UNIVERSITY OF PANNONIA

Analysis of composite materials in 3D printing technologies

by

Kámán András

DOI:10.18136/PE.2026.1017

A thesis submitted in fulfillment for the
degree of Doctor of Philosophy

in the
Chemical Engineering and Material Sciences Doctoral School

August 2026

Analysis of composite materials in 3D printing technologies

The thesis was prepared for the award of a doctoral degree (PhD) within the framework of the Doctoral School of Chemical Engineering and Material Sciences at University of Pannonia

in the discipline of Materials science and technology

written by: András Kámán

Supervisor: Dr. Attila Egedy

I recommend the dissertation for acceptance: yes / no.

…….
supervisor

I recommend the dissertation for peer review.

…….
chair of the DDHC

The PhD-candidate has achieved ……. % at the public debate.

The composition of the Final Examination Committee:

chair:…….…….

reviewers:.……

members:…….

Veszprém,

…….
chair of the committee

Qualification of degree: ….....

Veszprém,

…….
chair of the UDHC

Kivonat

A disszertáció célja a 3D nyomtatás területén folyó kutatások összehasonlíthatóbbá és megbízhatóbbá tétele. Ezeket főként a 3D nyomtatott struktúra egyedi tulajdonságai tartják vissza, különös tekintettel a szálerősített poliamid 3D nyomtatóanyagokra részletes nyomtatási paraméterhatás-vizsgálatokkal. Új módszereket mutattam be e cél elérése érdekében, beleértve a homogén struktúrarendszerek használatát és azok hatását a különböző méretű és alakú próbatesteknél.

Már vannak jól bejáratott standard próbatest-geometriák, amiket a műanyagipar használ, mint a "kutyacsont" alakú szakító próbatest, azonban a nagy strukturális sokszínűségnek hála, amelyet a 3D nyomtatással el lehet érni, a próbatestek nem feltétlenül viselkednek azonosan különböző struktúrák és paraméterek esetében. Ebből kifolyólag kérdéses a kutatások összehasonlíthatósága, amelyek különböző próbatest-geometriákat használtak fel. A doktori kutatásom alatt két fő struktúratípust vizsgáltam, amellyel minden 3D nyomtatott test rendelkezik, hogy meghatározzam, valóban változik-e a szilárdságuk a próbatest-geometria változásával. Továbbá, egy előtesztelő csoportot hoztam létrem és vizsgáltam komputertomográfiával, hogy meghatározzam a próbatestek porozitásának van-e hatása a szakítószilárdságukra, miután az anyag depozíció kalibrálva lett.

A fő nyomtatási paramétereket és azok hatását vizsgáltam a mechanikai tulajdonságokra kíséleti eredmények értékelésével és korrelációs vizsgálatokkal egyaránt mindhárom tárgyalt anyagrendszernél, amelyek a sima-, szénszállal erősített- és üvegszállal erősített poliamidok voltak. Míg a paraméterek hatásai drasztikusan változtak a struktúratípústól függően, általános megállapítások és viselkedési minták rajzolódtak ki az eredmények kiértékelése alatt.

A szakítóvizsgálatok során nyert adatokat tovább felhasználva, valamint a nyomtatási paraméterek alapján, modellillesztés segítségével prediktáltam a mechanikai tulajdonságokat. Ezzel kiváló teljesítményű nemlineáris modelleket sikerült előállítani, miközben más megközelítés is kipró- bálásra került. Ez az új, strukturális paraméterek alapján szétbontott csoportokat tartalmazó megkö- zelítés lineáris modell felhasználásával történt, azonban ez nem hozta a várt teljesítményeket, amit az előző vizsgálat is mutatott.

A célom az volt, hogy a 3D nyomtatott testek egyedi belső struktúráját a kutatás folyamatává tegyem, nem pedig egy hátráltató tényezővé, ami megnehezíti azok vizsgálatát. Továbbá, hogy egy átívelő kutatást végezzek a nyomtatási paraméterek a hatásáról a 3D-nyomtatott testek mechanikai tulajdonságaira és azok viselkedésére.

Abstract

This dissertation aims to make the process of 3D printing research more comparable and reliable, mainly set back by the unique quirks of printed structures, with special focus on polyamide filaments with fiber reinforcement, with detailed printing parameter effect tests and analysis. New methods were introduced to achieve this aim, including the use of homogeneous structure systems and inquiring into the effect these unique structures may have when using differently sized and shaped specimens.

There are already well established standardized specimen geometries in the plastic industry, like the typical dogbone shape used for tensile testing; however, due to the huge variety of structures that can be built with 3D printing, the differently shaped specimens may not behave the same when different structures or parameters are being examined. Stemming from this fact, the comparability between studies and specimens comes into question. During my doctoral research, I investigated the two main structural types that any 3D printed object has, to determine if any of them show different strength with the change of specimen geometry. Furthermore, a pretest group was created and investigated by computed tomography to determine whether, after material deposition calibration, the porosity of the specimens has any bearing on their tensile strengths.

After the initial aim, the study of primary parameters and their effect on mechanical properties was carried out by both experimental test results and correlation analysis for the three material groups: unreinforced, carbon fiber reinforced, and glass fiber reinforced polyamide blend. While the effect of parameters varied drastically with structure type, general observations and behaviour patterns emerged during the evaluation.

Further use of the testing data took shape in the form of mechanical property prediction by model fitting based on the printing parameter set. This produced outstanding model performances for the non-linear model, while another approach was also considered and attempted; the new, more fractured groups with a linear model did not bring the desired performances that the former analysis study suggested.

My goal is to make the unique inner structure of 3D printed objects part of the research process rather than it being a hindrance to it, and make an overarching printing parameter influence study regarding the behaviours of 3D printed objects and their mechanical properties.

Abstrakt

Diese Dissertation zielt darauf ab, den Forschungsprozess im Bereich des 3D-Drucks vergleichbarer und zuverlässiger zu gestalten, der vor allem durch die einzigartigen Eigenheiten der gedruckten Strukturen behindert wird, wobei ein besonderer Schwerpunkt auf faserverstärkten Polyamid-Filamenten mit detaillierten Tests und Analysen der Auswirkungen von Druckparametern liegt. Um dieses Ziel zu erreichen, wurden neue Methoden eingeführt, darunter die Verwendung homogener Struktur-Systeme und die Untersuchung der Auswirkungen, die diese einzigartigen Strukturen haben können, wenn Proben unterschiedlicher Größe und Form verwendet werden.

In der Kunststoffindustrie gibt es bereits etablierte, standardisierte Probengeometrien, wie beispielsweise die typische „Dogbone"-Form für Zugversuche; aufgrund der enormen Vielfalt an Strukturen, die mittels 3D-Druck hergestellt werden können, verhalten sich unterschiedlich geformte Proben jedoch möglicherweise nicht gleich, wenn verschiedene Strukturen oder Parameter untersucht werden. Aus dieser Tatsache ergibt sich die Frage nach der Vergleichbarkeit zwischen Studien und Proben. Im Rahmen meiner Doktorarbeit untersuchte ich die beiden wichtigsten Strukturtypen, die jedes 3D-gedruckte Objekt aufweist, um festzustellen, ob einer von ihnen bei einer Änderung der Probengeometrie eine unterschiedliche Festigkeit aufweist. Darüber hinaus wurde eine Vorversuchsgruppe erstellt und mittels Computertomographie untersucht, um festzustellen, ob die Porosität der Proben nach der Kalibrierung der Materialablage einen Einfluss auf ihre Zugfestigkeiten hat.

Nach der Festlegung des ursprünglichen Ziels wurden die primären Parameter und deren Einfluss auf die mechanischen Eigenschaften sowohl anhand experimenteller Testergebnisse als auch mittels Korrelationsanalyse für die drei Materialgruppen – unverstärkte, kohlefaserverstärkte und glasfaserverstärkte Polyamid-Mischungen – untersucht. Während der Einfluss der Parameter je nach Strukturtyp stark variierte, zeigten sich im Verlauf der Auswertung allgemeine Beobachtungen und Verhaltensmuster. Die weitere Nutzung der Versuchsdaten erfolgte in Form einer Vorhersage der mechanischen Eigenschaften durch Modellanpassung auf der Grundlage des Druckparametersatzes. Dies führte zu hervorragenden Modellleistungen für das nichtlineare Modell, während ein weiterer Ansatz ebenfalls in Betracht gezogen und erprobt wurde; die neuen, stärker gebrochenen Gruppen mit einem linearen Modell brachten jedoch nicht die gewünschten Leistungen, die die vorherige Analysestudie nahegelegt hatte.

Mein Ziel ist es, die einzigartige innere Struktur von 3D-gedruckten Objekten in den Forschungsprozess einzubeziehen, anstatt sie als Hindernis zu betrachten, und eine übergreifende Studie zum Einfluss der Druckparameter auf das Verhalten von 3D-gedruckten Objekten und deren mechanische Eigenschaften durchzuführen.

Acknowledgements

Here I would like to acknowledge the help of all those without whom I would not have succeeded in finishing this dissertation.

First of all, I wish to express my gratitude towards the members of the Department of Process Engineering for their continued support and valuable input during my doctorate journey.

I would like to especially thank my supervisor Dr. Attila Egedy for his guidance during my doctorate years. A special thanks goes to Dr. Miklós Jakab, who supported me as my supervisor even after he departed from the university and remained a constant source of inspiration and advice during my final years of study.

I would also like to offer my gratitude and express my love and thankfulness to my family and friends who supported me on this journey.

Contents

Kivonat i

Abstract ii

Abstrakt ii

Acknowledgements iv

List of Figures vii

List of Tables xi

Abbreviations xii

Symbols xiv

1 Introduction 1

2 Overview of the 3D printing technologies 4
2.1 Categorization of 3D printing . . . 4
2.1.1 Extrusion 3D printing methods . . . 7
2.1.2 Resin 3D printing methods . . . 8
2.1.3 Powder bed 3D printing methods . . . 9
2.2 Literature review of Extrusion 3D printing technology . . . 10
2.2.1 General overview . . . 11
2.2.2 Nylon as a matrix material in extrusion 3D printing . . . 12
2.2.3 Reinforcing materials used in extrusion 3D printing . . . 12
2.2.4 Relevant experimental developments supporting the research work . . . 14
2.2.5 Critical review of the literature . . . 14

3 Materials and methods 16
3.1 3D printing process . . . 16
3.1.1 Investigated parameters . . . 19
3.1.2 Tensile testing . . . 20
3.1.3 Scanning electron microscopy . . . 20
3.1.4 Computed tomography . . . 22
3.1.5 MATLAB . . . 24

4 Inquiry into the effect of specimen size and geometry on tensile strength 25
4.1 3D printing process . . . 26
4.2 Results . . . 30
4.3 Conclusion . . . 42

5 Investigation of the 3D printing process parameters and their effect on tensile properties 43
5.1 Main parameters of an extrusion based 3D printing process . . . 43
5.1.1 Nozzle diameter . . . 45
5.1.2 Layer height . . . 45
5.1.3 Extruded line cross-section area . . . 46
5.1.4 Printing temperature . . . 48
5.1.5 Infill orientation . . . 48
5.1.6 Nozzle types . . . 49
5.2 Tensile strength results . . . 50
5.3 Young's modulus results . . . 56
5.4 Pearson correlation analysis . . . 62
5.4.1 Pearson correlation between tensile strength and material groups categorized by their infill orientation . . . 68
5.4.2 Pearson correlation between Young's modulus and material groups categorized by their infill orientation . . . 69
5.4.3 Pearson correlation between tensile strength and material groups categorized by their nozzle diameter . . . 72
5.4.4 Pearson correlation between Young's modulus and material groups categorized by their nozzle diameter . . . 72
5.4.5 Conclusion . . . 73

6 Modeling and simulating the complex structural 3D printed specimens based on different printing parameters 78
6.1 The prediction of mechanical properties with model fitting . . . 78
6.1.1 Conclusion . . . 84

7 Conclusion 85
7.1 I. Thesis point . . . 85
7.2 II. Thesis point . . . 86
7.3 III. Thesis point . . . 87

Bibliography 89

Appendix 97

List of Figures

2.1 The wide variety of the 3D printing spectrum [1], [2], [3], [4], [5], [6] 5
2.2 3D printing technologies categorized 6
2.3 An extrusion based 3D printer [7] 7
2.4 A resin based 3D printer [8] 9
2.5 A powder bed 3D printer [9] 10

3.1 Rat Rig V-Core 3 modular FDM 3D printer [10] 17
3.2 ASTM D638 type V tensile testing specimen 20
3.3 SEM image of the distribution of the chopped glass fibers inside the filament . 21
3.4 SEM images of reinforcing chopped glass fibers after the plastic matrix has been burnt away, with their length (a) and width (b) measured 22
3.5 SEM images of reinforcing chopped glass fibers inside the nylon matrix after breakage 22
3.6 The orientation of fibers inside individual extruded lines at a cross-section of a sample 23
3.7 CT image of the porosity system of a 3D printed sample 23

4.1 A common 3D printed structure with the 3 main line structures, yellow lines are walls (vertical shell), purple lines are bottom layers (horizontal shell), and red lines are infill lines. 26
4.2 ASTM D638 type V tensile testing specimen with the 3 dimensions that have been changed 26
4.3 The visual representation between only wall specimens with their uppermost layer visible (a) and second uppermost layer visible (b), and only infill specimens with their uppermost layer visible (c) and second uppermost layer visible (d) 28
4.4 The visual difference in shape and size between individual specimens after tensile testing 29
4.5 The relation between the infill orientation and tensile testing 29
4.6 The tensile strengths of the pretest specimens compared by their porosity . . . 30
4.7 The porosity systems of an only infill specimen of the 0.53 Width/height ratio and 4.94 mm^2 cross section area group captured in the CT imaging software . . 31
4.8 The directional porosity analysis (a) and its cross section (b) of an only infill specimen of the 0.53 Width/height ratio and 4.94 mm^2 cross section area group 31
4.9 The tensile strengths of the only wall 3D printed specimens compared by their cross section area 33
4.10 The tensile strengths of the only infill 3D printed specimens compared by their cross section areas 33

4.11 The tensile strengths of the only wall 3D printed specimens compared by their width/height ratios . . . 34
4.12 The tensile strengths of the only infill 3D printed specimens compared by their width/height ratios . . . 34
4.13 The tensile strengths of the only wall 3D printed specimens compared by their width/nozzle diameters . . . 35
4.14 The tensile strengths of the only infill 3D printed specimens compared by their width/nozzle diameters . . . 35
4.15 The tensile strengths of the only wall 3D printed specimens compared by their height/layer heights . . . 35
4.16 The tensile strengths of the only infill 3D printed specimens compared by their height/layer heights . . . 36
4.17 Individual specimen group with their mean value and deviations . . . 36
4.18 Individual specimen group with their mean value and deviations . . . 37
4.19 The tensile strengths of the porosity specimens included in their specimen group compared by their cross section area . . . 37
4.20 The tensile strengths of the porosity specimens included in their specimen group compared by their width/height ratios . . . 37
4.21 Deviations represented inside the only wall 0.8 mm nozzle specimen group with their mean value and deviation . . . 40
4.22 Deviations represented inside the only wall 0.4 mm nozzle specimen group with their mean value and deviation . . . 40
4.23 Deviations represented inside the only infill 0.8 mm nozzle specimen group with their mean value and deviation . . . 41
4.24 Deviations represented inside the only infill 0.4 mm nozzle specimen group with their mean value and deviation . . . 41

5.1 The difference between the extruded lines of (a) 0.4 mm nozzle diameter; (b) 0.8 mm nozzle diameter . . . 45
5.2 The difference between layer heights concerning the surface quality of a cat model . . . 46
5.3 The correlation between nozzle diameter, layer height, real and theoretical ELCSA 47
5.4 SEM image of ELCSA inside a 3D printed layer . . . 47
5.5 The difference between the (a) MK8 nozzle and (b) V6 nozzle . . . 49
5.6 The change in tensile strength values of unreinforced nylon specimens based on different parameters . . . 51
5.7 The change in tensile strength values of carbon fiber reinforced nylon specimens based on different parameters . . . 52
5.8 The change in tensile strength values of glass fiber reinforced nylon specimens based on different parameters . . . 53
5.9 The change in tensile strength values of specimens printed with high temperature and 0° orientation . . . 54
5.10 The change in tensile strength values of specimens printed with high temperature and 45° orientation . . . 54
5.11 The change in tensile strength values of specimens printed with low temperature and 0° orientation . . . 55
5.12 The change in tensile strength values of specimens printed with low temperature and 45° orientation . . . 55

5.13 The change in Young's modulus values of unreinforced nylon specimens based on different parameters . . . 57
5.14 The change in Young's modulus values of carbon fiber reinforced nylon specimens based on different parameters . . . 57
5.15 The change in Young's modulus values of glass fiber reinforced nylon specimens based on different parameters . . . 58
5.16 The change in Young's modulus values of specimens printed with high temperature and 0° orientation . . . 59
5.17 The change in Young's modulus values of specimens printed with high temperature and 45° orientation . . . 59
5.18 The change in Young's modulus values of specimens printed with low temperature and 0° orientation . . . 60
5.19 The change in Young's modulus values of specimens printed with low temperature and 45° orientation . . . 60
5.20 The Pearson Correlation matrix regarding printing parameters and mechanical properties of unreinforced nylon samples . . . 63
5.21 The Pearson Correlation matrix regarding printing parameters and mechanical properties of carbon fiber reinforced nylon samples . . . 64
5.22 The Pearson Correlation matrix regarding printing parameters and mechanical properties of glass fiber reinforced nylon samples . . . 65
5.23 The tensile strength summarization of the Pearson coefficient values of all three matrices . . . 66
5.24 The Young's modulus summarization of the Pearson coefficient values of all three matrices . . . 66
5.25 The tensile strength summarization of the Pearson coefficient values of all three materials grouped by their infill orientation . . . 67
5.26 The Young's modulus summarization of the Pearson coefficient values of all three materials grouped by their infill orientation . . . 68
5.27 The tensile strength summarization of the Pearson coefficient values of all three materials grouped by their nozzle diameter . . . 71
5.28 The Young's modulus summarization of the Pearson coefficient values of all three materials grouped by their nozzle diameter . . . 71

6.1 The prediction model performance for unreinforced nylon samples' tensile strength (a) and Young's modulus (b) values. . . . 79
6.2 The prediction model performance for carbon fiber reinforced nylon samples' tensile strength (a) and Young's modulus (b) values. . . . 80
6.3 The prediction model performance for glass fiber-reinforced nylon samples' tensile strength (a) and Young's modulus (b) values. . . . 80
6.4 The prediction model performance for both infill orientation- and nozzle diameter categorizations in the case of tensile strength. . . . 82
6.5 The prediction model performance for both infill orientation- and nozzle diameter categorizations in the case of Young's modulus. . . . 82
6.6 Young's modulus and tensile strength heat map for unreinforced nylon . . . 83
6.7 Young's modulus and tensile strength heat map for carbon fiber reinforced nylon 83
6.8 Young's modulus and tensile strength heat map for glass fiber reinforced nylon 84

7.1 Individual specimen group with their mean value and deviations . . . 97
7.2 Individual specimen group with their mean value and deviations . . . 97

7.3 Individual specimen group with their mean value and deviations 97
7.4 Individual specimen group with their mean value and deviations 98
7.5 Individual specimen group with their mean value and deviations 98
7.6 Individual specimen group with their mean value and deviations 98
7.7 Individual specimen group with their mean value and deviations 99
7.8 Individual specimen group with their mean value and deviations 99
7.9 Individual specimen group with their mean value and deviations 99
7.10 Individual specimen group with their mean value and deviations 100
7.11 Individual specimen group with their mean value and deviations 100
7.12 Individual specimen group with their mean value and deviations 100
7.13 Individual specimen group with their mean value and deviations 101
7.14 Individual specimen group with their mean value and deviations 101
7.15 Individual specimen group with their mean value and deviations 101
7.16 Individual specimen group with their mean value and deviations 102
7.17 The prediction model performance for 0° infill oriented unreinforced nylon samples tensile strength (a) and Young's modulus (b) values. 102
7.18 The prediction model performance for 45° infill oriented unreinforced nylon samples tensile strength (a) and Young's modulus (b) values. 102
7.19 The prediction model performance for 0.4 mm nozzle unreinforced nylon samples tensile strength (a) and Young's modulus (b) values. 107
7.20 The prediction model performance for 0.8 mm nozzle unreinforced nylon samples tensile strength (a) and Young's modulus (b) values. 107
7.21 The prediction model performance for 0° infill oriented carbon fiber reinforced nylon samples tensile strength (a) and Young's modulus (b) values. 108
7.22 The prediction model performance for 45° infill oriented carbon fiber reinforced nylon samples tensile strength (a) and Young's modulus (b) values. 108
7.23 The prediction model performance for 0.4 mm nozzle carbon fiber reinforced nylon samples tensile strength (a) and Young's modulus (b) values. 109
7.24 The prediction model performance for 0.8 mm nozzle carbon fiber reinforced nylon samples tensile strength (a) and Young's modulus (b) values. 109
7.25 The prediction model performance for 0° infill oriented glass fiber reinforced nylon samples tensile strength (a) and Young's modulus (b) values. 110
7.26 The prediction model performance for 45° infill oriented glass fiber reinforced nylon samples tensile strength (a) and Young's modulus (b) values. 110
7.27 The prediction model performance for 0.4 mm nozzle glass fiber reinforced nylon samples tensile strength (a) and Young's modulus (b) values. 111
7.28 The prediction model performance for 0.8 mm nozzle glass fiber reinforced nylon samples tensile strength (a) and Young's modulus (b) values. 111

List of Tables

3.1 The properties of the carbon fiber-nylon filament measured through injection molded specimens provided by the manufacturer 18
3.2 The properties of the glass fiber-nylon filament measured through injection-molded specimens provided by the manufacturer 18
3.3 The properties of the unreinforced nylon filament measured through injection-molded specimens provided by the manufacturer 19

4.1 The parameter set for the ASTM D638 type V tensile testing specimen resizing . 27
4.2 Tensile strength values for the porosity pretest groups 32
4.3 Tensile strength values for the only wall specimens printed with a 0.4 mm nozzle 38
4.4 Tensile strength values for the only wall specimens printed with a 0.8 mm nozzle 38
4.5 Tensile strength values for the only infill specimens printed with a 0.4 mm nozzle 39
4.6 Tensile strength values for the only infill specimens printed with a 0.8 mm nozzle 39

5.1 The parameter matrix of the specimens 49

6.1 The values of received parameters of each mechanical property 81

7.1 The measured mechanical properties and used parameters of every unreinforced nylon samples 103
7.2 The measured mechanical properties and used parameters of every carbon fiber reinforced nylon samples 104
7.3 The measured mechanical properties and used parameters of every glass fiber reinforced nylon samples no. 1 105
7.4 The measured mechanical properties and used parameters of every glass fiber reinforced nylon samples no. 2 106

Abbreviations

FDM	Fused Deposition Modeling
FFF	Fused Filament Fabrication
FGF	Fused Granulate Fabrication
DED	Direct Energy Deposition
LENS	Laser Engineered Net Shaping
EBAM	Electron Beam Additive Manufacturing
VPP	Vat Photopolymerization
SLA	Stereolithography
MSLA	Masked Stereolithography
DLP	Digital Light Processing
CLIP	Continuous Liquid Interface Production
MJ	Material Jetting
PJ	PolyJet technology
NPJ	NanoParticle Jetting
DOD	Drop-On Demand
SBS	Selective Beam Sintering
SLS	Selective Laser Sintering
SLM	Selective Laser Melting
EBM	Electron Beam Melting
SBJ	Selective Binder Jetting
BJ	Binder Jetting
MJF	Multi Jet Fusion
PLA	Polylactic acid
ABS	Acrylonitrile Butadiene Styrene
PC	Polycarbonate

PA Polyamide

PPS Polyphenylene sulfide

PETG Polyethylene terephthalate with Glycol additive

Symbols

N	Unreinforced nylon
CFN	Carbon fiber reinforced nylon
GFN	Glass fiber reinforced nylon
T	Temperature
D_N	Nozzle diameter
H_L	Layer height
α	infill orientation
σ_t	Tensile strength
E	Young's modulus
$N0$	Unreinforced nylon specimens printed in a 0° infill orientation
$N45$	Unreinforced nylon specimens printed in a 45° infill orientation
$N04$	Unreinforced nylon specimens printed with a 0.4 mm nozzle
$N08$	Unreinforced nylon specimens printed with a 0.8 mm nozzle

Chapter 1

Introduction

In recent years, the 3D printing industry has not only been able to reach everyday homes but also simplified the whole process of 3D printing to such an extent that almost anyone can start printing at home with enough disposable income and minimal knowledge. Due to the explosive growth of the industry, the number of scientific papers discussing 3D printing has been steadily growing each year; furthermore, this relatively new technology (only a few decades old) makes it a hot topic among researchers. These factors make the standardisation of the 3D printing industry and its research rather difficult; the main research gap that can be found among the scientific papers is the description of the printing process parameters and conditions.

In this dissertation, the author will be focusing on creating a thorough overview of the most recent 3D printing techniques, with special focus on the most widely available and used Fused Deposit Modeling (FDM) process. The dissertation contains three main thesis points which address contemporary challenges in the 3D printing landscape; these are:

- Inquiry into the effect that the specimen size and geometry have on the final tensile strength.
- Investigation of the 3D printing process parameters and their effect on tensile properties of finished products with:
  - unreinforced,
  - carbon fiber reinforced,

  - and glass fiber reinforced nylon.

- Modeling the complex structural 3D printed specimens based on different printing parameters.

In the last 10 years, the main breakthroughs happened in the material, slicer, and firmware fields as the hardware of the 3D printers already reached a mature state. The materials that can be used hassle-free expanded exponentially from the old PLA and ABS pair with the rapid advancement of additives that made the printing of other materials possible, such as PC, PA, or PPS more recently. The slicers also went through a great deal of change in this time period as the commercially free and open-source slicers, such as Cura, PrusaSlicer, and OrcaSlicer, dominated the slicer software space and ultimately made the monetized slicers almost completely disappear. Few of the most recent additions include Arachne perimeter generation, which can generate different extrusion widths with the same nozzle, or the Scarf joints, which mimic the matching of sloping surfaces used in carpentry instead of the original simple line start and finish next to each other. Firmware advancements brought forth much more of the already matured hardware's potential, more refined control, and the ability to improve many of the printing aspects with extensive calibrations, as well as ease of operation and setup.

With the development of slicers and materials, the ability to tailor the material properties with the adjustment of printing parameters in slicers became an opportunity and a desired feature as well. As of the first quarter of 2025, PrusaSlicer (which was used for creating all the GCODEs in this dissertation), for example, has over 300 parameters that can be modified. This already large number of parameters is always expanding as the open-source nature of the software makes for a great breeding ground for innovation; a lot of private projects found their way into the later versions of PrusaSlicer in order to be used by everyone.

In the following chapter, I will introduce the different printing technologies based on my own categorization, then I will show the state of the scientific research in the field of 3D printing and the research gap.

In chapter 3, I will be discussing the materials, machines, and methods utilized during research and their importance.

In chapter 4, I will show the porosity pretest carried out and the investigation into the relationship between tensile strength and specimen size/geometry.

In chapter 5, the effects of process parameters on the mechanical properties of 3D printed objects are discussed with both experimental test values and Pearson correlation analysis.

In chapter 6, the prediction of mechanical properties based on process parameters by model fitting is introduced and discussed with evaluated model performances in two approaches.

Finally, in chapter 7, I conclude the dissertation in three thesis points summarizing and distinguishing the most important parts.

Chapter 2

Overview of the 3D printing technologies

The amount of relevant literature on 3D printing is very small to begin with; however, a large portion of it is obviously written by researchers from a different field of study. Due to these circumstances, it is quite difficult to find a study which dwells into the 3D printing process aspect in adequate detail. Also, there are a lot of different categorizations for 3D printing technologies, which are often nonsensical, but some kind of categories need to be established in order to discuss them properly. This dissertation will focus on the properly detailed 3D printing process both for the sake of repeatability and transparency.

2.1 Categorization of 3D printing

Before going into the topic of different 3D printing technologies, their place among the traditional manufacturing processes must be discussed, as these "traditional" subtractive ones like milling and drilling achieve a desired shape and form by taking material away, while the additive manufacturing processes like 3D printing achieve the same by adding material. The subtractive methods generally make a significant amount of waste material, especially when compared to the additive ones; also, they are limited in their capability of achieving complex inner structures. However, it is also true that traditional manufacturing methods usually produce parts with better mechanical properties and in higher production quantities; they are much more desirable compared to the additive manufacturing methods, and stemming

from this fact, usually these two radically different types of manufacturing approaches are not competing with one another, but rather have different use cases.

The differentiation between 3D printing solutions is always a difficult question, as the methods are numerous and the differentiating factors between them are often narrow or non-existent; for example, the following three technologies: binder jetting, selective laser sintering, and selective laser melting. Furthermore, there are 3D printing method names that only certain companies can use, which are usually very similar to other methods and only differ in small detail. For this reason, I have created the following 3D printing technology categorization of various 3D printing methods with 3 large groups and more subgroups inside of them based on the following factors:

- layer making method,
- inner structure,
- printing time,
- scalability,
- machine and material cost,
- type of material that is used (liquid, pellet, filament, powder, etc.),
- target production quantity range.

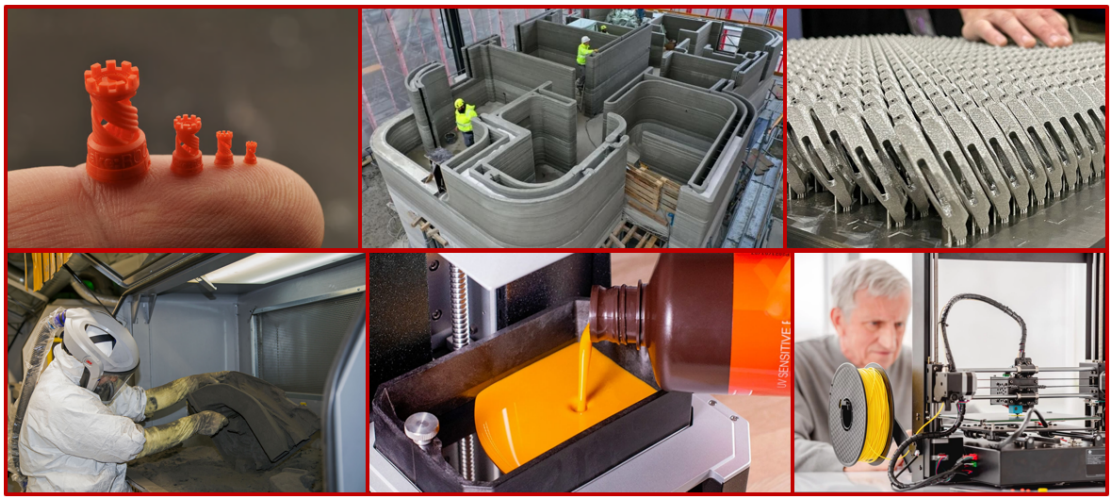


FIGURE 2.1: The wide variety of the 3D printing spectrum [1], [2], [3], [4], [5], [6]

Based on the above mentioned criterion, the 3 main groups are the extrusion 3D printing methods (FDM, FFF, DED, etc.), resin-based 3D printing methods (SLA, MSLA, DLP, etc.), and powder bed 3D printing methods (SLS, SEBM, BJ, etc.). Within each of these groups, the different technologies are very similar in terms of the factors listed and can be further categorized in Figure 2.1. Similar but not extensive categorization can be seen in the article made by Ma et al. [11] and Zhou et al. [12], where they separated the material jetting from photo-polymerization and powder bed fusion. However, categorization of the different printing technologies is rare, as most of the articles simply list the different technologies and methods after one another based on how close they are to each other in layer-making method or how widespread they are, like in the case of Ilbey et al. [13] and Chadha et al. [14].

Examples for these methods can be seen in Figure 2.1 with varying scale, inner structure, and production quantity [15]. There are hybrid technologies as well (UV resin being extruded), but their use is limited, so they are not categorized here.

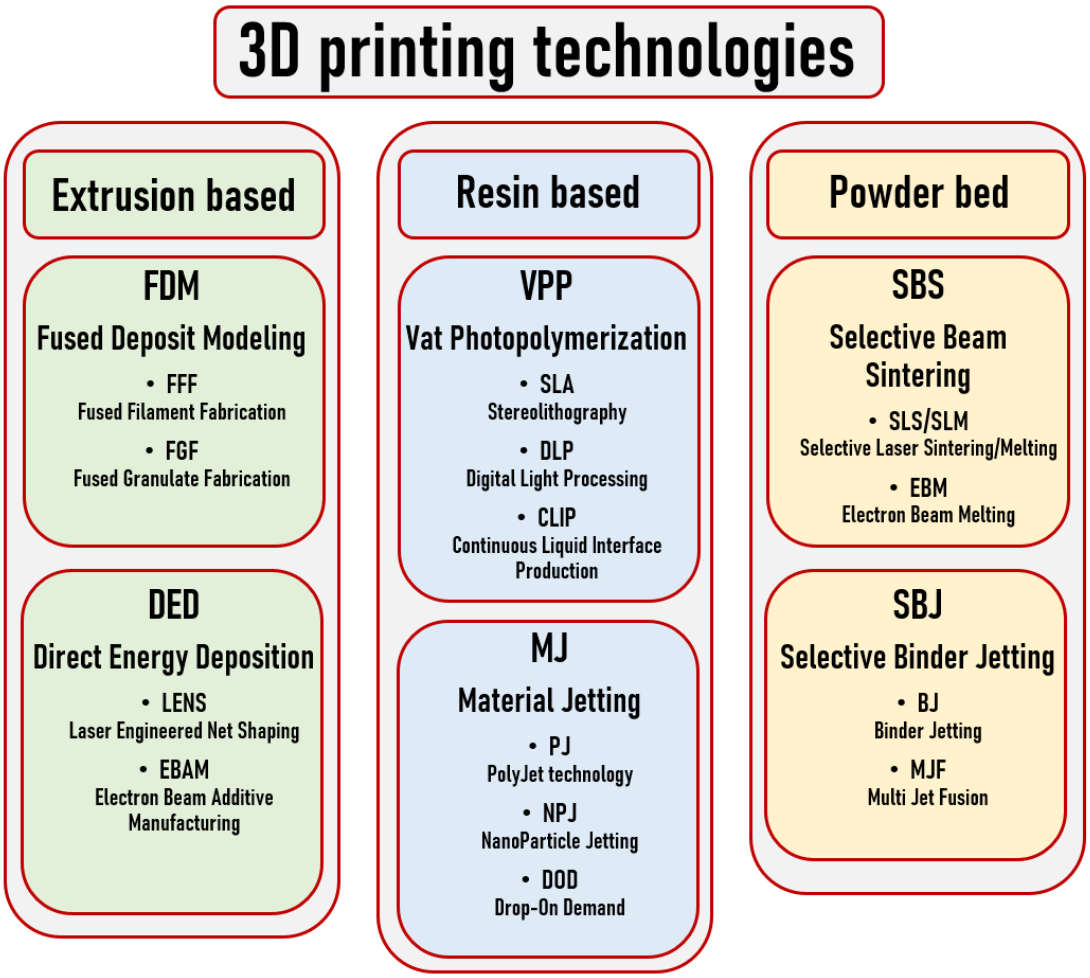


FIGURE 2.2: 3D printing technologies categorized

2.1.1 Extrusion 3D printing methods

Extrusion-based 3D printing is the most widely used 3D printing method, which is flexible enough to use for almost every application adequately, ranging from the low-end consumer 3D printers to the several meters long industrial ones. For this reason, among others, this dissertation focuses on this 3D printing method.

Its layer making happens with the extrusion and deposition of individual layers (Figure 2.3), which causes some unique properties and characteristics of the structures 3D printed with this type of technology [16]. Mainly that any type of inner infill can be printed and the orientation of the individual extrusion lines affects the mechanical properties [17], which is especially the case when fiber reinforced materials are being extruded [18]. Due to depositing the layers by individual lines [19], the printing time greatly depends on the size of an object as well as the height and width of the individual extruded lines; generally, it is the most time consuming printing method of the three.



FIGURE 2.3: An extrusion based 3D printer [7]

Regarding the methods scalability it is by far the most scalable of the 3 methods, as even the consumer grade printers can be equipped with a 0.1 mm nozzle and print at a layer height of 0.02 mm for printing small parts as well as with a 1.5 mm nozzle and 1 mm nozzle and print at a 1 mm layer height for much larger parts, also there is no issue with increasing the dimensions of a extrusion based 3D printer other than added cost, which are not exponential as with other printers. Not only is the scaling of the printer relatively low cost, but the basic machine costs and materials are the cheapest among the 3 technologies, as the most used materials are in the form of filaments and pellets, both of which require very few added manufacturing steps [20]. This method favors low production quantities, usually getting less efficient as it increases; for one machine, the sensible production quantity limit for complex

or bigger objects is in the two-digit range, and for simpler or smaller objects the three-digit range. For further manufacturing capabilities, the forming of printer farms is usually utilized; sometimes even several hundred printers are used to compensate for the relatively slow printing process that characterizes the extrusion-based 3D printing methods.

2.1.2 Resin 3D printing methods

The second most widely used 3D printing method, which usually shines when very detailed or small objects need to be printed, or special properties are required (biocompatibility, very low shore hardness, great transparency, etc.).

Its layer making method varies between the different subcategories as SLA uses a laser point that cures resin in a layer, DLP uses a light source, which is projected with mirrors, and MSLA uses a type of LCD screen to light the whole layer of resin at the same time [21], however every method is very efficient with using the entire plane for printing so there is not a huge difference in printing time between 1 or 10 objects as only the scanning of a beam is necessary. Most of the methods utilizes a resin bath, which makes the printing of enclosed structures almost impossible, usually if the wall of an object is above a given threshold it can only be printed hollow with a hole left for residual resin drainage as the post UV radiation cannot penetrate unlimited wall thickness the inner side of an object would contain uncured resin, which causes fractures in the structure later on [22]. The resin bath (Figure 2.4) is a limiting factor when it comes to scalability, as the resin is a viscous liquid it exerts considerable force on the print bed and already printed object on the bed as they are moving upwards between layers thus usually maximizing the print surface for these resin bath printers around 60000 mm^2, for other printers like inkjet types the build surface can be scaled indefinitely, however for practical purposes it rarely reaches even the 500 mm size for any dimension. As far as machine costs go, the bath types are usually among the cheapest options for any kind of 3D printer, while the more sophisticated inkjet types are among the most expensive industrial printers, both of which are usually paired with expensive liquid resin materials. The bath types can be used for single-object prints but work better with their whole build surface being filled, as they are very efficient when the whole building surface is being used. However, high production quantity is not the best fit for this printing type either, so they really shine in the low to mid manufacturing ranges; this cannot be said about the inkjet types as they

are almost exclusively used for singular printing or very low numbers of objects due to their nozzle-depositing nature [23].

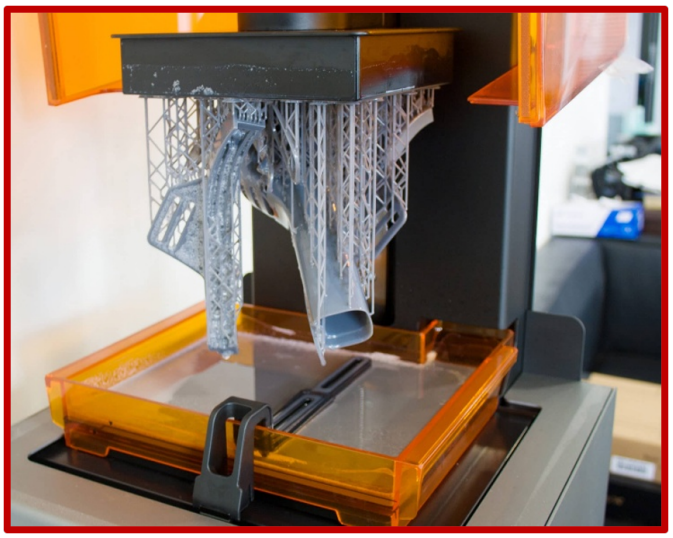


FIGURE 2.4: A resin based 3D printer [8]

2.1.3 Powder bed 3D printing methods

This method is exclusively used in industrial applications; there have been attempts to bring this method to the homes of people (Micron desktop SLS 3D Printer), but it never got into fruition mainly due to safety concerns.

The layer-making method involves spreading thin powder layers on top of each other and sintering/melting/binding the specific areas of said layers, leaving the residual powder in the printing volume (Figure 2.5). This residual powder has a few implications; this makes the involvement of supports unnecessary and essentially makes the inner structure only capable of 3 different kinds; these are solid structure, powder-filled structure, and similar to the resin-based hollow structure with drainage holes. Printing time is a tricky subject for these types of printers, as usually a whole process of printing is around a day; however, it can contain a high number of objects, so its productivity is high. The scalability is also limited, not by physics but rather costs; usually they have similarly sized print volumes as the resin-based printers, but their printer size is much larger because of preheating requirements and the nature of powder deposition; a few of the largest printers can get up to several meters high. Thus, these industrial printers are the most expensive by far compared to the other two methods, and their material cost is also the highest, as they are very fine powders, which are hard to manufacture and require special handling, as its particle are so small that health and safety

issues (explosion) arise when they are in the air. This method is by far most suited for high and very high production quantities; this is the method used when a product can only be manufactured by additive technology, but the production quantities are the same as the traditional subtractive technologies, like the US Army's new suppressors.



FIGURE 2.5: A powder bed 3D printer [9]

There are a lot of ways to group the different technologies ([24], [25]), which is increasingly difficult with the rapid development of new types of printers; this dissertation uses the above presented groups with special focus on extrusion 3D printing as its main topic.

2.2 Literature review of Extrusion 3D printing technology

Before reviewing the literature in this field, it is paramount to highlight major concerns about repeatability and usability of scientific studies conducted. Unfortunately, the majority of researchers and papers are mainly focusing on other fields of study and only using 3D printing as a novel tool to achieve results or as a new focus of already existing research. Stemming from this, the bulk of these studies are quite lacking in presenting important parameters and conditions of the printing process ([26], [27]) or contain nonsensical and arbitrary information ([28], [29]), worst cases even present outright wrong parameters or conditions that should have been avoided, for example the feed rate/flow rate in [27] which is highly dependent on the printer hardware and material being used and only serve as a limiting process parameter for the various printing speed parameters to safeguard against someone setting too high printing speeds for the printer or material.

Another characteristic of these studies is the use of low-end consumer printers utilized with factory settings, which require modification immediately to tailor them to the specific material and brand being used as well as the outcome users need. On the other end of the spectrum is the utilization of high-end industrial printers, which usually boast remarkable reliability; however, these are designed to be used by workers not proficient with 3D printers and lack any form of adjustment of the printing process.

Taking these factors into consideration, a major part of the literature overview will discuss the shortcomings of studies relevant to my thesis points.

2.2.1 General overview

In recent years, the 3D printing industry has experienced explosive growth in both household and industrial applications. Depending on the printing parameters, the properties of the end product can vary greatly, so in order to determine the parameters to meet the demands of different applications, the effects of individual parameters must be studied. Numerous studies that discuss different parameters and their effects on the 3D printing process and end product can be found. However, due to the rapid development in this area, most of these studies are either out of date, and the 3D printer used, slicing software, firmware, and materials are not consistent or lack the adjustability and sufficient documentation in order to reproduce the researched results.

Muhammad et al. investigated the effects of 8 parameters that could change the properties of PLA 3D printed products [30]. These were the layer height, perimeter line count, infill density, infill angle, printing speed, printing temperature, bed temperature, and print orientation. There are parameters that cannot be modified due to the materials being used, the geometry of the object, or the printing hardware and therefore, the investigation of such parameters is questionable; for example, the temperature of the build plate is usually chosen based on the printing material to ensure the adhesion of the printed parts and the threshold in which the adhesion is adequate is usually quite narrow.

The effect of parameter changes when fibers are added to the materials [31]; therefore, composited and unreinforced plastic filaments should be studied separately. Also, because of the added composite particles, the effect of a single parameter could also vary at different sizes

[32], and because these particles can not be compressed like the molten plastic matrix, the lower end of the used nozzle diameter is limited.

2.2.2 Nylon as a matrix material in extrusion 3D printing

Nylon is one of the most widely used polymers worldwide; it is a thermoplastic that has great mechanical properties and a low price, frequently used with some kind of fiber reinforcement. Due to its high strength, impact resistance, UV and chemical resistance, lightweight nature, and durability, nylon can be used in various applications, such as clothing or paracord manufacturing, as a fiber, lightweight, high strength and durable solid plastic in small arms and machine parts manufacturing, or in the electronics sector, to name a few. Their reinforcement is usually done by mixing chopped glass or carbon fibers into the plastic matrix [33],[34], [35], which oftentimes makes the orientation of said fibers random, especially when one of the most common manufacturing methods, injection moulding, is used; the orientation and distribution of fibers inside the injection moulded chopped fiber reinforced plastic bodies are challenging to change from the random nature that the flow of plastic inside moulds provides [36], [37], [38]. However, during an extrusion 3D printing process, the fibers inside the molten plastic naturally orient themselves in the direction of the extrusion [39], [40], [41], so the desired orientation can be achieved more easily. Furthermore, not only the fibers but the porosity system of a printed body is also naturally oriented in the direction of extrusion [42], so a planned/desired porosity system can be achieved.

2.2.3 Reinforcing materials used in extrusion 3D printing

One of the most used fiber-reinforced composite filaments in functional 3D printing is the chopped glass or carbon fiber-reinforced nylon filaments due to their mechanical, chemical, and thermal properties [43]. Research on the effect of infill of such materials can already be found [44], [45], [46], [47], mainly due to the fact that the orientation of fibers inside the nylon should contribute to its mechanical properties significantly, and the most investigated mechanical properties are the tensile and compressive strength of the samples, which is quite strange considering the fact, that fiber reinforcement is commonly used to enhance materials flexural strength.

The fiber-reinforced 3D printing is an emerging area with a wide range of possibilities not only in the field of engineering, but also in medical or consumer fields [48]. There are several different 3D printing methods (FDM, SLA, SLS, Binder jet, etc.); however, this paper focuses on FDM/FFF printing, because it is the most widely used and customizable additive manufacturing method.

Natural and bio-inspired fibers and matrix compounds as well as synthetic ones can be incorporated. However, most of the applied matrix compounds are PLA or nylon, due to the superior characteristics [49]. The applied fibers should increase some of the characteristics (mechanical, thermal, and elastic properties); however, we should keep in mind that for a detailed comparison, a proper optimization of the printing parameters and the use of adequate printers and parameters is key to achieve an optimal product.

Besides polymer 3D printing, other emerging fields are using similar manufacturing processes (extrusion based as FDM):

- geopolymers [50],
- cement including rubber particles [51],
- cement including fibers [52], [53],
- metal 3D printing [54],
- polymer-ceramic filaments [55].

Toth et al, investigated the behaviors of basalt fiber- reinforced PLA in both injection molding and 3D printing with special focus on the fiber content and distribution. They found that the strength of a 3D printed specimen can be predicted with an error of 5% [56].

There are two main reinforcement types in extrusion-based 3D printing, those being continuous and short chopped fibers [57]. Both types of fibers enhance specific material properties; however, their behaviour can slightly differ, also continous fiber printing is still in an infantile state, can only be performed with specifically built DIY printers and expensive industrial or semi-industrial printers. In contrast, the chopped fiber reinforced 3D printing can be done in any commercially available printer (besides the abrasion-resistant nozzle), and the prices for these materials usually stop at about twice the price of the pure matrix material; for these reasons, this study solely focuses on the chopped fiber reinforced material.

2.2.4 Relevant experimental developments supporting the research work

There have been an increasing number of studies relating to 3D printing, such as Sun et al, who used continuous fiber-reinforced composites and calculated the optimal turning radius for a nylon-carbon fiber system [58]. 7 mm fiber was used, and eSun PA6/1.75 mm nylon with a robot-based system. They created an excellent turning model and validated the model against measurement data. Zhang et al examined the conservative lower bound for strengths of fused filament fabrication and selective laser sintering [59]. eSun PLA filaments were used for the FFF, while PA12 was used for the SLS experiments. Based on the results, they created a new quadratic strength criterion. Wang et al proposed a novel topology optimisation for continuous fiber 3D printing [60]. With the optimised structure, better microstructure and stress distribution can be achieved while avoiding the possible defects (overlapping, sharp corners, not sufficient infill). Long et al aimed to improve the mechanical properties of continuous fiber composites by optimisation [61]. They focused on printing efficiency while maintaining acceptable tensile strengths.PLA and flax yarn fibers were applied, and the printing speed and printing line width were used in a Response Surface Optimisation method; the printing efficiency resulted in a 40 percent increase. Ding et al examined the effect of printing design on the pseudo-ductility in continuous fiber-reinforced glass/carbon nylon composites [62]. They found that the layer thickness does not affect the pseudo-ductility, while the printing platform temperature can decrease defect generation. Liu et al created a finite element model to simulate the printing process focusing on the effects of pressure on the continuous fiber reinforced composites [63]. They validated the model, and they found that the optimisation of the printing temperature and speed can eliminate the warping issues, and with the use of mathematical models, the optimisation process can be optimised. Peng et al examined the application of nacre-based topologies for the creation of carbon-fiber composites [64]. Light and scanning electron microscopy was also included in the detection and evaluation of the microstructure. They concluded that the interlocking composites have superior performance, and multi-material FDM-based printing has vast opportunities in biomimetic applications.

2.2.5 Critical review of the literature

However, these studies are quite limited in their scope and do not investigate other important parameters; the choice of other parameters is hardly stated, and often, when they are stated,

they seem to be chosen randomly or are the factory presets, which should be modified based on a lot of factors like Grgic et al [65] had done. Furthermore, the almost total lack of information on printing conditions often makes it difficult to replicate the results obtained in said studies and the use of low-end commercial 3D printers can be quite limiting in terms of parameter thresholds (e.g. PTFE tube cannot withstand temperatures above 240-250 °C without severe degradation, which makes the likes of nylon filaments not able to be printed at higher temperatures), usable hotend and nozzle types, and advanced features, which are crucial for calibration. Aside from these deficiencies, studies investigating this field of technology are few and far between, making the citation of such studies quite challenging. Therefore, in this study, all of the used printing parameters (over 450), chief 3D printer components, and printing conditions are available.

So, in order to ensure the repeatability of the study and make the conditions clearer, the full list of parameters is included. Also, to try to alleviate the problematic aspect of imperfections during 3D printing, extensive testing and calibration of both the printer and material were carried out. Lastly, the 3D printers used in studies fall between two groups: the industrial and semi-industrial printers, which are great for production purposes but are quite lacking in terms of customization, adjustability of the parameters, and usability of filaments that are not from the manufacturer. The other group is the cheap commercial printers, which have the aforementioned qualities but lack quality parts and usually run on some type of Marlin firmware, which lacks the advanced features that other firmware provides. These are the reasons that, in this study, one of the highest quality, expansively customizable 3D printers was used with the most recent features that can be found in any firmware.

Chapter 3

Materials and methods

Repeatability and transparency regarding the printing process were an essential aim of this dissertation; the full list of components used during printing, as well as processes before and during printing, is stated below.

3.1 3D printing process

All the specimens were made on a Rat Rig V-Core 3 (Faro, Portugal) machine that can be seen in Figure 3.1. It was chosen mainly for its modularity and high-quality mechanical components. Also, because this printer is designed to be run on Klipper firmware (v.0.11.0) [66], with RatOS (V 2.0.2) [67], the possibility to tweak settings down to the most basic levels is available.

For the mechanical parts its outfitted with MGN12 linear rails with MGN12C carriages, a 6 mm thick aluminium bed, and 30 mm x 30 mm aluminium extrusions that make up the frame of the printer. For the material deposition part, the two main components are the Orbiter V1.5 extruder (Shenzhen, China) and Slice Engineering Mosquito hotend (Gainesville, FL, USA) with E3D V6 steel nozzles; all the PTFE tubing used was Capricorn PTFE tube.

The Slicer used for the G-code generation was PrusaSlicer (V 2.7.0), and the non-adjusted parameter list can be seen in the appendix.

Before the specimen printing took place, the following calibrations were carried out to ensure the best results possible for every material used:

- Extrusion multiplier [68]
- Retraction length [69]
- Retraction speed [69]
- Resonance compensation [70]
- Pressure advance [71]
- Skew correction [72]

These calibrations are essential for ensuring the best possible material deposition available; for example, the Pressure advance calibration calculates the amount of material being deposited based on chamber pressure inside the hot end, which gives better results than the approach that other printers use [73].



FIGURE 3.1: Rat Rig V-Core 3 modular FDM 3D printer [10]

During the experimental work, 3 types of filaments were used, these being eSUN ePA 6/66 nylon or Polyamid blend (as a mixture of nylon 6 and nylon 66 polymers, as stated by the manufacturer), unreinforced, chopped glass fiber reinforced (25 wt%), and chopped carbon fiber reinforced (20 wt%) of 1.75 mm diameter. It was manufactured by Shenzhen Esun Industrial Co., Ltd. (Shenzhen, China), which has a reputation for its great performance/cost ratio.

Due to the hydrophilic nature of nylon filaments, they were dried at 70 °C for 24 hours before printing, and they remained in it during the whole process of 3D printing in order to negate

any moisture absorption of the nylon matrix [74], [75]. The main properties of the filaments can be observed in Table 3.1 [76], Table 3.2 [77], and Table 3.3 [78].

TABLE 3.1: The properties of the carbon fiber-nylon filament measured through injection molded specimens provided by the manufacturer

Properties	**Testing method**	**Typical value**
Density	GB/T 1033	1.24 (g/cm^3)
Melt flow index	GB/T 3682	11.46 (275 °C/5 kg)
Tensile strength	GB/T 1040	140 (MPa)
Elongation at break	GB/T 1040	10.61 (%)
Flexular strength	GB/T 9341	140 (MPa)
Flexular modulus	GB/T 9341	4363 (MPa)
IZOD impact strength	GB/T 1843	18.67 (kJ/m^2)
Heat distortion temperature	GB/T 1634	155 (°C, 0.45 MPa)

TABLE 3.2: The properties of the glass fiber-nylon filament measured through injection-molded specimens provided by the manufacturer

Properties	**Testing method**	**Typical value**
Density	GB/T 1033	1.35 (g/cm^3)
Melt flow index	GB/T 3682	1.45 (220 °C/2.16 kg)
Tensile strength	GB/T 1040	76.93 (MPa)
Elongation at break	GB/T 1040	20.07 (%)
Flexular strength	GB/T 9341	77.75 (MPa)
Flexular modulus	GB/T 9341	1714.63 (MPa)
IZOD impact strength	GB/T 1843	14.68 (kJ/m^2)
Heat distortion temperature	GB/T 1634	120 (°C, 0.45 MPa)

TABLE 3.3: The properties of the unreinforced nylon filament measured through injection-molded specimens provided by the manufacturer

Properties	**Testing method**	**Typical value**
Density	GB/T 1033	1.12 (g/cm^3)
Melt flow index	GB/T 3682	12.3 (230 °C/2.16 kg)
Tensile strength	GB/T 1040	52.45 (MPa)
Elongation at break	GB/T 1040	175.32 (%)
Flexular strength	GB/T 9341	58 (MPa)
Flexular modulus	GB/T 9341	1370 (MPa)
IZOD impact strength	GB/T 1843	18.4 (kJ/m^2)
Heat distortion temperature	GB/T 1634	50 (°C, 0.45 MPa)

3.1.1 Investigated parameters

Previous tests showed that the behaviour of the used materials was more predictable when printing was done with only walls or only 100% infill due to the more homogeneous nature of end products. In real-world applications, horizontal and vertical perimeters (walls) as well as a low percentage of infill must be used to ensure objects' dimensional accuracy and a favorable strength-to-weight ratio. The inclusion of these 3 structure types skewed previous tests, as the different specimens all shared the same horizontal and vertical shell. Thus, from an investigation standpoint, the perimeters of a 3D-printed object make it more difficult to measure the impacts of parameters, so only the homogeneous structure types were examined. The four investigated parameters were the following:

- Printing temperature (temperature of the printing head)
- Nozzle diameter
- Layer height
- Infill orientation

Furthermore, the nozzle diameter and layer height were later merged into a single virtual parameter as a way to measure the amount of material extruded in a single line.

All the parameters used can be observed in the config text file in the appendix, which contains more than 320 parameters used during printing but not changed except for the 4 investigated parameters.

3.1.2 Tensile testing

The tensile strength tests were conducted on an INSTRON 3385H universal testing machine (250 kN) with a 5 kN static load cell that made the measurements much more precise for forces that arise during the testing of the specimens. Additionally, a distance of 40 mm between the clamps and an extension rate of 2 mm/min has been chosen. Specimens that were mainly used in this dissertation were ASTM D638 type V (Figure 3.2) and their modified versions due to their smaller size. The elongation was measured through the testing machine's internal testing head displacement, as the small sizes of the specimens did not allow for the placement of an extensometer and the forces that arose during testing were small enough that they would not contribute to any problem.

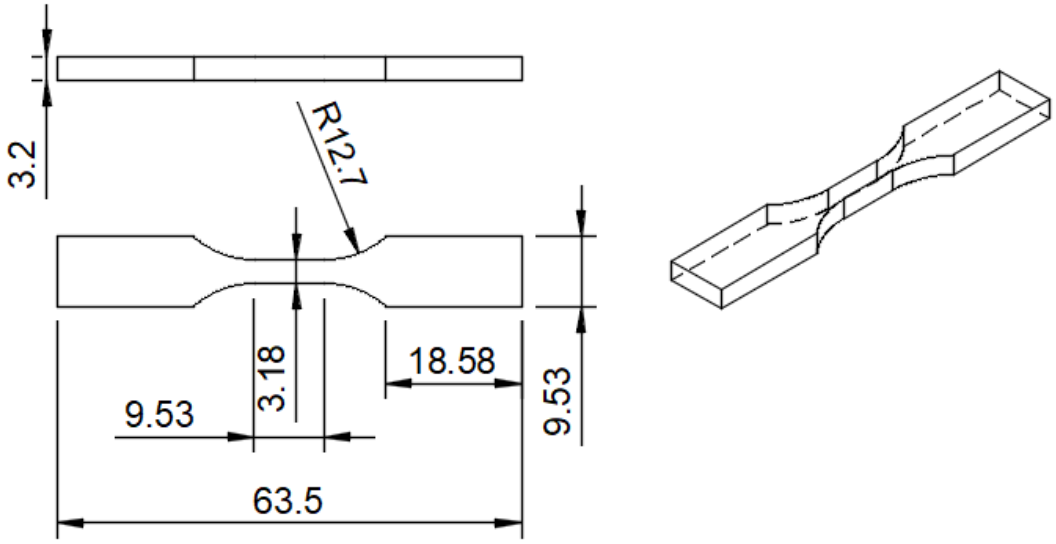


FIGURE 3.2: ASTM D638 type V tensile testing specimen

3.1.3 Scanning electron microscopy

The investigation of different characteristics of the fracture surfaces was done by an FEI/ThermoFisher Apreo S LoVac scanning electron microscope (SEM)(Brno, Czech Republic). The

length of chopped glass fibers was measured with it; prior to it, the nylon matrix of the reinforced filament was burnt away, so the individual glass fibers were exposed entirely. It was done in a Nabertherm 30-3000 furnace at 700 °C with a 5 °C/min heating rate and 1 hour dwell time, and the exposed glass fibers were then placed onto a sample holder manually. The diameter of the fibers varied between 10 and 15 µm, and their length could reach up to 475 µm (3.4), which is not only comparable to the diameter of the nozzle used (400 µm) but exceeds it. A distribution of the fibers across the cross-section of the filament can be seen in Figure 3.3.

Furthermore, images after tensile testing have also been made to determine that the glass fibers have sufficient bonding with the nylon matrix; such images can be seen in Figure 3.5.

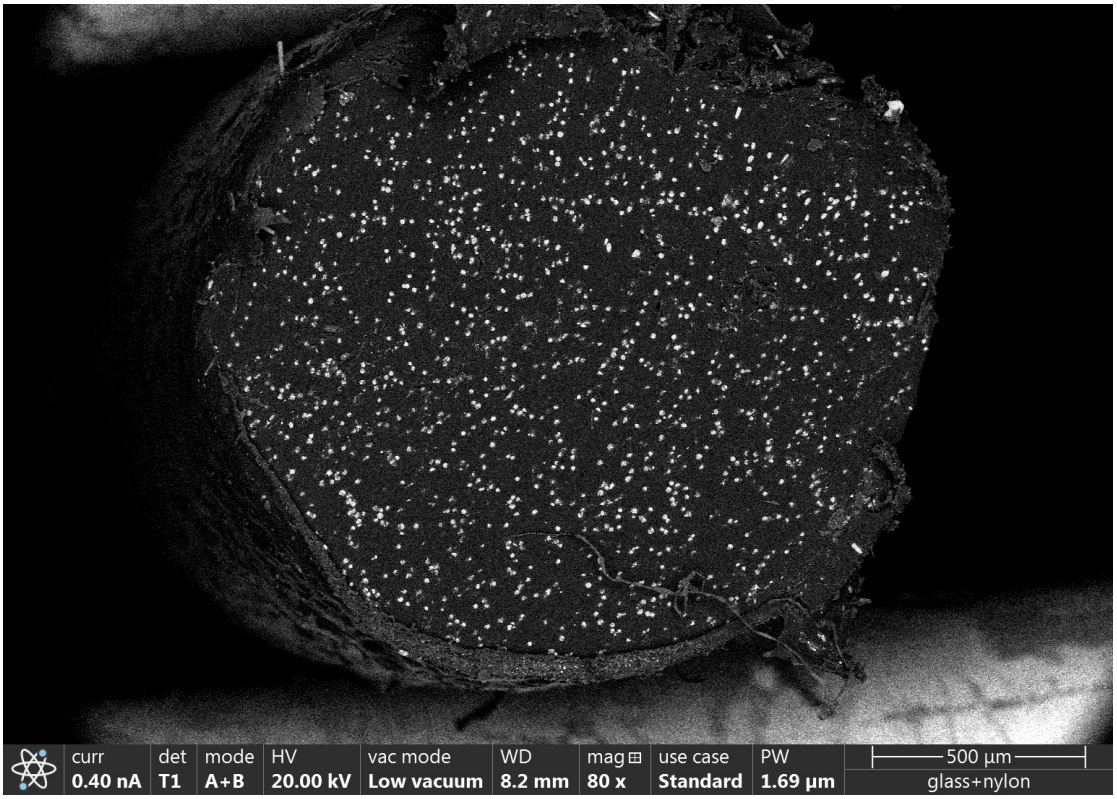


FIGURE 3.3: SEM image of the distribution of the chopped glass fibers inside the filament

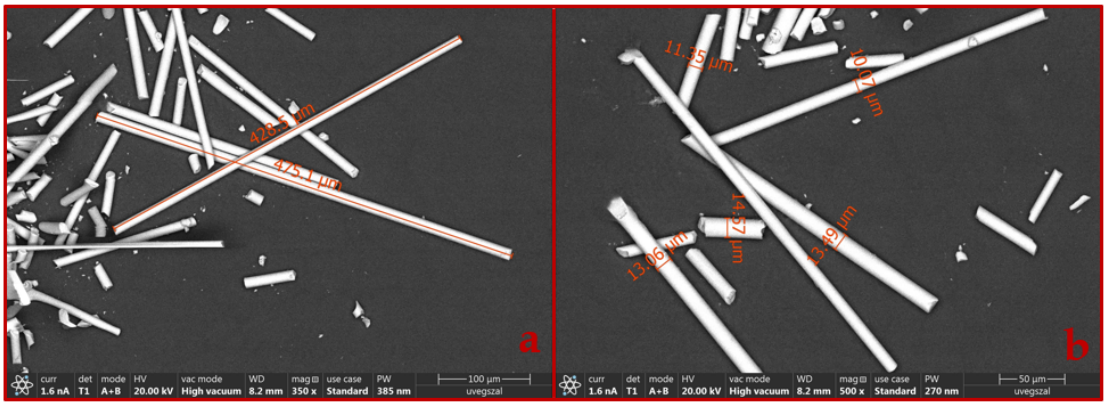


FIGURE 3.4: SEM images of reinforcing chopped glass fibers after the plastic matrix has been burnt away, with their length (a) and width (b) measured

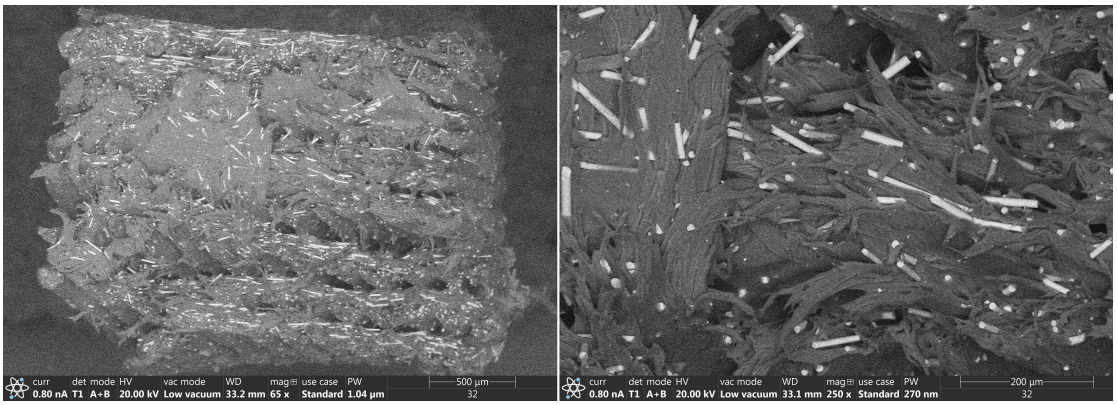


FIGURE 3.5: SEM images of reinforcing chopped glass fibers inside the nylon matrix after breakage

3.1.4 Computed tomography

Nikon XT H 225 ST X-ray computed tomography (CT, Tokyo, Japan) was used for the porosity and fiber orientation analysis. The sample's porosity was analysed with the VGStudio Max Porosity/Inclusion Analysis module, while the fiber orientation analysis was carried out by the VGStudio Max Fiber Composite Material Analysis module. The fibers are oriented in the direction of extrusion by the flow of the polymer, meaning that the orientation of fibers can be adjusted with infill orientation. Figure 3.6 shows the orientation map of the fibers inside individual extruded lines, where red means the parallel orientation of fibers with the plane of the image, blue means a perpendicular orientation of fibers with the plane of the image, and green means an orientation between the two. The mostly blue and green parts are cross-sections of multiple extruded lines, while the mostly red and green parts are along the axis of three separate extruded lines.

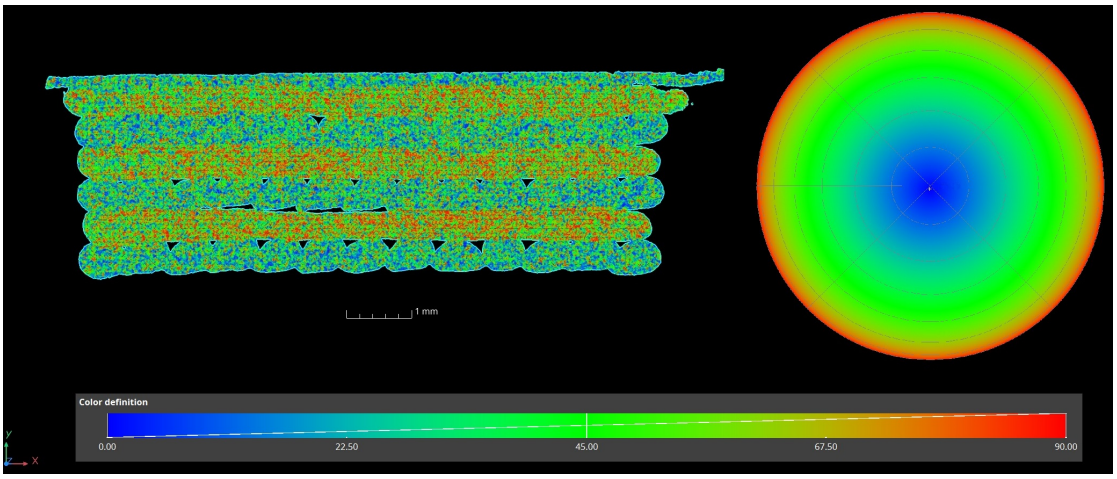


FIGURE 3.6: The orientation of fibers inside individual extruded lines at a cross-section of a sample

The porosity of particular samples was also measured with computed tomography; these showed a well-defined porosity system built up from the cavities that can be found between extruded lines and follow the direction of the line (Figure 3.7).

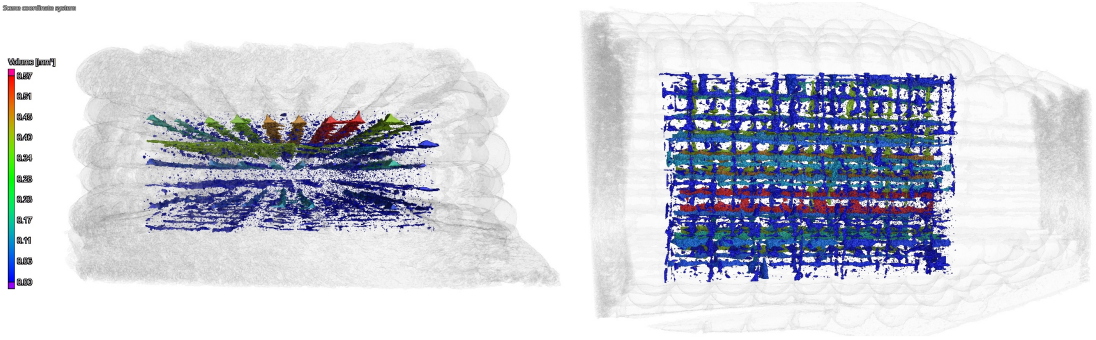


FIGURE 3.7: CT image of the porosity system of a 3D printed sample

3.1.5 MATLAB

For data processing and analysis, I used MATLAB R2023a. Complex visualizations were also carried out in MATLAB:

- complex tensile testing figures,
- Pearson coefficient matrices,
- model fitting figures,
- contour plots of the model fitting results.

Where the capabilities of MATLAB were not needed, simple visualizations of test values were created in Excel.

Chapter 4

Inquiry into the effect of specimen size and geometry on tensile strength

In this chapter, I will review the chief reasons why the problem of specimen size and geometry arose and showcase studies that suffer from the lack of consideration between different specimen sizes. The standardised specimen geometries were created for the purpose of tests being comparable; however, they differ depending on the material group and property being analysed. Usually, researchers in the additive manufacturing field use dog-bone-shaped specimens of varying size and shape. Based on the fact that widely used extrusion 3D printing processes inherently have a structure that is made up of extruded lines of various shapes and sizes (chiefly influenced by the nozzle size being used and layer height). This chapter aims to determine the impact that specimen geometry and size have on the final tensile strength of a specimen.

One of the most widely used engineering materials, chopped carbon fiber reinforced nylon was used for this end, 4 main specimen groups were examined, these are the following: specimens containing only walls and specimens containing only infill printed with both a 0.4 mm and 0.8 mm nozzle (to determine that the size of the extrusion lines have any effect on the tensile strength with different specimen sizes) achieving a solid body with two different line structures that can be found in a 3D printed part, them being the vertical (walls) and horizontal shell (top/bottom layers) (Figure 4.1).

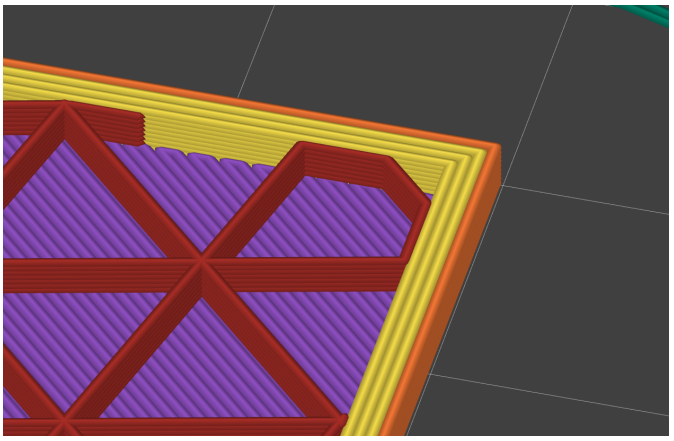


FIGURE 4.1: A common 3D printed structure with the 3 main line structures, yellow lines are walls (vertical shell), purple lines are bottom layers (horizontal shell), and red lines are infill lines.

4.1 3D printing process

To create a variety of specimen sizes and geometries, simple scaling of the ASTM D638 Type V tensile bar has been done with the same gauge length (Figure 4.2 and Table 4.1); during testing, none of the specimens suffered breakage outside of the middle gauge section. The tensile test specimens were created using an extrusion 3D printing process; the material used in this chapter was exclusively the chopped carbon fiber reinforced PA6/PA66 blend. This chapter focuses on the two main load-carrying structures of 3D printed objects.

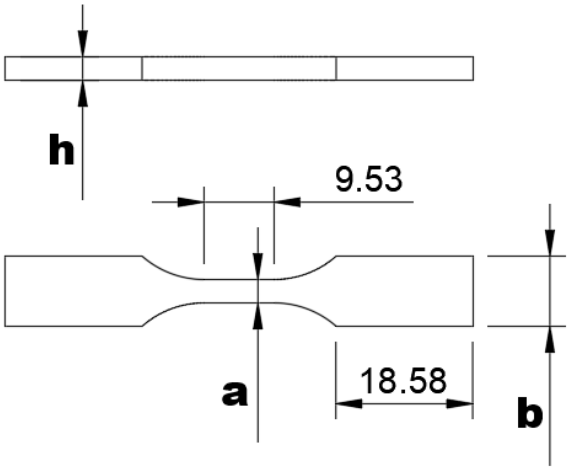


FIGURE 4.2: ASTM D638 type V tensile testing specimen with the 3 dimensions that have been changed

TABLE 4.1: The parameter set for the ASTM D638 type V tensile testing specimen resizing

h (mm)	**a** (mm)	**b** (mm)
3.2	1.59	4.77
6.4	1.59	4.77
3.2	3.18	9.53
6.4	3.18	9.53
12.8	3.18	9.53
3.2	6.36	19.06
6.4	6.36	19.06
1.6	12.72	38.12
3.2	12.72	38.12
6.4	12.72	38.12
3.2	15.9	47.65
3.2	19.08	57.18
6.4	19.08	57.18
3.2	22.26	66.71
3.2	25.44	76.24

One of these is the only infill group, in which the specimens only consist of alternating layers of parallel extruded lines, where the lines inside a particular layer are perpendicular to the neighbouring layer lines. This group represents the horizontal shells of a printed part, known also as top and bottom layers.

The other group is the only wall specimens, in which all the layers are identical to one another; this group represents the vertical shell of printed parts, also known as wall, wall lines, or wall loops. The main difference between these groups are the orientation of the chopped fibers, as the fibers inside the extruded lines naturally orient themselves in the direction of the print head movement ([18] and [79]), the only infill group is made up of layers where half of them are oriented in the direction of the tensile testing and the other half perpendicular to it as seen in Figure 4.3. In the only wall group, all the layers and extruded lines in them are oriented in the direction of the tensile testing.

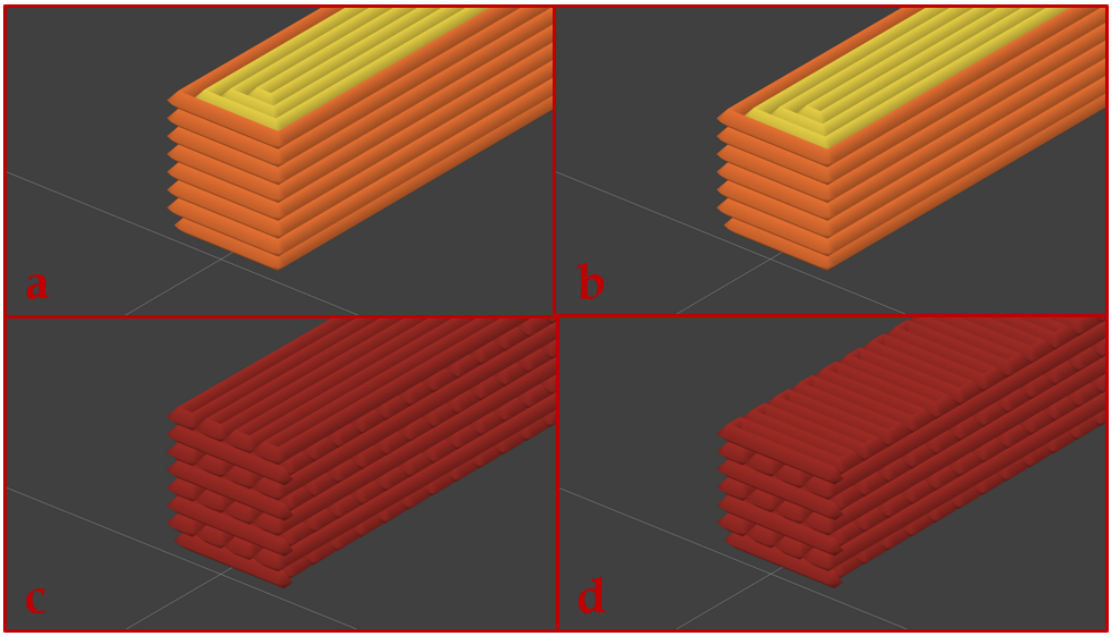


FIGURE 4.3: The visual representation between only wall specimens with their uppermost layer visible (a) and second uppermost layer visible (b), and only infill specimens with their uppermost layer visible (c) and second uppermost layer visible (d)

Furthermore, all the 3D printing parameters of the specimens were the same, except for the nozzle diameter and structure. The two nozzle diameters were the most widely used 0.4 mm and 0.8 mm nozzles, in order to determine if the nozzle diameter has any effect on the overall impact of the specimen geometry, as this parameter determines the size of the extruded lines a printed part is made up of. The two structures were the only infill and only wall structures already discussed above, both achieving a 100% solid part which is structurally homogeneous (almost exclusively, both of them have to be used for printing in real life, resulting in a heterogeneous structure [80]).

The width/height ratio of specimens ranged between a value of 0.22 and 8.5; their cross section area was between a value of 9.11 mm^2 and 120.27 mm^2, their layer count was between 4 and 32 and inside those layers, the extruded line count in parallel lines varied between 2 and 56. So the very low layer/extruded line count samples were also represented, which is important for composite structures as their behaviours can change in the lower ranges. For better understanding of the difference between sizes and geometries of the specimen groups, they can be seen after testing in Figure 4.4

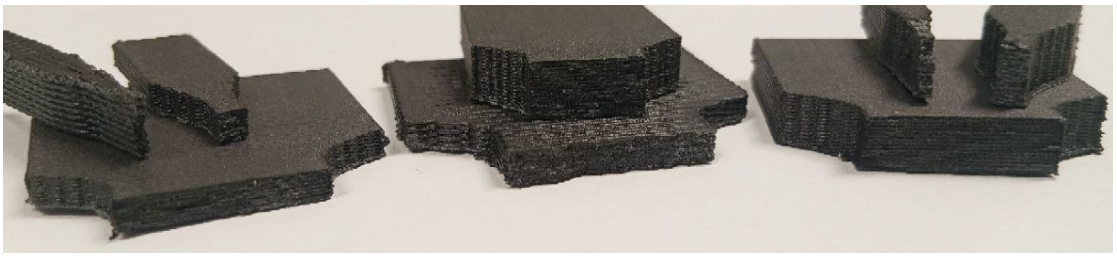


FIGURE 4.4: The visual difference in shape and size between individual specimens after tensile testing

The primary printing parameters were:

- 50% layer height (relative to the nozzle diameter)
- 0° infill orientation (relative to the direction of tensile testing, Figure 4.5)
- no top and bottom layer
- arachne perimeter generation [81]
- all printing speeds were set to 40 mm/s except the first layer for increased adhesion, which was 15 mm/s
- 250 °C printing temperature
- Part cooling disabled

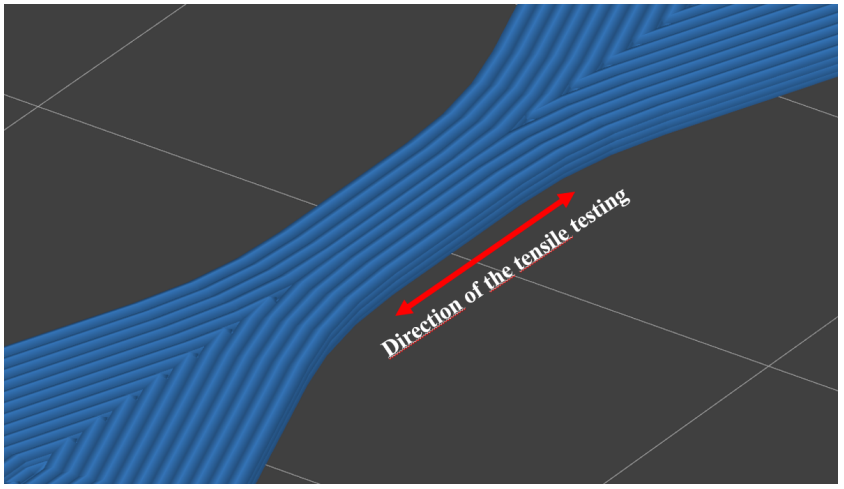


FIGURE 4.5: The relation between the infill orientation and tensile testing

4.2 Results

A special specimen group was also created in order to determine that the different porosities would yield different strengths; such a porosity system can be seen from different angles in Figure 4.7, which shows the middle section of a specimen where the breakage would occur. The special specimens were printed with a 0.4 nozzle and only infill (Table 4.2), with CT porosity analysis done before tensile testing. Figure 4.6 shows that the porosity had no effect on tensile strength in this 3-6 $vol\%$ range, keeping in mind that material deposition was calibrated beforehand for this exact reason, validating that the mentioned calibrations are a necessity.

Computed tomography results revealed that even with all the calibration done beforehand, the porosity of specimens could not be lowered below 1.5 $vol\%$, but in most cases the porosity was between 3-6 $vol\%$.

Figure 4.7 and 4.8 show the same specimen in 3D rendering and a 2D slice; the 3D rendering shows that the porosity system of a specimen runs through the whole middle section of a specimen like channels and has smaller spikes situated sideways where the voids of extruded lines intersect. From the 2D analysis in Figure 4.8, a directional porosity density can be observed; from left to right in the analysis corresponds with the specimen's top-to-bottom direction, showing an even distribution of porosity among the layers excluding the very bottom one, where the extruded lines are squished.

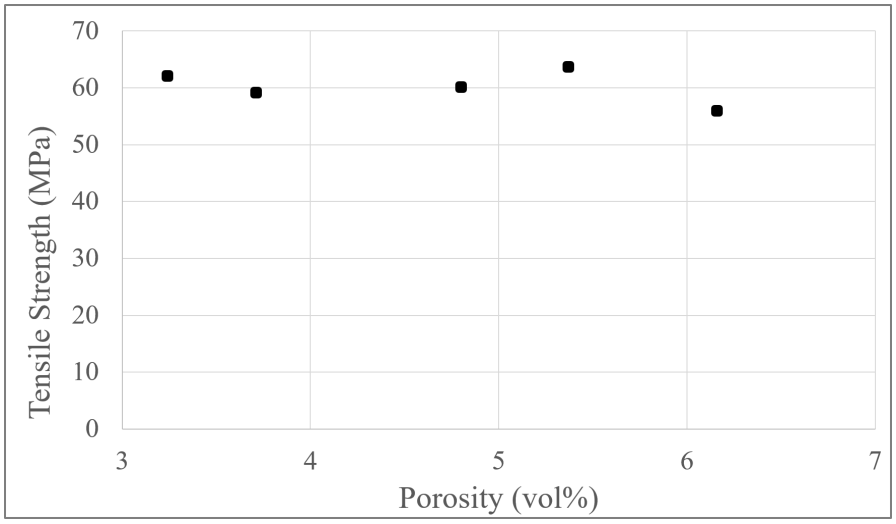


FIGURE 4.6: The tensile strengths of the pretest specimens compared by their porosity

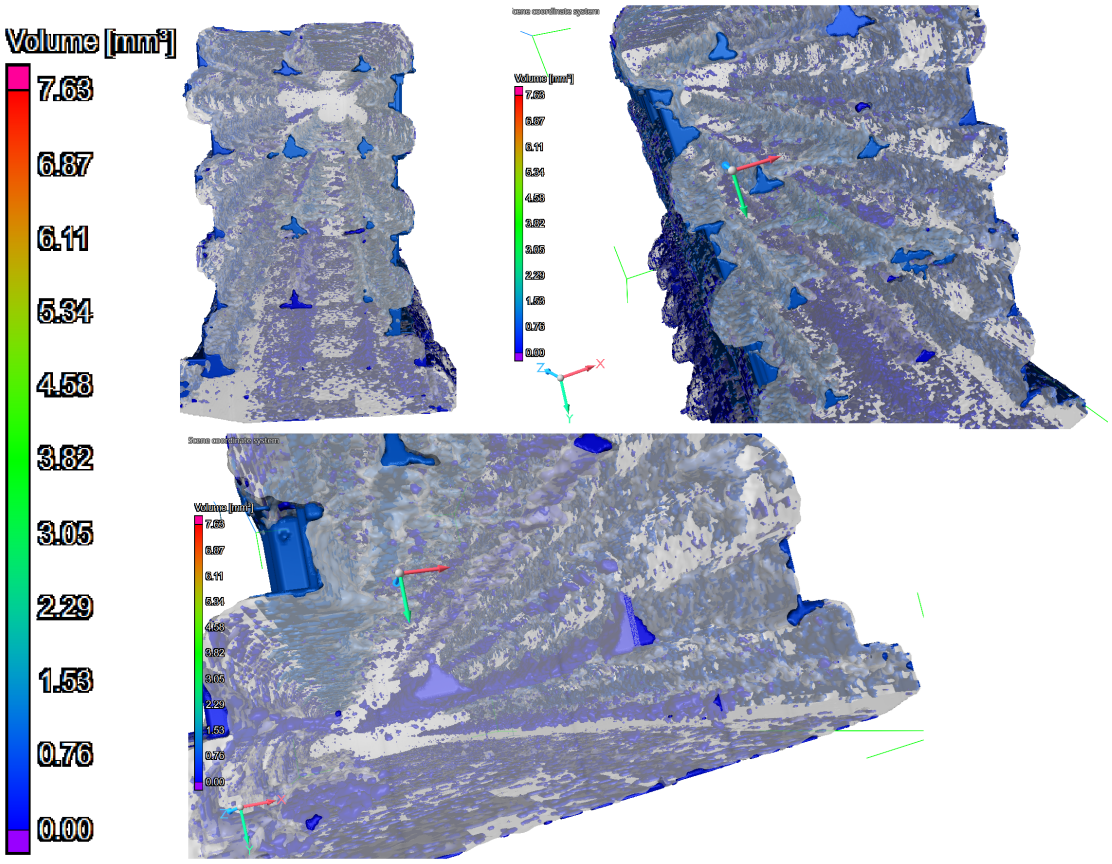


FIGURE 4.7: The porosity systems of an only infill specimen of the 0.53 Width/height ratio and 4.94 mm^2 cross section area group captured in the CT imaging software

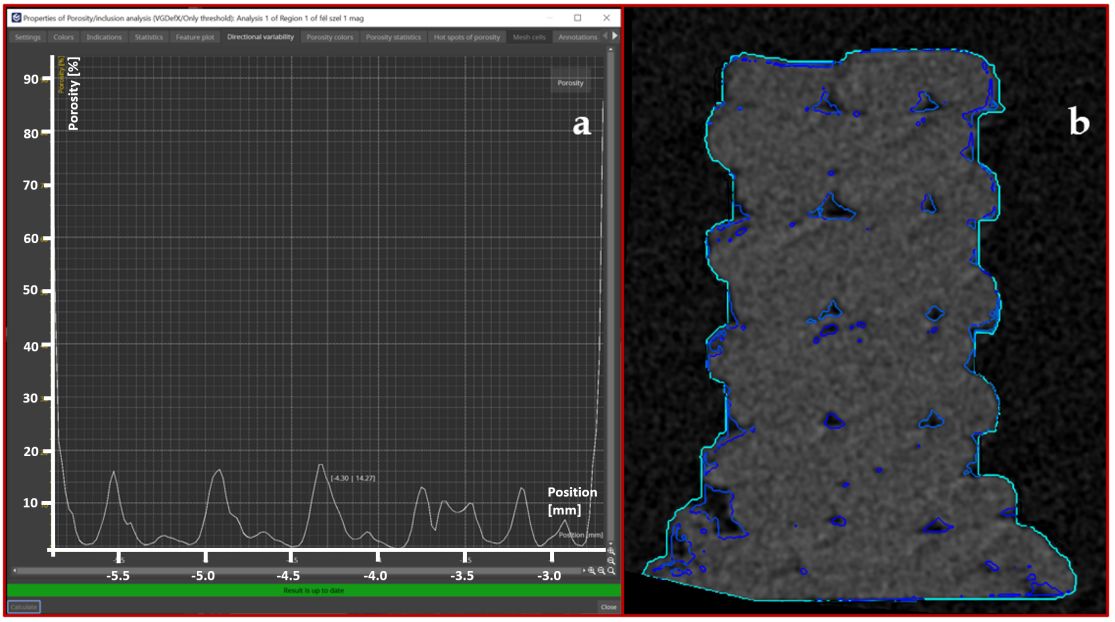


FIGURE 4.8: The directional porosity analysis (a) and its cross section (b) of an only infill specimen of the 0.53 Width/height ratio and 4.94 mm^2 cross section area group

TABLE 4.2: Tensile strength values for the porosity pretest groups

Width/height ratio (-)	**Cross section area** (mm^2)	**Tensile strength** (MPa)	**Tensile strength deviation** (MPa)	**Porosity** ($vol\%$)	**Porosity deviation** ($vol\%$)
0.50	18.42	60.11	3.63	4.80	1.61
0.53	4.94	55.92	0.90	6.16	1.43
0.96	8.94	63.70	5.97	5.37	1.48
2.06	19.00	62.10	6.13	3.24	0.63
2.24	4.02	59.14	7.81	3.71	1.15

The final 4 specimen groups were compared by their cross section area, width/height ratio, width/nozzle diameter, and height/layer height. The meaning behind these geometric parameters is the following:

- Cross section area indicates the overall bulk of a specimen.
- Width/height ratio indicates how the deposited material is distributed between layers and extruded lines inside of those layers.
- Width/nozzle diameter ratio simply corresponds to the number of extruded lines inside a layer which is perpendicular to the tensile testing.
- Height/layer height ratio gives the information of how many layers the specimens are made up from.

The final results in all 4 comparisons were very similar; some variation between the specimens was present, however the lack of trend inside of each specimen group as a whole is evident from the results listed below. The corresponding values can be seen in Figures 4.9 to 4.16, where each point represents the mean value of 4 specimens, except for a few groups where outlier values have been omitted when they showed a strength value <10% less than their group's mean value, as they definitely show some flaw in the 3D printing process. Furthermore, each of the 4 specimen groups can be seen with the exact values and tensile strength deviation in Tables 4.3 to 4.6.

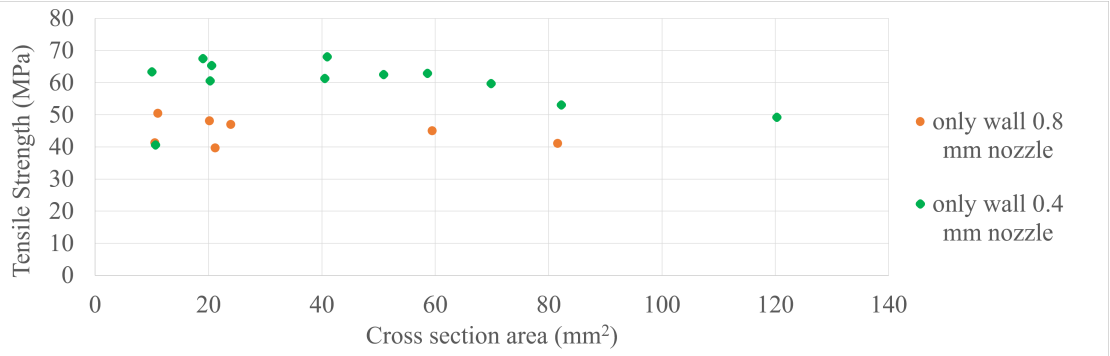


FIGURE 4.9: The tensile strengths of the only wall 3D printed specimens compared by their cross section area

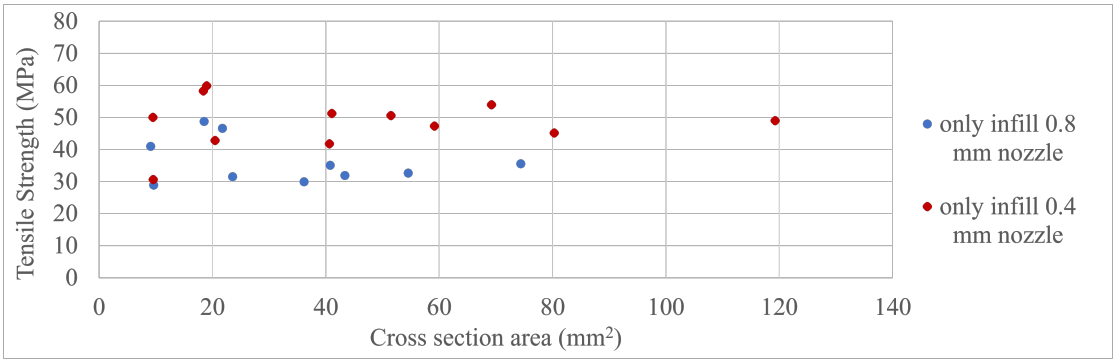


FIGURE 4.10: The tensile strengths of the only infill 3D printed specimens compared by their cross section areas

The 0.4 mm nozzle specimens in Figure 4.9 show a drop in strength after 60 mm^2 in cross section area; however, no other group showed such behaviour, and it is well within the deviation, so a conclusion cannot be drawn. Also, the 0.8 mm nozzle group in Figure 4.10 has 3 outliers in them, as they are 10-20 MPa stronger than the other ones with almost the same cross section area, the fact they are within the strength range of the 0.4 mm nozzle group further proves that they are outliers as the 0.4 mm nozzle specimens almost always fair better and have higher tensile strength than their 0.8 mm nozzle specimen counterparts. Calignano et al. [82] also investigated this material group from another manufacturer with 0.4 mm nozzle 100% infill samples with a tensile strength of around 45 MPa and cross section area around 10 mm^2, which are in line with the lower end of these types of specimens presented above. Blok et al. 2018 [83] had examined the same kind of material group and structure, albeit with a larger 41.6 mm^2 cross section area specimen geometry and presented a much lower 33.5 MPa tensile strength value. The difference between these strength values presented in this chapter and the aforementioned papers is most likely due to the numerous calibrations done beforehand listed in the previous section; the average tensile strength value for the 0.4

mm nozzle diameter and only infill specimen group was 50 MPa. The comparison by cross section area had been deemed the most important as it determines how many extruded lines a specimen is made up of, and the relation between specimen size and nozzle diameter can be more easily understood.

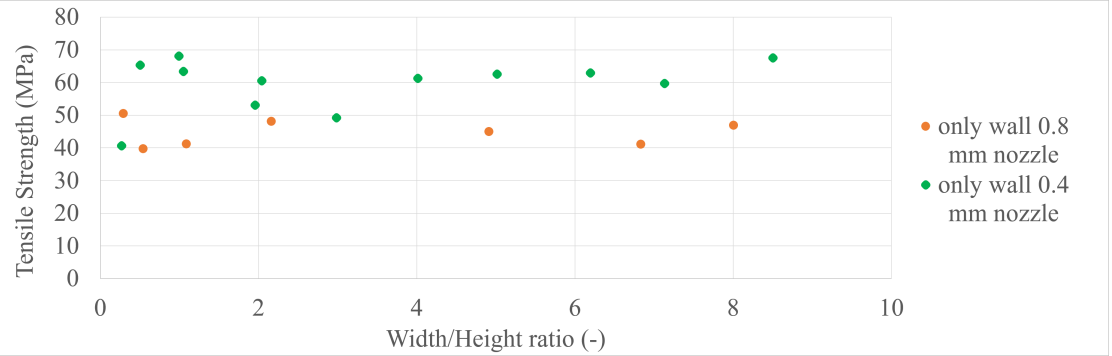


FIGURE 4.11: The tensile strengths of the only wall 3D printed specimens compared by their width/height ratios

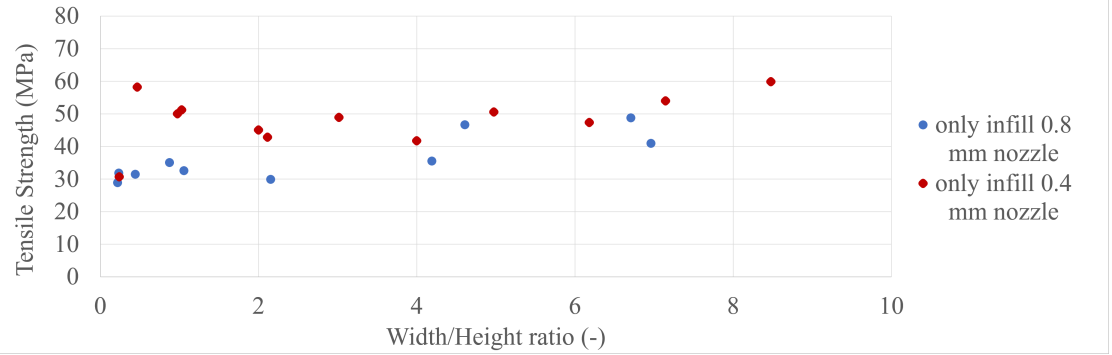


FIGURE 4.12: The tensile strengths of the only infill 3D printed specimens compared by their width/height ratios

In Figure 4.11, the 0.4 mm nozzle group seems to show a downward trend below a 4 width/height ratio; however, above it they settle around the 60 MPa mark, with a single outlier at around 0.25 width/height ratio. The 0.8 mm nozzle group again shows the 3 outliers at the last 3 values in Figure 4.12; they are again within the strength range of the 0.4 mm nozzle group.

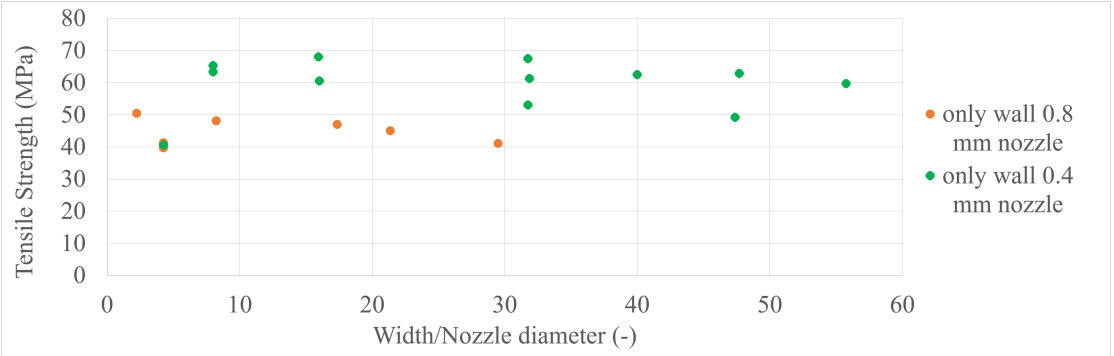


FIGURE 4.13: The tensile strengths of the only wall 3D printed specimens compared by their width/nozzle diameters

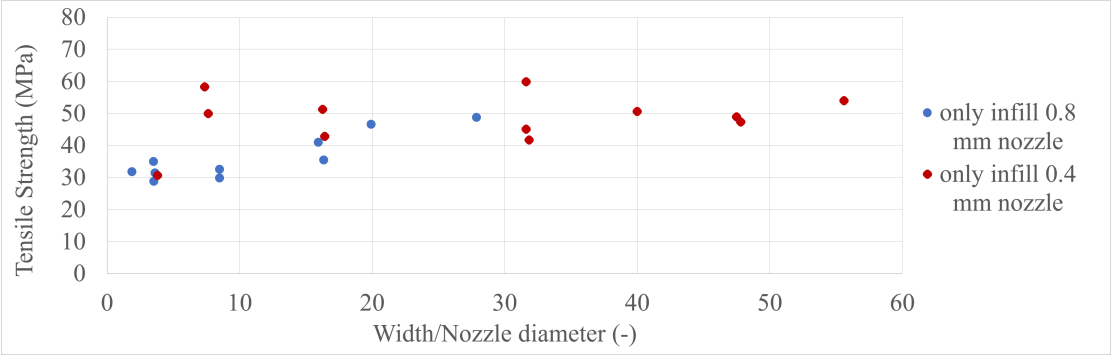


FIGURE 4.14: The tensile strengths of the only infill 3D printed specimens compared by their width/nozzle diameters

The comparison by width/nozzle diameter in Figure 4.13 and 4.14 shows more specimens with a single width/nozzle diameter, with the 0.8 mm nozzle only infill still having the 3 outliers separate.

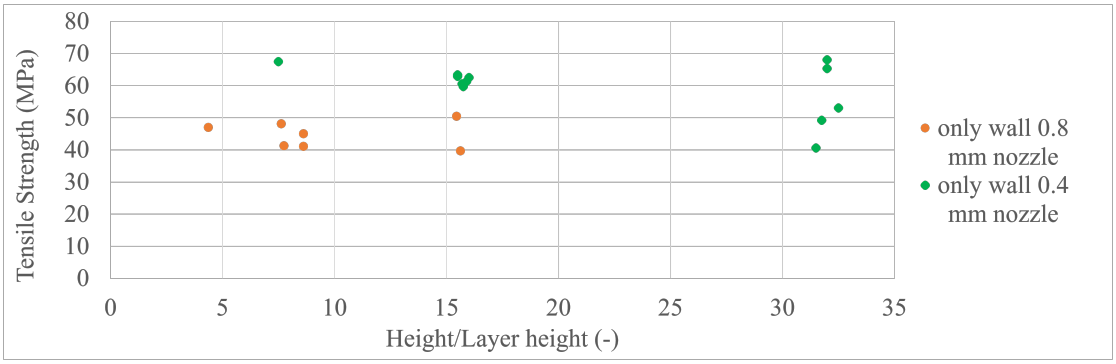


FIGURE 4.15: The tensile strengths of the only wall 3D printed specimens compared by their height/layer heights

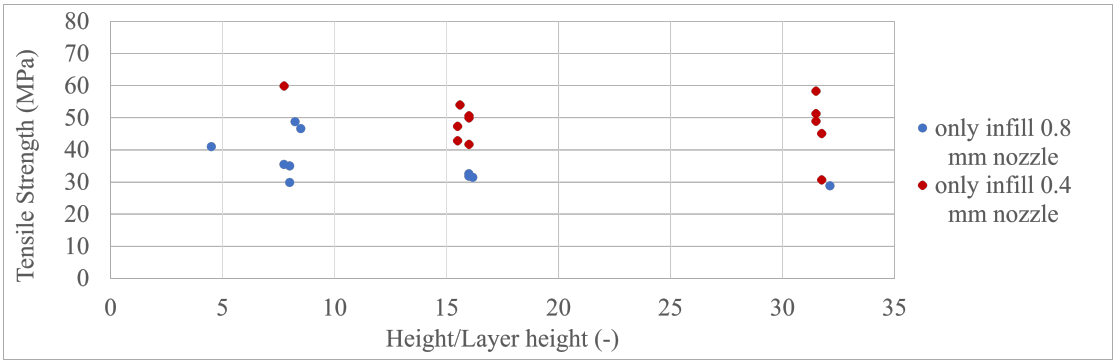


FIGURE 4.16: The tensile strengths of the only infill 3D printed specimens compared by their height/layer heights

The height/layer height comparisons (Figure 4.15 and 4.16), which again describes the number of layers a specimen consists of, have a more interesting content as the for both the only infill and only wall 0.4 mm nozzle groups show the same behaviour that the 3 main group gathered around the 8, 16, and 32 layer lines have a member which is among the highest strength values and the 32 layer line members have a greater spread than the 16 layer line members.

To further clarify that the above presented values have no trend in them, two individual sample groups can be observed in Figure 4.17 and 4.18 with their mean values as a solid line and deviations as dotted lines. None of these is included in the main text as the paired-up figures are already lengthy enough, so they are included in the appendix from Figure 7.1 to Figure 7.16.

Also, the porosity pretest samples were added to their specimen group, which was the only infill 0.4 mm nozzle group, to provide more data; the values can be seen in Figure 4.19 and Figure 4.20. The added data show that they are in line with the upper values of their group.

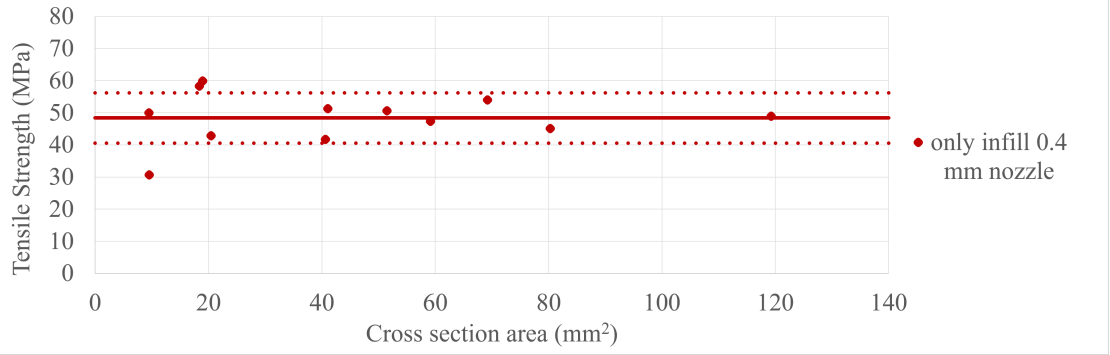


FIGURE 4.17: Individual specimen group with their mean value and deviations

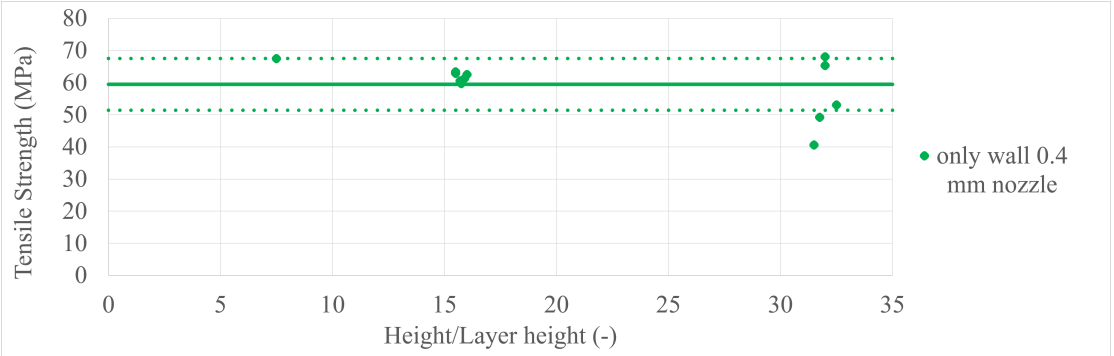


FIGURE 4.18: Individual specimen group with their mean value and deviations

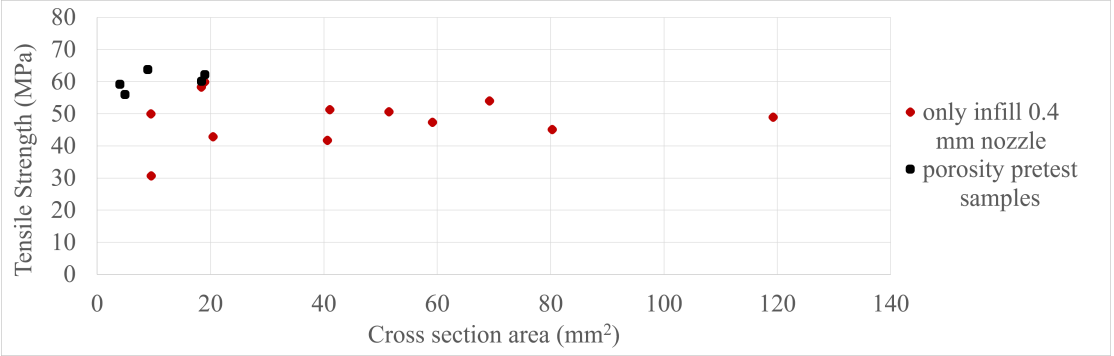


FIGURE 4.19: The tensile strengths of the porosity specimens included in their specimen group compared by their cross section area

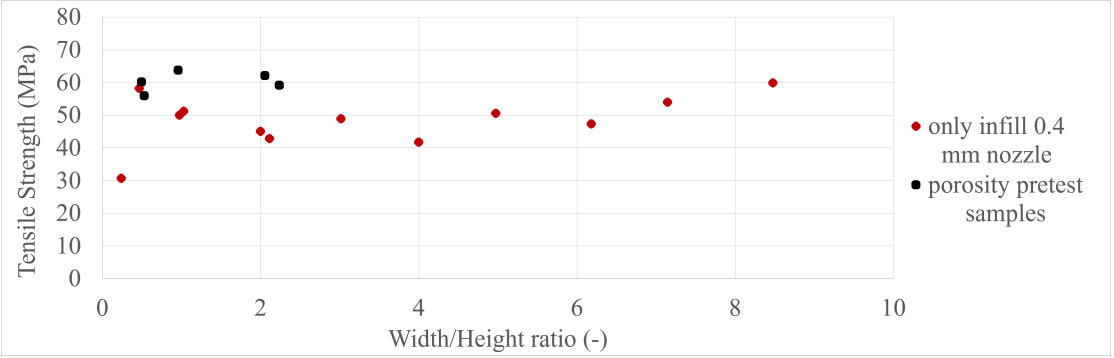


FIGURE 4.20: The tensile strengths of the porosity specimens included in their specimen group compared by their width/height ratios

The exact values can be seen in Tables 4.3 to 4.6 divided by the same groups as before. Almost all the tensile strength deviations are lower than 5% of their corresponding strength values, with some exceptions like the 10.99 MPa deviation in Table 4.3 and the 5.11 MPa deviation in Table 4.6.

TABLE 4.3: Tensile strength values for the only wall specimens printed with a 0.4 mm nozzle

Height/width ratio	**Cross section area**	**Tensile strength**	**Tensile strength deviation**
(-)	(mm^2)	(MPa)	(MPa)
0.27	10.66	40.62	2.13
0.50	20.58	65.33	2.37
0.99	40.93	68.03	1.77
1.05	10.03	63.39	10.99
1.96	82.23	53.04	0.84
2.04	20.27	60.49	1.66
2.99	120.27	49.21	3.83
4.02	40.52	61.25	2.18
5.02	50.91	62.52	3.92
6.19	58.62	62.92	1.23
7.13	69.86	59.71	0.49
8.50	18.99	67.48	0.53

TABLE 4.4: Tensile strength values for the only wall specimens printed with a 0.8 mm nozzle

Height/width ratio	**Cross section area**	**Tensile strength**	**Tensile strength deviation**
(-)	(mm^2)	(MPa)	(MPa)
0.29	11.10	50.47	2.67
0.54	21.18	39.69	0.74
1.09	10.54	41.21	2.36
2.16	20.17	48.11	0.55
4.91	59.46	44.99	3.67
6.84	81.60	41.06	0.53
8.00	23.95	46.92	1.18

TABLE 4.5: Tensile strength values for the only infill specimens printed with a 0.4 mm nozzle

Width/height ratio	**Cross section area**	**Tensile strength**	**Tensile strength deviation**
(-)	(mm^2)	(MPa)	(MPa)
0.24	9.54	30.67	0.25
0.47	18.37	58.26	1.74
0.97	9.49	50.00	1.96
1.03	41.06	51.26	1.37
2.00	80.29	45.10	0.65
2.11	20.44	42.82	2.72
3.02	119.26	48.96	2.91
4.00	40.60	41.76	1.81
4.98	51.47	50.60	4.41
6.18	59.13	47.33	1.52
7.14	69.24	53.96	1.83
8.48	18.94	59.86	0.78

TABLE 4.6: Tensile strength values for the only infill specimens printed with a 0.8 mm nozzle

Width/height ratio	**Cross section area**	**Tensile strength**	**Tensile strength deviation**
(-)	(mm^2)	(MPa)	(MPa)
0.22	36.20	28.84	1.24
0.24	9.63	31.84	2.22
0.44	18.53	31.44	0.86
0.88	9.11	34.99	1.62
1.06	43.35	32.55	1.71
2.16	21.75	29.85	3.32
4.19	40.80	35.49	5.11
4.61	54.54	46.59	0.26
6.71	74.39	48.72	0.43
6.96	23.56	40.95	0.84

To visually represent these deviations, all the values can be seen from Figure 4.21 to Figure 4.24. The group with the highest individual deviation value can be seen in 4.22, still covering most of the whole only wall 0.4 mm nozzle group's entire deviation.

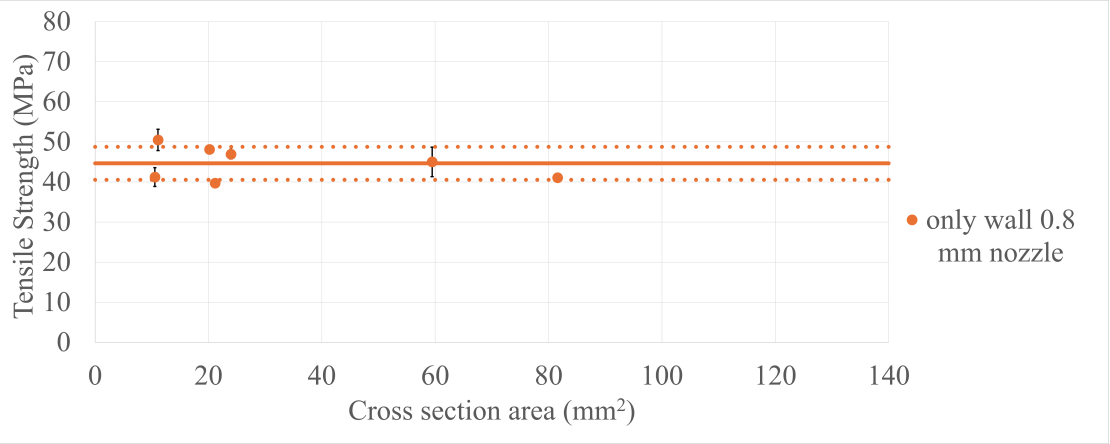


FIGURE 4.21: Deviations represented inside the only wall 0.8 mm nozzle specimen group with their mean value and deviation

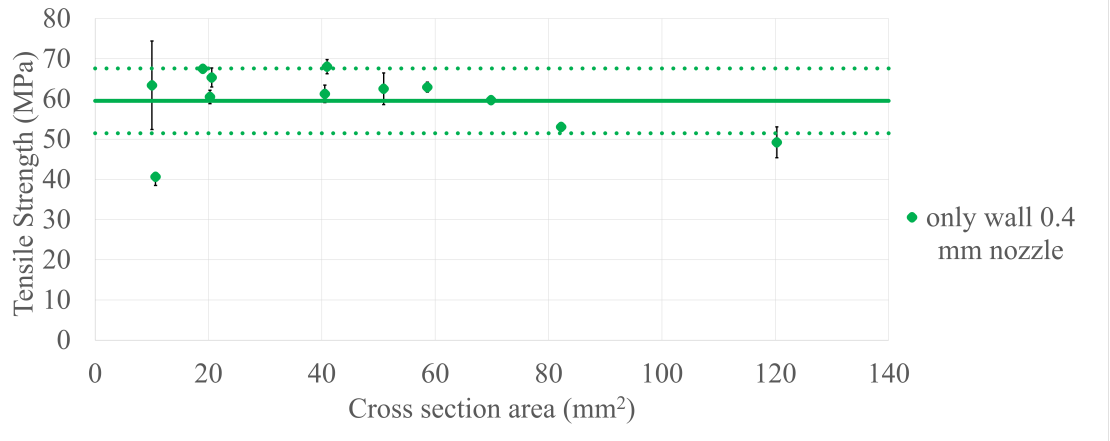


FIGURE 4.22: Deviations represented inside the only wall 0.4 mm nozzle specimen group with their mean value and deviation

Furthermore, the individual deviations are mostly insignificant and cannot even be seen in these figures.

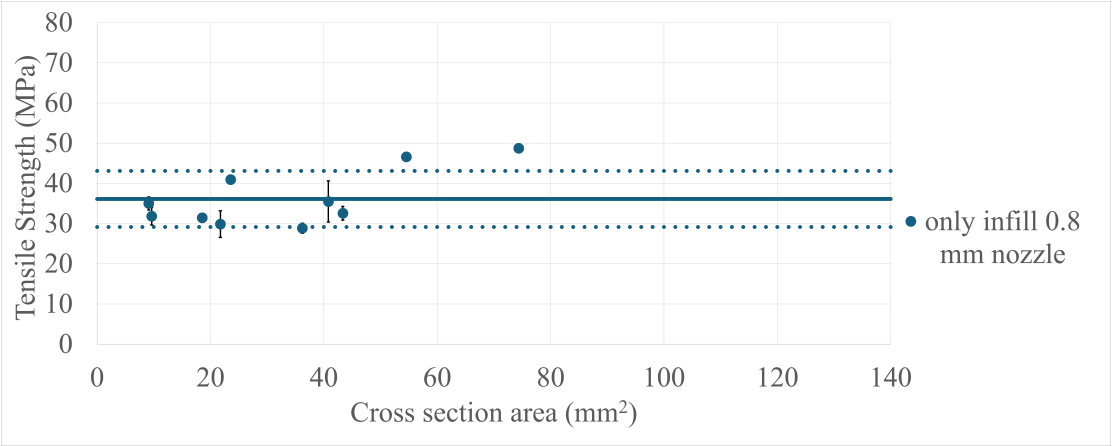


FIGURE 4.23: Deviations represented inside the only infill 0.8 mm nozzle specimen group with their mean value and deviation

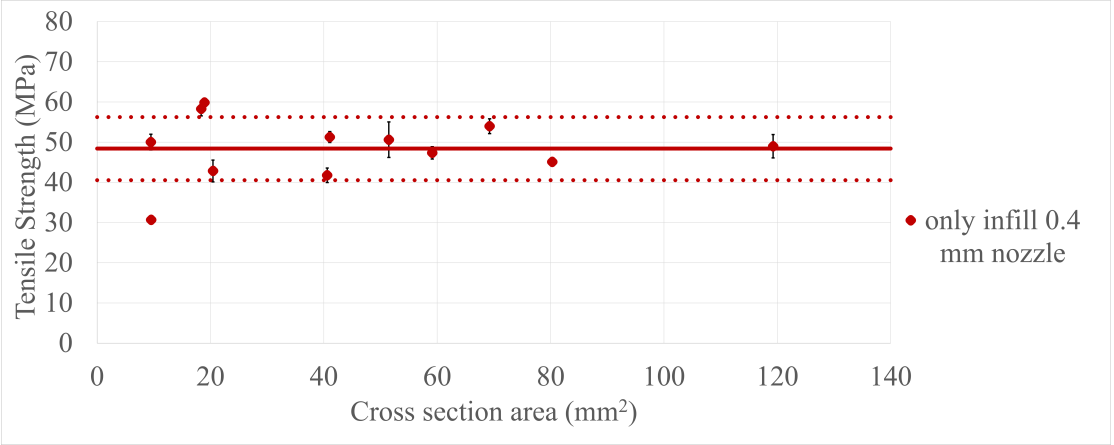


FIGURE 4.24: Deviations represented inside the only infill 0.4 mm nozzle specimen group with their mean value and deviation

The initial aim for these experiments was to determine the effect that the geometry of the various modified specimens has on the tensile strength based on the assumption that a body composed of numerous extruded lines of different sizes and shapes would be influenced by the shape and size of the lines that they are made of; however, the opposite case have been observed later during the evaluation stage.

All the 4 specimen groups studied showed the same behaviour, that the geometry and size of the specimen had not influenced the tensile strength; rather, the different specimen strength values were around their mean value and within their deviation. The difference between the two nozzle sizes and structures used (wall and infill, representing vertical and horizontal shells of a 3D printed object respectively) is quite clear from the presented figures. All of the 0.4 mm nozzle specimens showed higher tensile strength values than their 0.8 mm nozzle

counterparts, while all the specimens consisting of only walls consistently showed higher strength values than their counterparts consisting of only infills, typically in the range of 10-15 MPa.

While the only wall samples higher strength can be easily explained by the fact that in them all the extruded lines (and by extension all the embedded chopped carbon fibers) are parallel to the direction of tensile testing, while in the all infill samples it is only true for every second layer.

4.3 Conclusion

The conclusion can be drawn that the geometry and overall size of a 3D printed specimen has no influence on its final tensile strength, making the comparison between studies using different specimen types valid and warranted even down to very few layers and extruded lines inside a layer.

Furthermore, an additional observation had been made that the specimens consisting of only walls and 0.4 mm nozzle diameter showed greater tensile strength than their counterparts, only infill and 0.8 mm nozzle diameter, respectively. Therefore, the strongest group measured were the only wall 0.4 mm nozzle diameter group with a mean value of 60 MPa and a top value of 68 MPa.

Chapter 5

Investigation of the 3D printing process parameters and their effect on tensile properties

In this chapter, I introduce the main printing parameters commonly adjusted in slicers and the theories behind why someone would use different values for them instead of there being one "optimal" value. I will also show the not-so-scientific approaches and results of some prolific members of the 3D printing community and compare them with actual papers on the matter. After the introduction, I will present the investigation of the main process parameters I studied and the results obtained.

5.1 Main parameters of an extrusion based 3D printing process

First and foremost, the most important detail that will shape the parameters is the material being used, for example the most commonly used filament PLA is usually printed with a nozzle temperature of 200-230 °C, with a print speed of how swiftly a printer can melt/deposit material with sufficient cooling, that is one reason it is usually the choice for Speed Benchy challenges [84], while another material like PPS-CF, which is an engineering polymer containing a huge amount of crystalline phase, needs at least 320 °C to be printable and does not like to be printed fast, so a maximum of 5 mm/s printing speed is advisable (while PLA can reach 1000 mm/s easily).

Another huge deciding factor is the printing hardware one is using; a cheap commercial bed slinger 3D printer can't compete with a custom-built CoreXY one, neither in speed nor in temperature range. A lot of parameters are decided by the printer components one will use for printing; for example, if we want to print the above-mentioned PPS-CF but our printer hotend can only achieve the minimum requirement of 320 °C but cannot really go above it, the printing speed needs to be lowered for the layers to have more bonding time in that lower temperature range.

Lastly, the third factor that one needs to take into account is the properties of the end product, which is the main focus of the printing, be it strength, quality, cost, speed, or any kind of mix of these goals. The parameters need to be set according to the properties desired; for example, if we want to print only one instance of a sculpture, the strength, cost, and speed will not play a huge role in the parameter setting, while the quality of the surface will decide everything. This changes if we want to print a lot of these bodies; then the cost and speed start to play a bigger role in the decision-making depending on the desired outcome.

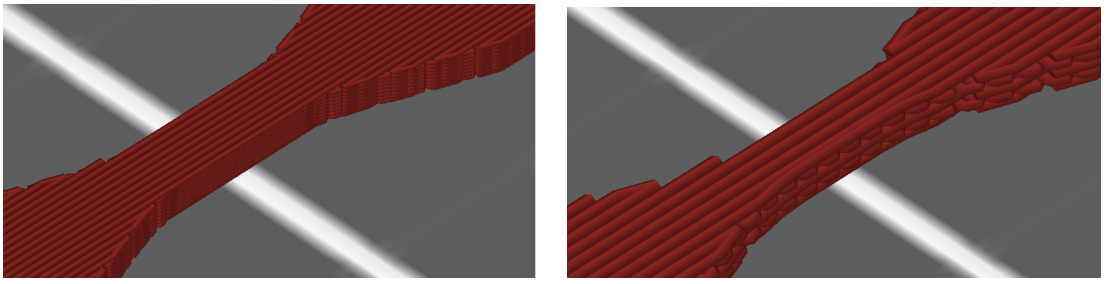
Another example is an engineering application of a certain machine component; then the strength usually plays the biggest role, while the cost and speed are dependent on the scenario, and lastly the quality is all but negligible.

For scientific research, the same principles apply, especially considering that most of the studies done in this field utilize a commercially available, often low-end 3D printer; the use of industrial machines is very limited mainly due to the fact that they are designed not to be adjustable by the end user.

Previous tests showed that the behaviour of the used materials was more predictable when printing was done with no wall, top, or bottom solid layers and infill only due to the more homogeneous nature of end products. In real-world applications, horizontal and vertical perimeters (walls) must be used to ensure objects' dimensional accuracy. However, from an investigation standpoint, the perimeters of a 3D-printed object make it more difficult to measure the impacts of parameters, so the horizontal shell had been omitted. The four investigated parameters were the printing temperature (temperature of the printing head), nozzle diameter, layer height, and infill orientation. Furthermore, the nozzle diameter and layer height were later merged into a single virtual parameter as a way to measure the amount of material extruded in a single line.

5.1.1 Nozzle diameter

The nozzle diameter is the only hardware-related parameter and can only vary based on the type of nozzle used. It is a deterministic dimensional parameter that mainly affects the amount of material that can be extruded and the number of extruded lines a body is made of across the XY plane (Figure 5.1). It mainly influences the printing process's speed and the surface quality of the end product.



(a) (b)

FIGURE 5.1: The difference between the extruded lines of (a) 0.4 mm nozzle diameter; (b) 0.8 mm nozzle diameter

5.1.2 Layer height

Similar to nozzle diameter, layer height is a dimensional parameter and mainly affects the geometry of extruded lines. The lower end of layer heights corresponds to a flat extruded line, while the higher end of it means an extruded line similar to the geometry of a squashed circle. It can play a role when air- or watertight products are being printed, as a flatter extruded line has more contact area with its downward and upward neighbors; also, similarly to the nozzle diameter, it influences the printing speed and surface quality of a printed object (Figure 5.2).

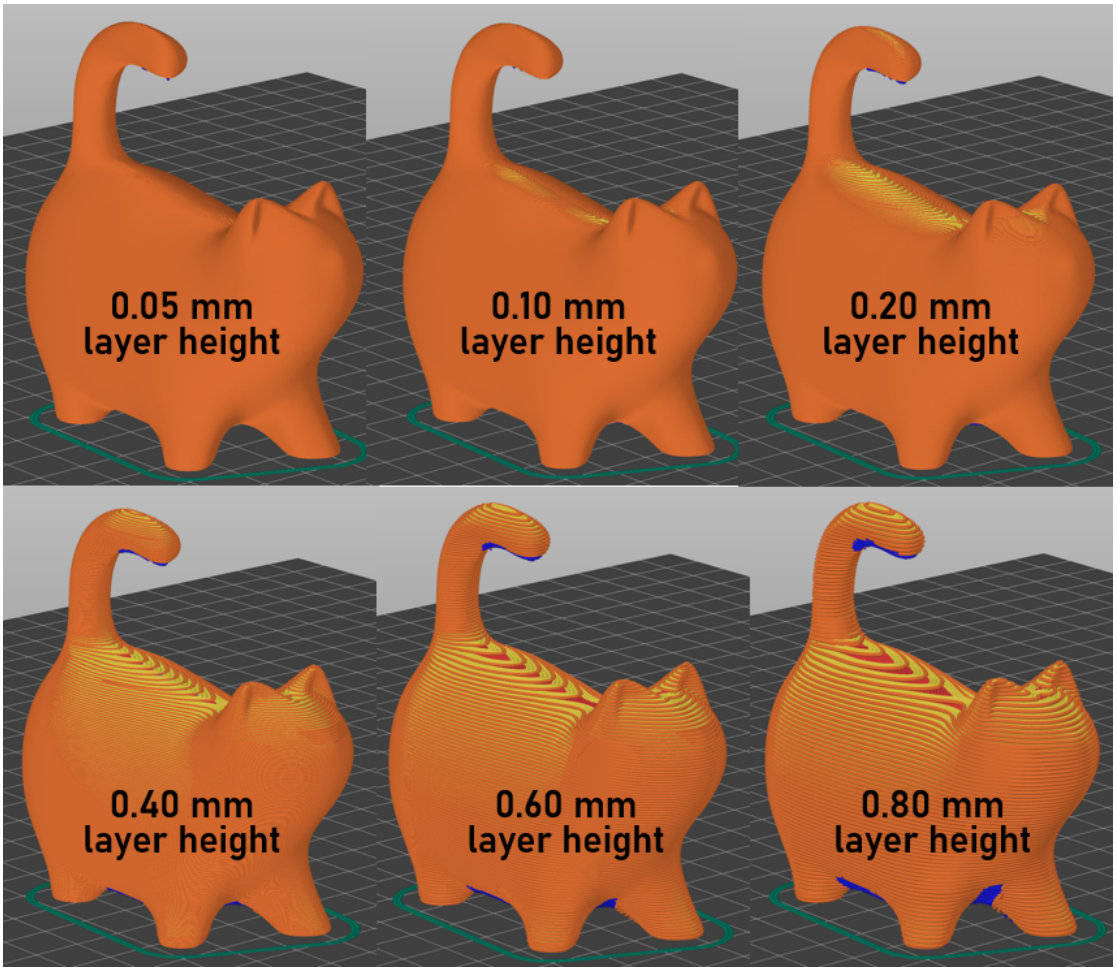


FIGURE 5.2: The difference between layer heights concerning the surface quality of a cat model

5.1.3 Extruded line cross-section area

During the evaluation of test results, the problem arose that the nozzle diameter determines the usable layer height range, and therefore these two parameters are not independent of each other. To ensure the independence of the investigated parameters, the nozzle diameter and layer height were incorporated into a new theoretical parameter called extruded line cross-section area or ELCSA, which is the product of nozzle diameter and layer height (Figure 5.3). The ELCSA simply shows the amount of material extruded in a single line. The difference between the theoretical and ideal ELCSA and the real life equivalent of it can be observed between Figure 5.3 and 5.4, showing how an extruded line looks like during the printing process after it leaves the nozzle, mathematically it is a square with the two sides

being exactly the nozzle diameter and layer height, however in reality it is much closer to a ellipsis.

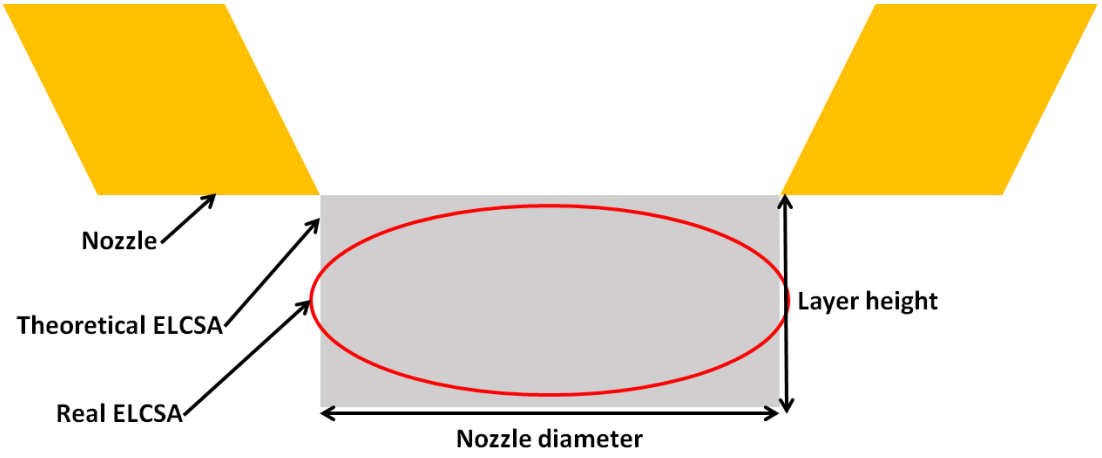


FIGURE 5.3: The correlation between nozzle diameter, layer height, real and theoretical ELCSA

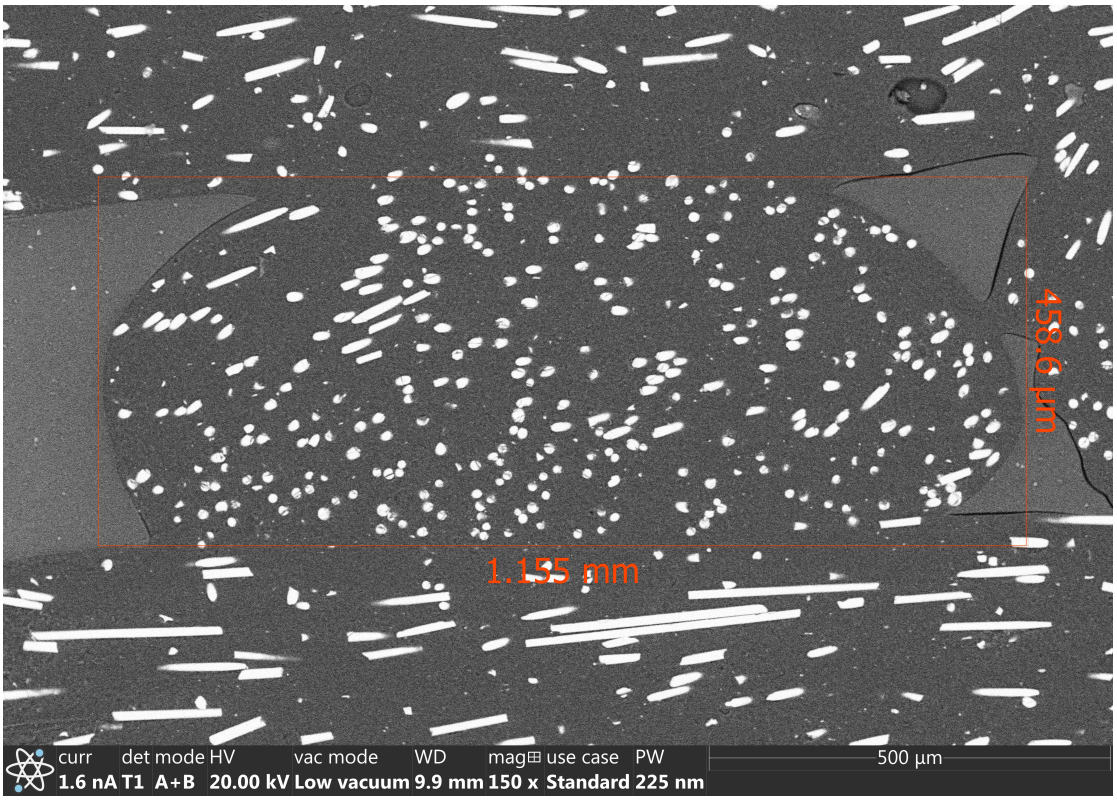


FIGURE 5.4: SEM image of ELCSA inside a 3D printed layer

5.1.4 Printing temperature

One of the most impactful factors in the final properties of 3D printed objects is the temperature of the nozzle, which contributes to the bonding of extruded lines. There is a general rule in FDM/FFF 3D printing that the lower end of the printing temperature range produces better aesthetic features but weaker mechanical properties, and the opposite is true for the higher end of the printing temperature range.

The used temperature is mostly determined by the material extruded; in the case of a nylon 6/66 blend, the usual printing temperature range is between 220-260 °C, and when they are reinforced with fibers, the temperature tends to be on the higher end. The printing speed or volumetric speed depends greatly on the temperature used, as to achieve higher printing and volumetric speed, the temperature also has to be higher, so the used default and maximum printing speed was 40 $\frac{mm}{s}$ and the maximum volumetric speed was 12 $\frac{\mathrm{mm}^3}{s}$ to ensure sufficient bonding even at lower temperatures. This parameter also influences a lot of factors, such as the printing speed, surface quality, strength, and ductility of the end product.

5.1.5 Infill orientation

Also known as raster angle in other slicer software, it determines the orientation of the parallel infill lines inside the 3D printed bodies. In the case of this study, 100 % infill was used exclusively in order to ensure the homogeneity of the samples. In the case of 100 % infill, the bodies build up from layers, and the layers build up from parallel extruded lines; these layers are stacked on top of each other perpendicular to the one below them. So an infill orientation of 0° also means orientation of +90°; due to this fact, the infill orientation can only be varied between 0° and 45°, where the 0° means that half of the number of layers (inside them parallel lines) rounded up are parallel to the axis of the samples and half of the number of layers rounded down are perpendicular to the axis of the samples, and 45° means that all of the layers and the extruded lines inside them are in a 45° orientation to the axis of the samples.

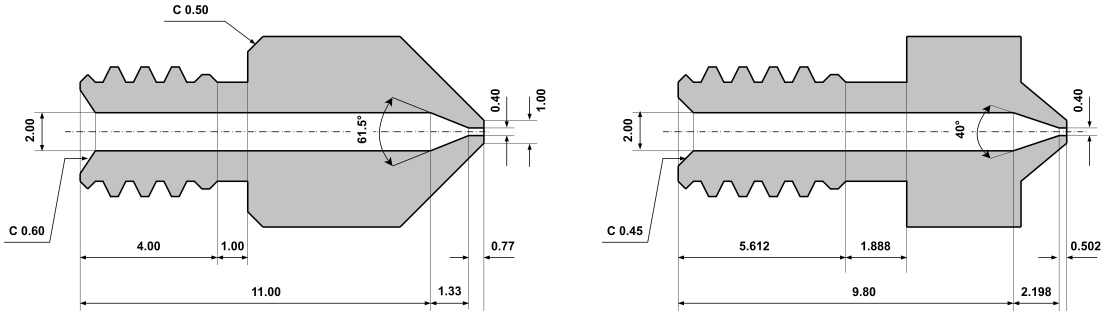
The unevenness of the layer counts means that if the number of layers is not an even number, the result of the 0° and 90° infill orientation could differ, but in most of the real-world applications, its significance is so low that it makes no sense to investigate this disparity.

TABLE 5.1: The parameter matrix of the specimens

Parameter value	**Nozzle diameter** (mm)	**Layer height** (%)	**Temperature** ($°C$)	**Infill orientation** (°)
Low	0.4	25	220	0
High	0.8	62.5	250/260	45

5.1.6 Nozzle types

During testing, two types of nozzles were studied in the case of glass fiber reinforced nylon, the first being the manufacturer recommended V6 style nozzle and the other being the widely available MK8 nozzle which, in theory, is too short (5 mm neck size instead of the V6's 7.5 mm) for the hotend used and a small gap between the bi-metal heatbreak and nozzle can be observed (Figure 5.5). However, the samples printed with this shorter MK8 nozzle did not show any visible flaws or printing artefacts, so their usage was also considered. Due to the fact that two nozzle types and different horizontal and vertical perimeter counts were studied and showed flawed behaviour and lower strength values, the sample number starts from 35 in the case of glass fiber reinforced nylon, which means that there were 34 probing test sample groups and 16 final sample groups, which can be observed in the specimen table included in the appendix Table 7.3 and 7.4. Since the MK8 nozzles were insufficient to print with the hotend used it had been omitted from further testing with the other two materials.



(a) (b)

FIGURE 5.5: The difference between the (a) MK8 nozzle and (b) V6 nozzle

To make the parameter matrix easier to understand, it can be seen in Table 5.1.

5.2 Tensile strength results

Because of the complexity of the mechanical property figures, the deviation of the values is presented in Tables 7.3 and 7.4, furthermore the figures have labels on top of them, which are duplicates of their text, to better differentiate between different materials, parameters, and mechanical properties as they are very similar in appearance and thus very hard to recognize what figure is being observed only by reading their description. The values presented below mainly try to demonstrate the different trends observable between different materials; their individual exact values also give important information; however, for the sake of focusing on the bigger trends, the individual values are not emphasized. For this reason, specific Y-axis scales are being used, which at first glance might seem misleading as they do not include the lower values such as under 40 MPa and under 2500 MPa for the tensile strength and Young's modulus, respectively. Furthermore, some of the figures include big empty spaces, such as Figure 5.13, where the values are between 2500 and 3500 MPa but the Y-axis scale is going up to 6000 MPa, there characteristics of the Y-axis scaling are to facilitate the ease of comparability across figures and to distinguish the differences between sample groups.

Also, the figures showing the two main mechanical properties are of high complexity, thanks to cramming as much information as possible into a single figure to further highlight the main trends being present in a whole specimen group. The main points that have to be taken into consideration when reading these figures are the following:

- ELCSA is being used as the X axis in order to show each group how much bulk their individual layers have.
- Same color means same printing temperature and infill orientation or the same material.
- Same marker type (triangle, square, circle) being linked together with a dotted line represents the same temperature, infill orientation, and nozzle diameter but different layer height.

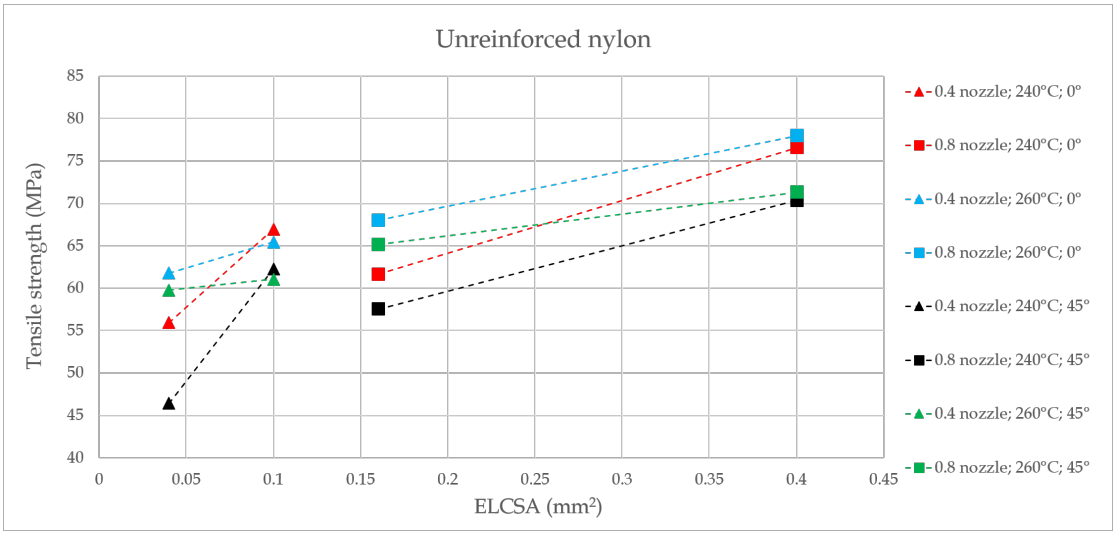


FIGURE 5.6: The change in tensile strength values of unreinforced nylon specimens based on different parameters

Firstly, regarding the unreinforced nylon (in later figures referred as N) specimen groups, on Figure 5.6 the different behaviour between low and high temperature prints can be observed (blue and green being high temperature, red and black being low) as both groups show a very similar change in tensile strength between the two layer heights (connected by a dotted line) for the 0.4 mm (left side of the figure with triangles) and 0.8 mm (right side of the figure with squares) nozzles. It can be said that higher layer heights yield better tensile strength in every specimen group for unreinforced nylon, going further for high temperature specimen groups the same can be said about ELCSA as well, every instance a higher ELCSA group yielded higher strength as well, while for the lower temperature groups this is not the case as the 0.4 mm nozzle and high layer height groups showed greater strength than the 0.8 mm nozzle and low layer height groups, which have larger ELCSA than the previous group.

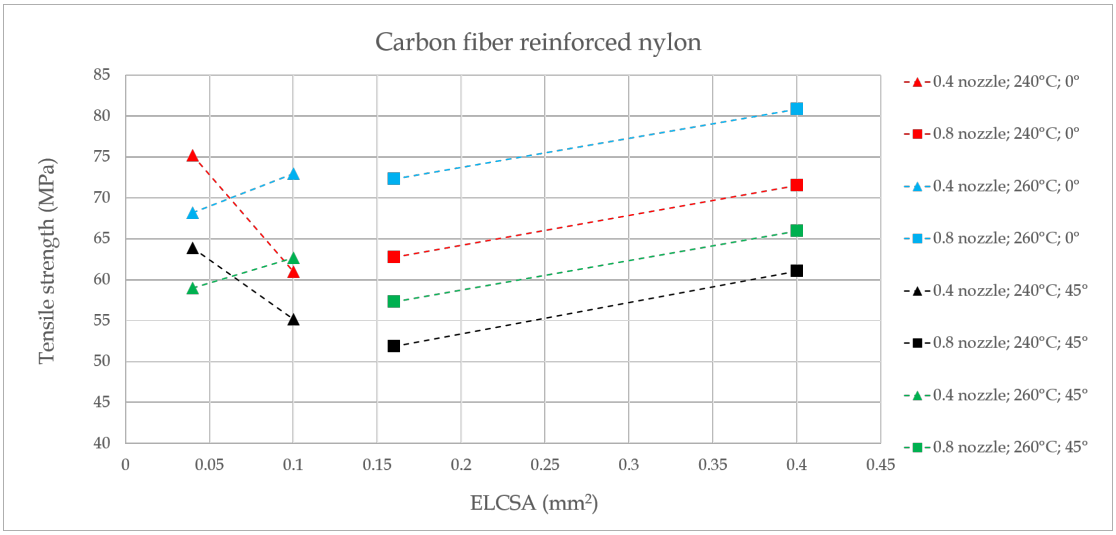


FIGURE 5.7: The change in tensile strength values of carbon fiber reinforced nylon specimens based on different parameters

The carbon fiber reinforced nylon (in later figures referred to as CFN) specimen groups showed similar behaviour to the unreinforced groups with a few changes (Figure 5.7). All 0.8 mm nozzle groups showed the same behaviour between different layer heights, as well as the 0.4 mm nozzle groups with high printing temperature; however, the low printing temperature specimens of the 0.4 mm nozzle group showed the opposite behaviour. Furthermore, not only is the effect of layer height different for the low temperature 0.4 mm nozzle specimens, but they also exceed the tensile strength values of their 0.8 mm counterparts, completely flipping the previous trends that higher layer height means a higher strength value. Also, for these low temperature carbon fiber-reinforced nylon groups, the lowest ELCSA value meant the highest strength values. The fact that the 0° groups outperformed their 45° counterparts regardless of temperature means that the infill orientation played the biggest role in the specimens' strength values.

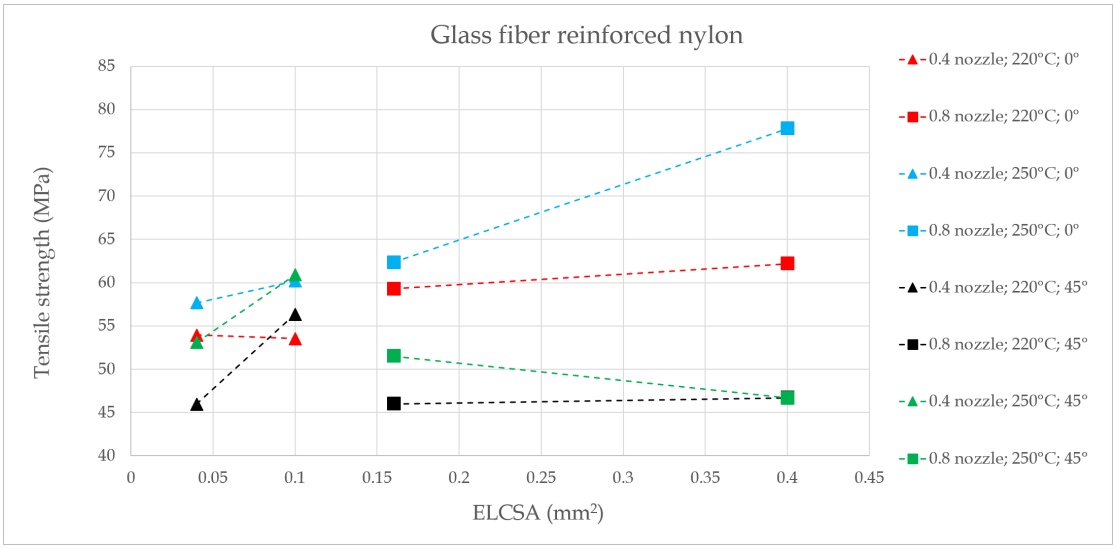


FIGURE 5.8: The change in tensile strength values of glass fiber reinforced nylon specimens based on different parameters

Lastly, the glass fiber reinforced nylon (in later figures referred to as GFN) specimens' behaviour was much more complex than the previous two (Figure 5.8). For starters, in the 0° oriented groups, a higher ELCSA was always paired with a higher tensile strength value, while the 45° oriented groups showed the complete opposite. Also, the layer height change trend inside a specimen group remains the same in each color for both nozzle diameters, except for the 0.8 mm nozzle, 250 °C, and 45°. However, this specific specimen group is an outlier (and the high layer height value in particular) not just among the other glass fiber reinforced nylon groups but in the others as well, which can be seen much more clearly below (Figure 5.9 and 5.10).

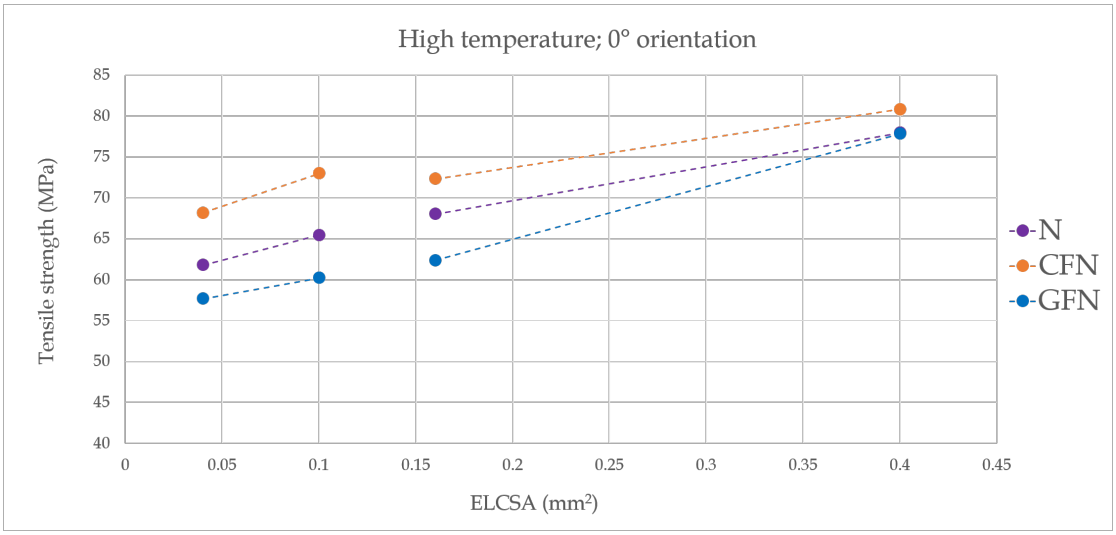


FIGURE 5.9: The change in tensile strength values of specimens printed with high temperature and 0° orientation

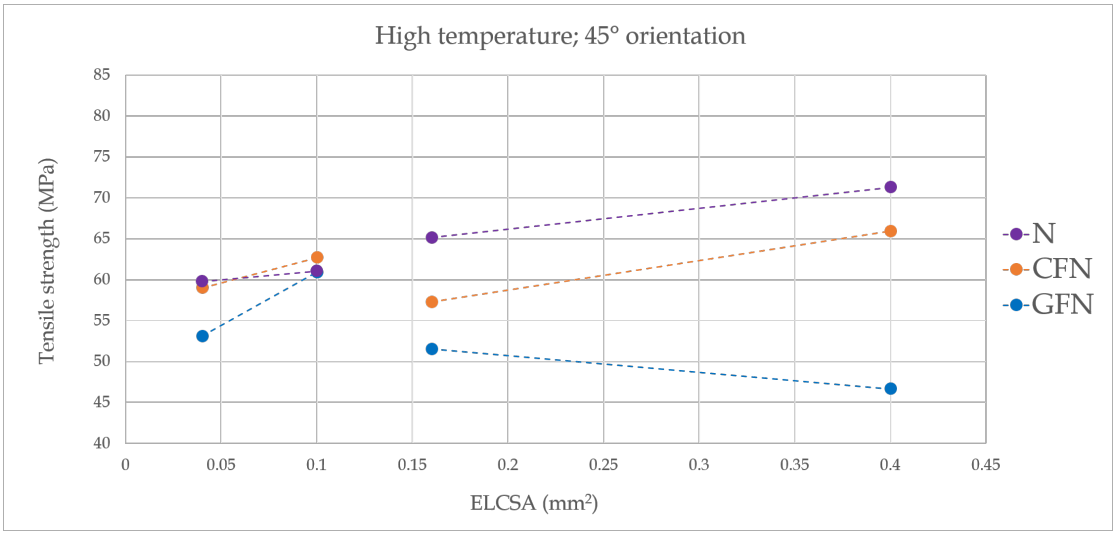


FIGURE 5.10: The change in tensile strength values of specimens printed with high temperature and 45° orientation

The results from the 3 materials highlight the trends they show when presented next to each other for the four major parameter groups (Figures 5.9 and 5.10), in particular the low and high temperature groups shown next to each other. Their behaviour is very similar in the same temperature range, with a few changes between different orientations.

All the high temperature specimens showed higher tensile strength with higher layer height, except the glass fiber reinforced nylon, 0.8mm nozzle, high temperature, and 45° oriented group, which was already distinguished in the previous paragraph. Also, the difference between different materials is lower for the 0.8 mm nozzle specimens when they were printed

with a 0° orientation than with a 45° orientation; the opposite case was true for the 0.4 mm nozzle specimens.

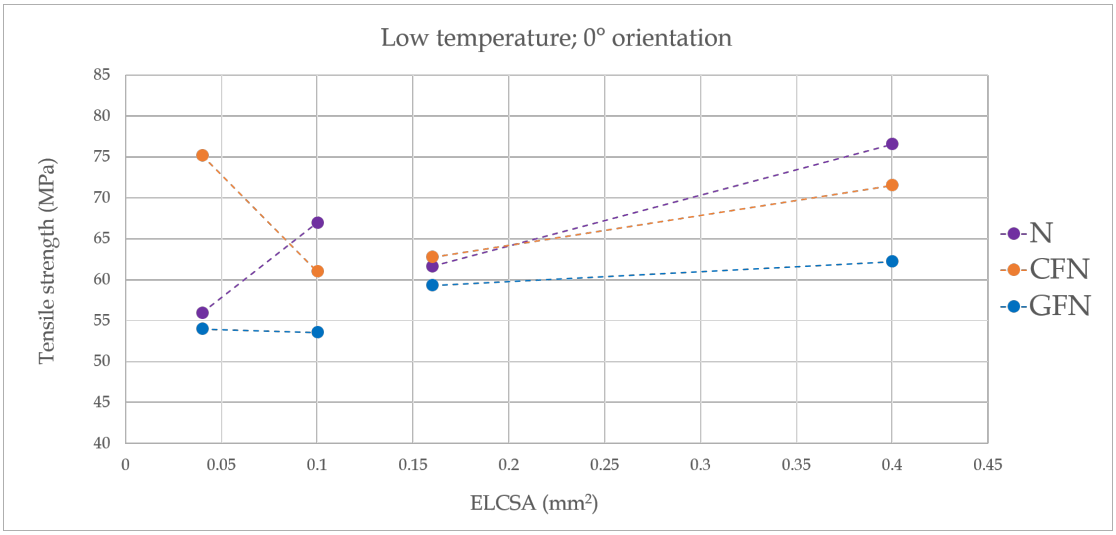


FIGURE 5.11: The change in tensile strength values of specimens printed with low temperature and 0° orientation

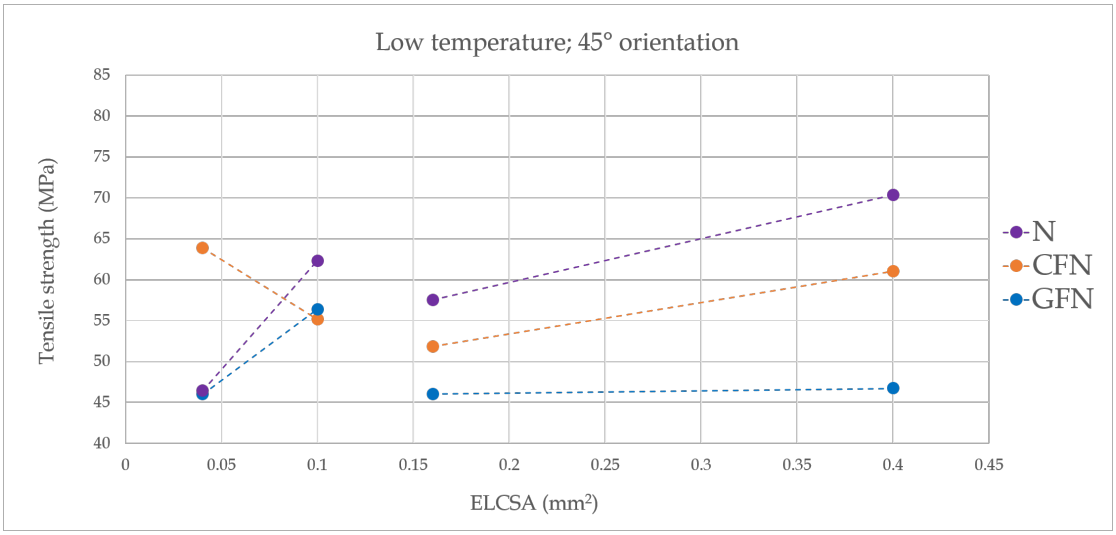


FIGURE 5.12: The change in tensile strength values of specimens printed with low temperature and 45° orientation

For the low temperature results (Figures 5.11 and 5.12), the same behaviour can be observed going from 0° orientation specimens to 45° ones as the higher temperature specimens showed. A very similar trend among the two layer heights, except again for the glass fiber reinforced ones at 0.1 mm^2 ELCSA. And again, the 0.8 mm nozzle specimens' values were much closer to each other in the 0° orientation case than in the 45° one.

The general observations that can be made for every specimen group and material regarding tensile strength are the following:

- Every 0.8 mm nozzle specimen group showed greater strength when printed with a higher layer height (except for the above-mentioned one outlier), which was also true for the high temperature 0.4 mm nozzle groups.
- Only the carbon fiber reinforced nylon specimens showed greater strength at lower layer height when printed with low temperature and a 0.4 mm nozzle; however, their strength was so high that both times they outperformed every other group with higher ELCSA.
- Only in the High temperature, 0° groups did a higher ELCSA also mean a higher tensile strength value.
- Switching from 0° infill orientation to a 45° one always meant a drop in overall strength with every material; this was also the case for switching from high temperature to low temperature, with the only exception being the already mentioned CFN specimen with the lowest ELCSA value.
- Glass fiber reinforced specimens always had the lowest strength out of the three materials printed with the same parameters.

5.3 Young's modulus results

The same principles used for visualizing the tensile strength results apply to the Young's modulus results as well, with the same specimen group pairings and parameter group presentation.

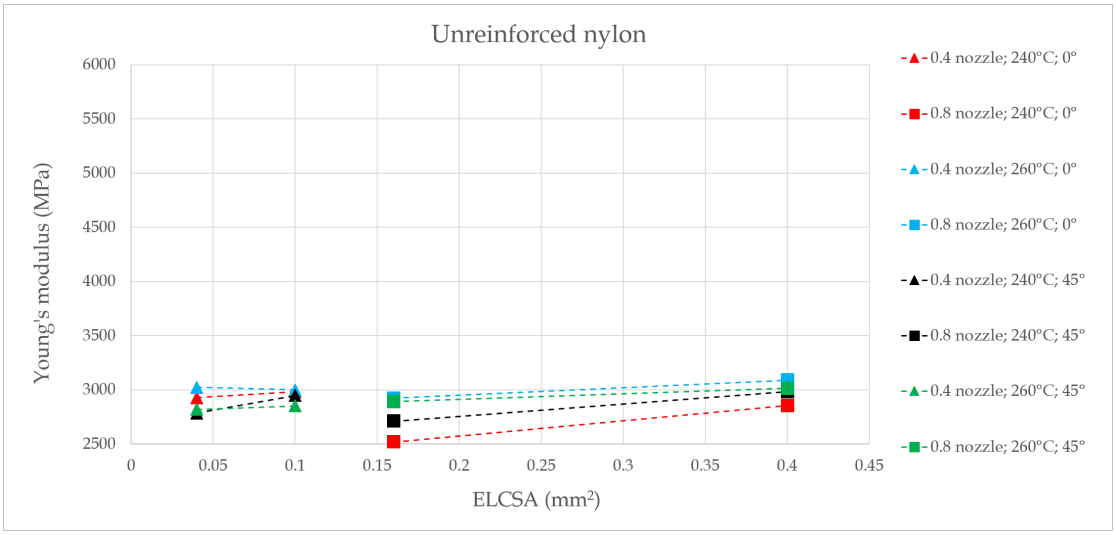


FIGURE 5.13: The change in Young's modulus values of unreinforced nylon specimens based on different parameters

The Young's modulus values for unreinforced nylon specimens can be observed in Figure 5.13. They show a clear increase in Young's modulus with the increase of layer height; however, the ELCSA did not play any role. For the 0.8 mm nozzle groups, the temperature clearly played a major role, as the high temperature ones yielded higher Young's modulus values, while for the 0.4 mm nozzle groups the orientation was a bigger factor, as the 0° oriented groups had higher values than the 45° oriented ones.

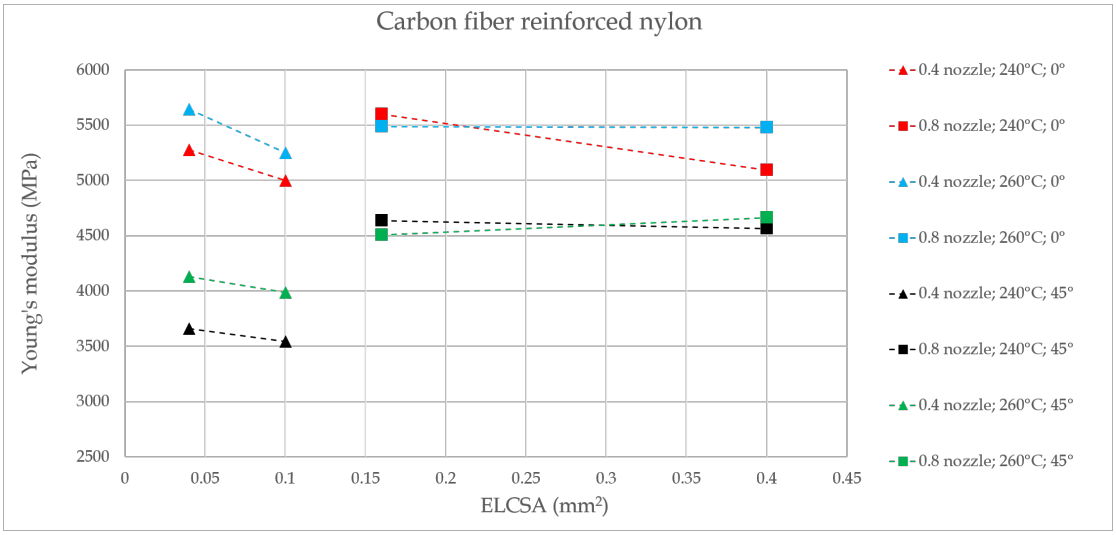


FIGURE 5.14: The change in Young's modulus values of carbon fiber reinforced nylon specimens based on different parameters

The case for the carbon fiber-reinforced nylons is very different; their values clearly place them into two groups based on their infill orientation (Figure 5.14). They also differ from the

unreinforced nylon specimens as the increase in layer height decreases their Young's modulus with two 45° oriented exceptions. For the 0° oriented groups, the nozzle diameter had no effect on their Young's modulus, while the 45° oriented groups showed higher values with a 0.8 mm nozzle diameter.

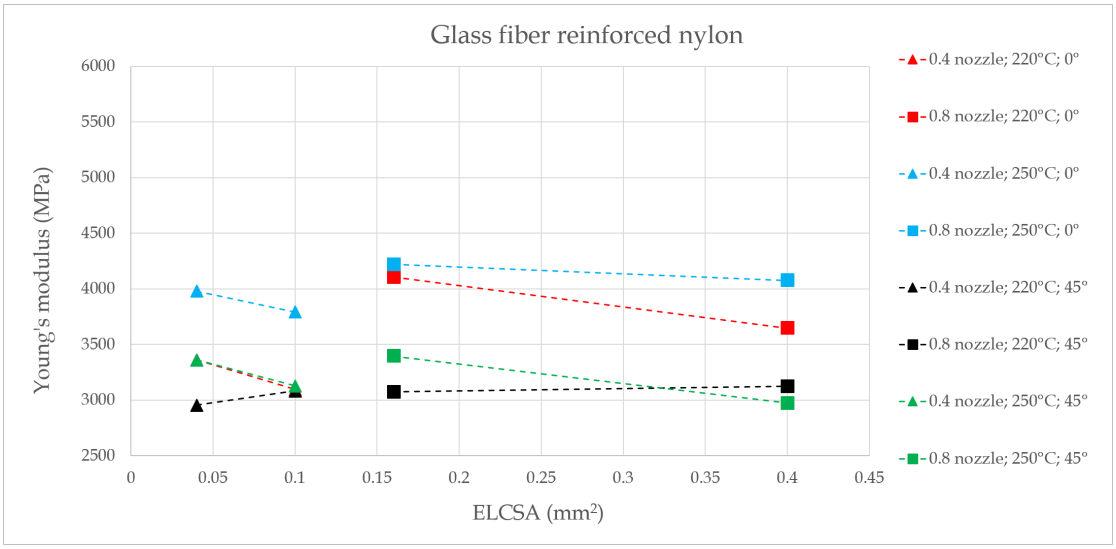


FIGURE 5.15: The change in Young's modulus values of glass fiber reinforced nylon specimens based on different parameters

The glass fiber reinforced nylon specimens (Figure 5.15) behaved very similarly to their carbon fiber counterparts, not surprising thanks to their similar nature of short fiber reinforcement. They can also be put into two distinct groups based on orientation, and their Young's modulus values also decrease with the increase of layer height with the exact same exception group. The two main differences are that the 45° oriented groups did not show an increased value when printed with a 0.8 mm nozzle, and the other being that the two 0.4 mm nozzle groups that should have a significant difference in their value showed exactly the same values.

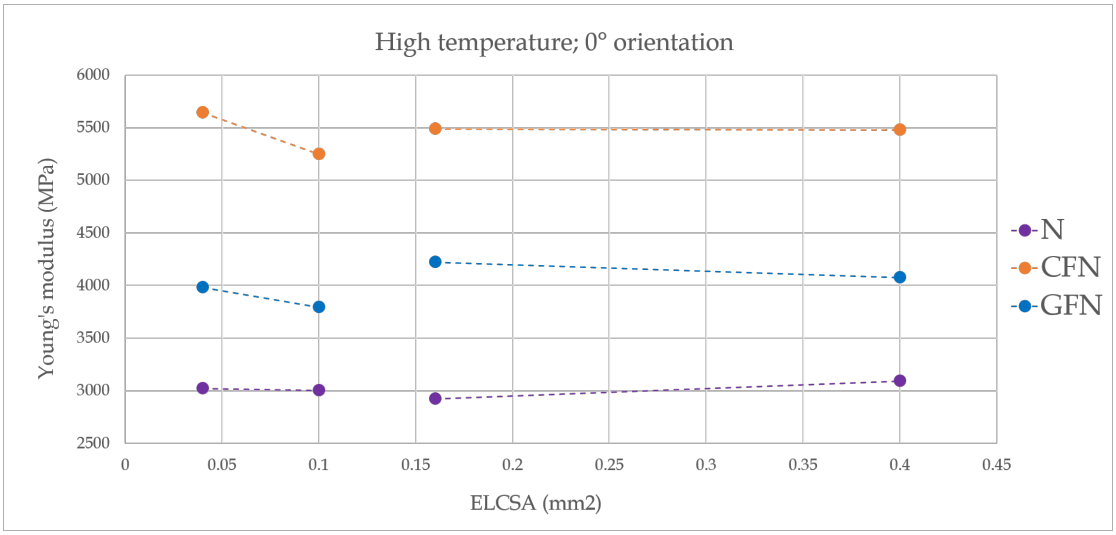


FIGURE 5.16: The change in Young's modulus values of specimens printed with high temperature and 0° orientation

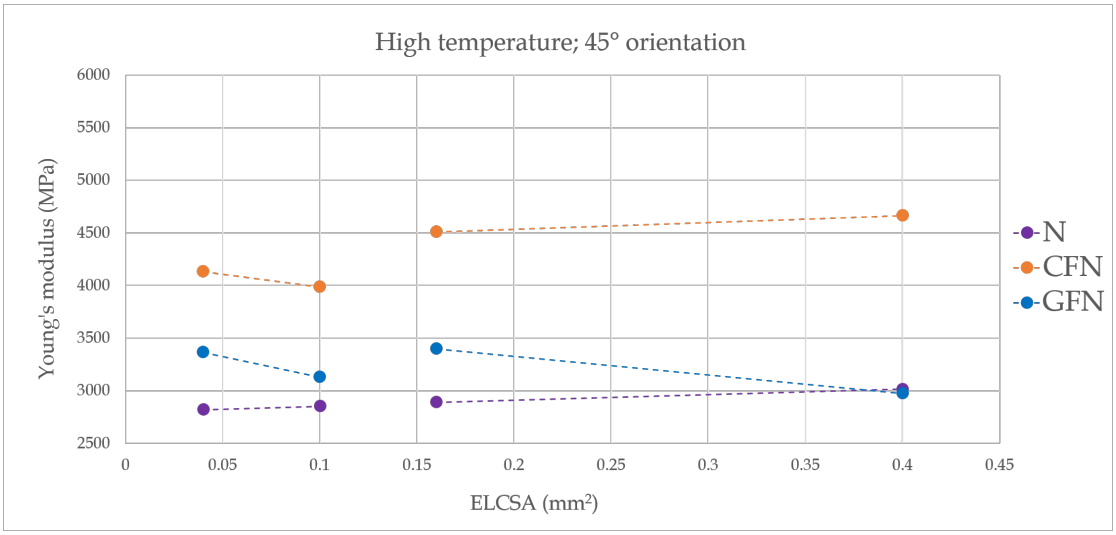


FIGURE 5.17: The change in Young's modulus values of specimens printed with high temperature and 45° orientation

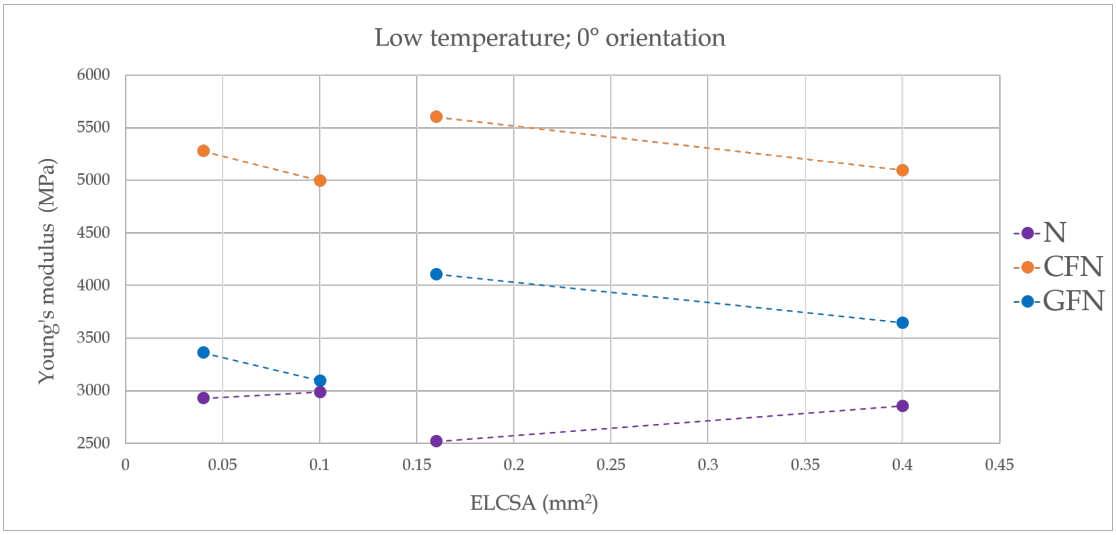


FIGURE 5.18: The change in Young's modulus values of specimens printed with low temperature and 0° orientation

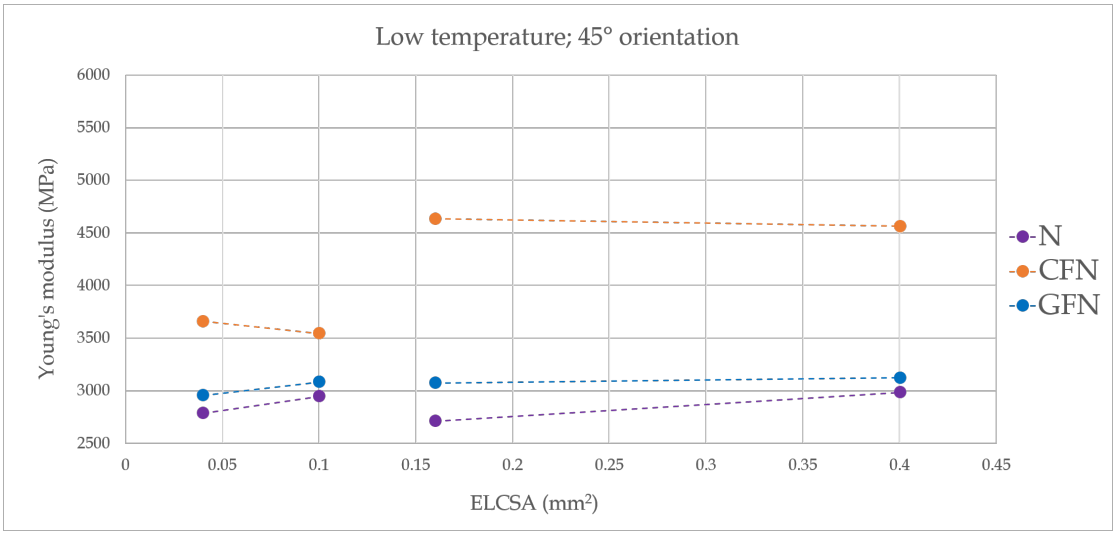


FIGURE 5.19: The change in Young's modulus values of specimens printed with low temperature and 45° orientation

When comparing the different materials based on printing temperature and infill orientation (Figures 5.13 to 5.15) the strange observation can be made that the unreinforced and carbon fiber reinforced nylon specimens trends does not change significantly from one orientation to the other in both high and low temperatures and that the glass fiber reinforced and unreinforced nylon values are pretty close to one another in every 45° orientation case.

The general observations that can be made for every specimen group and material regarding Young's modulus are the following:

- ELCSA does not play a role in the shaping of a specimen's Young's modulus.
- Trends are consistent across different nozzle diameters.
- Carbon fiber reinforced specimens always had the highest Young's modulus out of the three materials printed with the same parameters, while unreinforced nylon ones were the lowest, with glass fiber reinforced being a close second when the orientation of the infill was 45°.
- Layer height had a much lesser impact on the Young's modulus values compared to the tensile strength values.

In this section, the effect of the main 3D printing process parameters has been introduced and discussed for unreinforced, carbon fiber reinforced, and glass fiber reinforced PA 6/66 polymer blends entirely based on measured data.

Firstly, there are some general conclusions that can be drawn for every material and instance, and there are some conclusions that are specific to one type of parameter group or another.

Glass fiber reinforced nylon samples always showed lower tensile strength than their unreinforced and carbon fiber reinforced counterparts and consistently were in between the two in terms of Young's modulus.

Another one is the role that ELCSA plays in the shaping of Young's modulus and tensile strength values, which is close to zero, with the only exception being that in the high temperature, 0° groups, a higher ELCSA value always translated to a higher strength value as well.

Also, the Young's modulus ranking is consistent across all parameter groups, carbon fiber reinforced nylon being the highest, then glass fiber reinforced nylon in the middle, and unreinforced nylon being the lowest. This was not the case for Tensile strength values, where a clear ranking could not be established even inside a single parameter group (for example Figure 5.11).

The individual trends between different orientations but the same temperatures are almost always consistent, from Figure 5.9 to 5.10, Figure 5.11 to 5.12, Figure 5.16 to 5.17, and Figure 5.16 to 5.17.

5.4 Pearson correlation analysis

To determine and visualize the effect of printing parameters on mechanical properties, Pearson correlation analysis was used; it measures a linear correlation between variables divided by the product of their standard deviations. In our case, we want to show the effects of printing parameters on the mechanical properties of the printed material. So we analyzed the unique parameters and the combinations of the parameters so we can get a complete picture of the effects that the parameters have. The equation (5.1) shows the calculation of the Pearson coefficient (ρ) for general variables (P_i, P_j).

$$\rho(P_i, P_j) = \frac{\operatorname{cov}(P_i, P_j)}{\omega_{P_i}\omega_{P_j}} = \frac{1}{N-1}\sum_{k=1}^{N}\left(\frac{P_{i,k}-\mu_i}{\omega_{P_i}}\right)\left(\frac{P_{j,k}-\mu_{P_j}}{\omega_{P_j}}\right) \tag{5.1}$$

If we calculate every variable we can get, as a result, a matrix (Φ) which contains the Pearson coefficient for every variable. That can be represented by the following equation (equation (5.2)) for the two general variables.

$$\Phi = \begin{pmatrix} 1 & \rho(P_i, P_j) \\ \rho(P_j, P_i) & 1 \end{pmatrix} \tag{5.2}$$

Based on this, we can calculate this matrix for our data, and the corresponding 95% confidence interval matrix based on the Fisher distribution can be found in the appendix.

Firstly, to estimate the correlation between each parameter and mechanical property, a Pearson Correlation analysis was carried out (Equation 5.1). The values of all parameters were normalised between -1 and 1, where -1 is the lower end, and 1 is the higher end of the parameters, in order to ensure that their original numerical values do not skew the correlation analysis. The results of the correlation analysis for every material can be seen as the whole matrix in Figures 5.20 to 5.22. Generally, the corresponding thresholds for these Pearson coefficients are the following:

- No correlation between values of 0 and 0.1;
- Low correlation between values of 0.1 and 0.3;
- Medium correlation between values of 0.3 and 0.5;

- Strong correlation between values of 0.5 and 1.

These thresholds can be seen as black lines for ease of understanding in Figures 5.23 and 5.28.

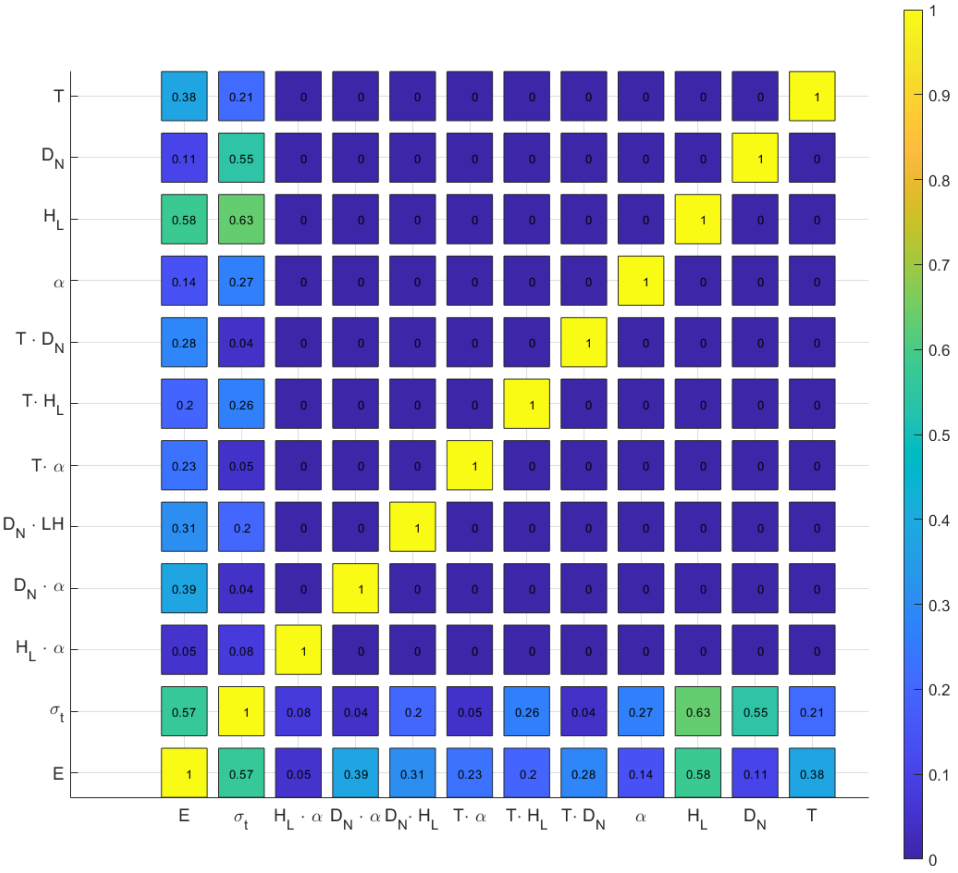


FIGURE 5.20: The Pearson Correlation matrix regarding printing parameters and mechanical properties of unreinforced nylon samples

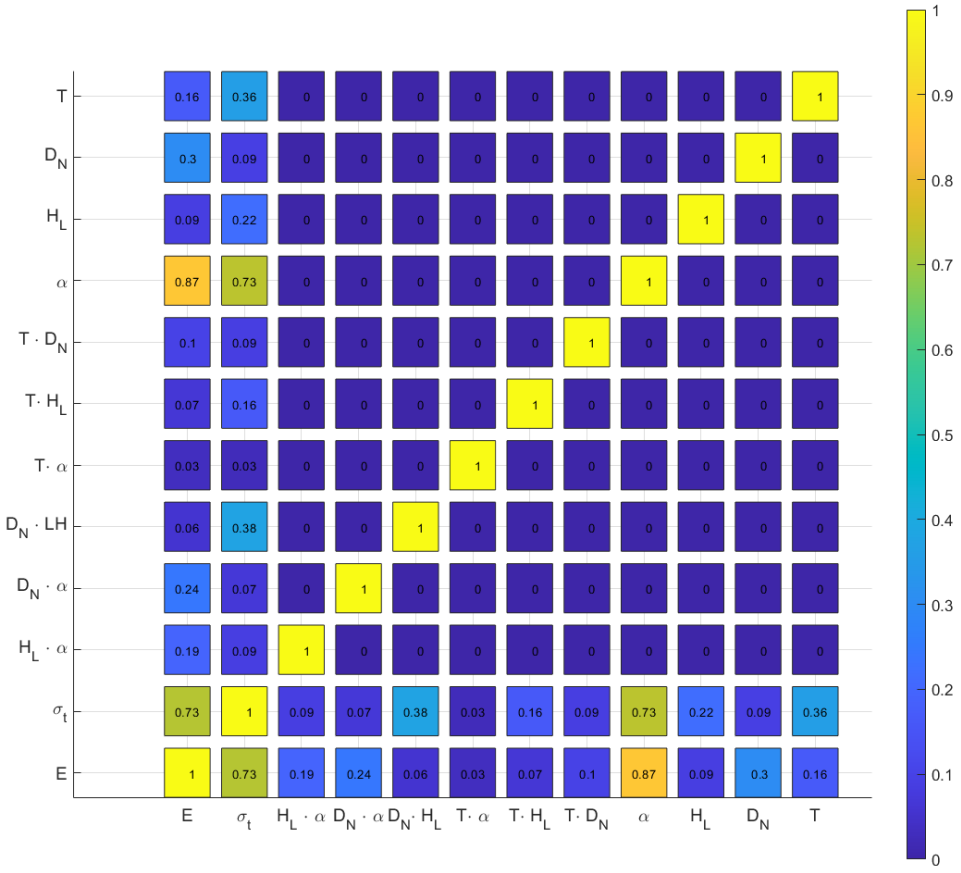


FIGURE 5.21: The Pearson Correlation matrix regarding printing parameters and mechanical properties of carbon fiber reinforced nylon samples

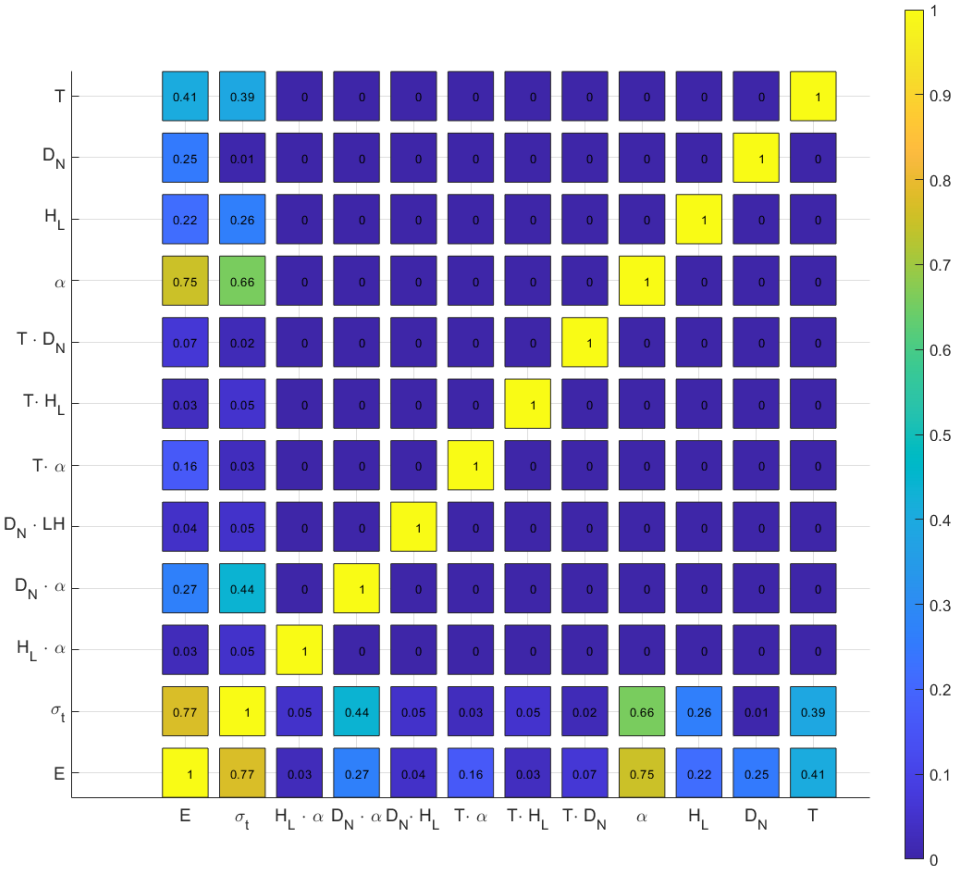


FIGURE 5.22: The Pearson Correlation matrix regarding printing parameters and mechanical properties of glass fiber reinforced nylon samples

These matrices are generally difficult to read due to their complex nature, so a summarization of the important parts has been compiled in Figure 5.23 and 5.24.

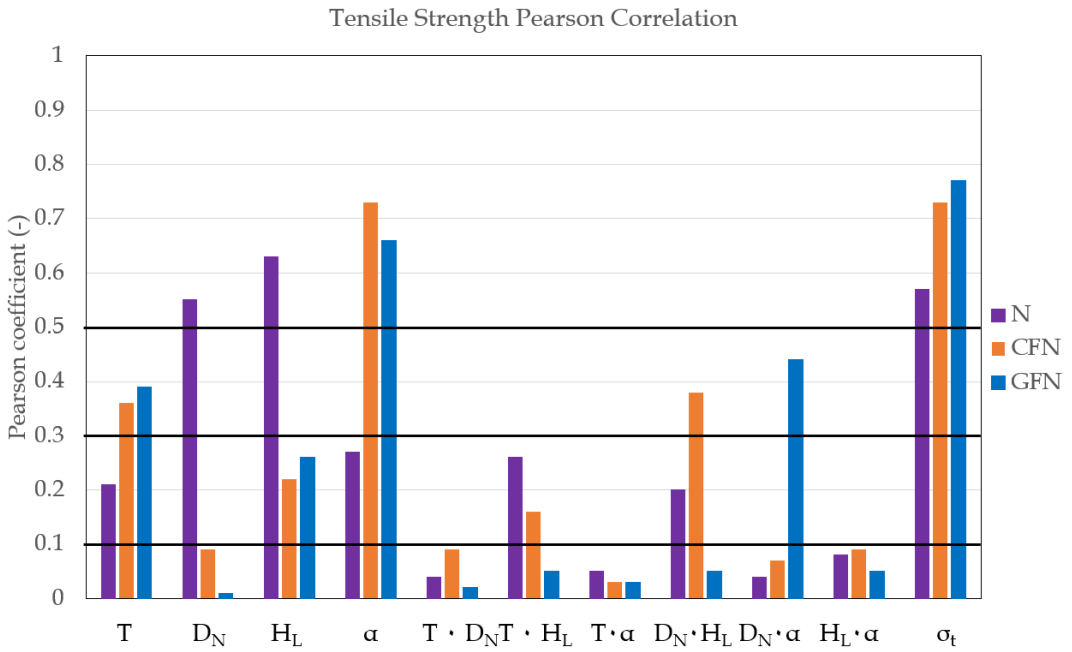


FIGURE 5.23: The tensile strength summarization of the Pearson coefficient values of all three matrices

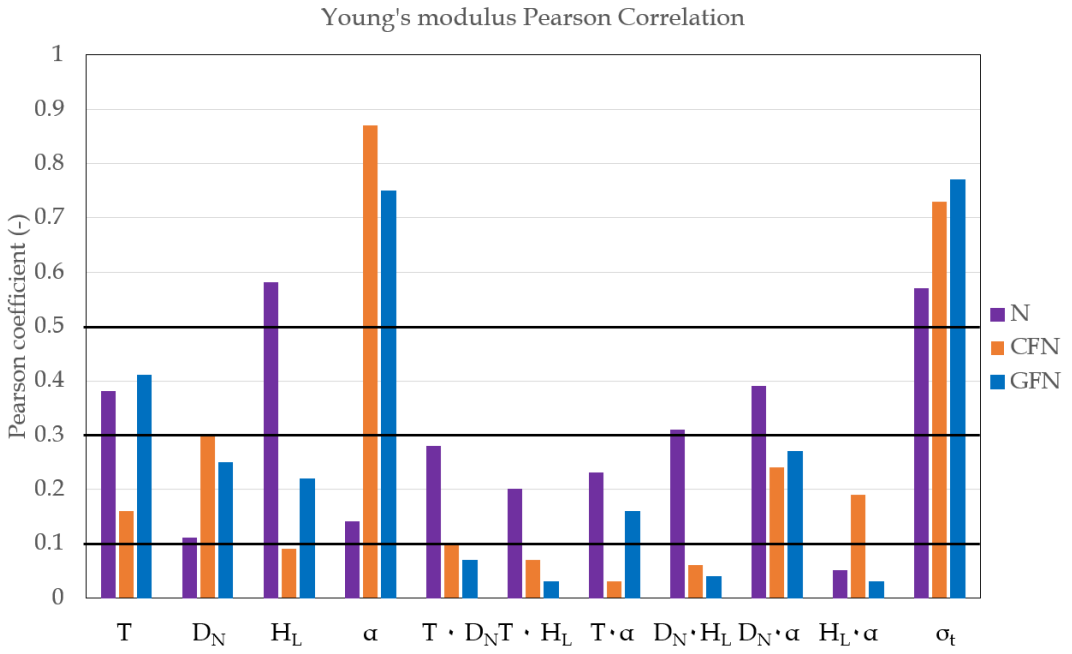


FIGURE 5.24: The Young's modulus summarization of the Pearson coefficient values of all three matrices

After matching the resulting Pearson coefficients (Figures 5.23 and 5.24) with the measured values and trends discussed in the previous section, it was clear that they do not match up with one another. So, to further differentiate groups inside the three material groups, the

specimens were categorized by their two structural parameters, which were the infill orientation and nozzle diameter. These two parameters already showed different trends inside them in the previous section, so this new categorization made the most sense; for example, the 45° and 0° oriented samples sometimes showed different behaviours inside the same material group. Furthermore, after creating new diagrams for these categories, the analysis of the combined effect of two parameters was nonsensical, as the groups formed around infill orientation or nozzle diameter made the values 0 or the same as the previous ones. The new categorized figures can be seen from Figure 5.25 to 5.28.

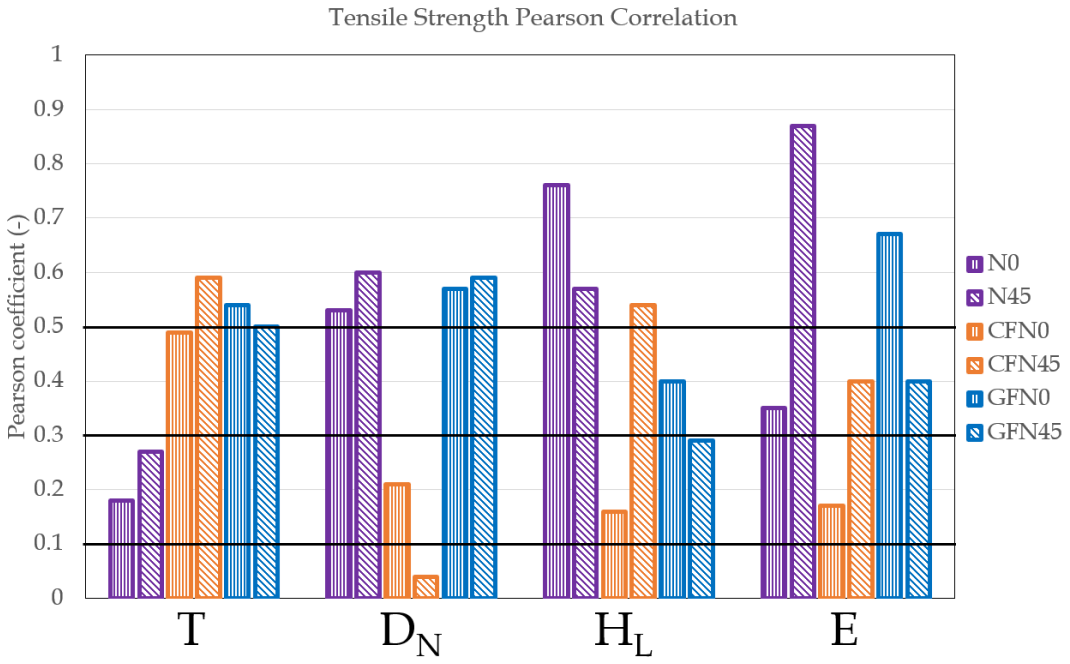


FIGURE 5.25: The tensile strength summarization of the Pearson coefficient values of all three materials grouped by their infill orientation

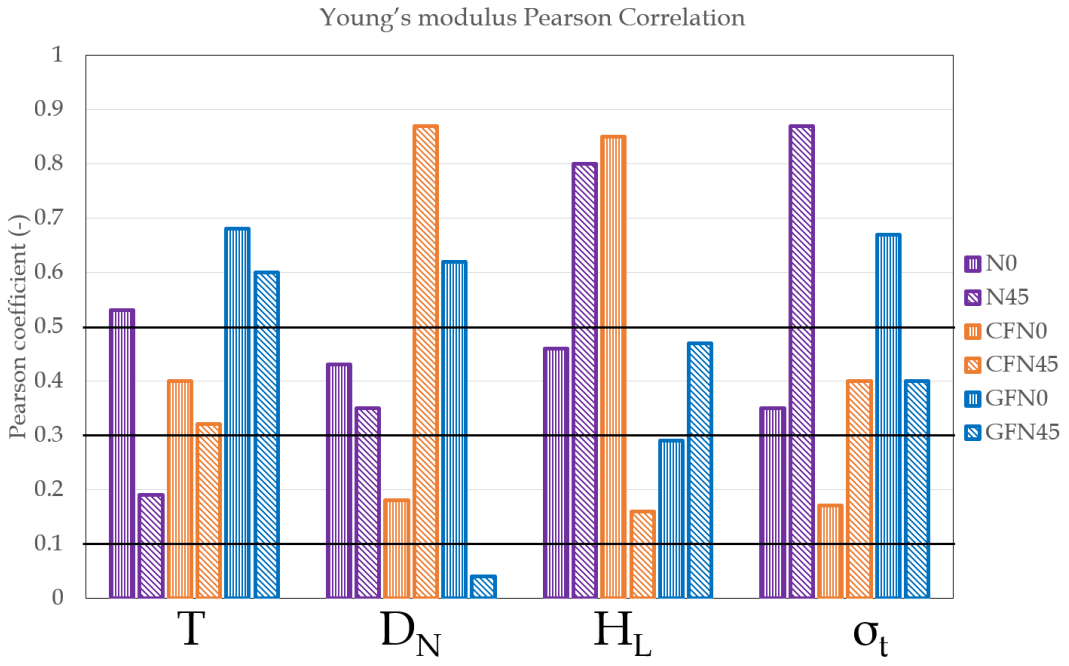


FIGURE 5.26: The Young's modulus summarization of the Pearson coefficient values of all three materials grouped by their infill orientation

5.4.1 Pearson correlation between tensile strength and material groups categorized by their infill orientation

When differentiating within a material group based on infill orientation, the only coefficients that are not significantly changed are the tensile strength values of unreinforced nylon. As for fiber-reinforced nylons, both their 0° and 45° oriented samples showed a very similar and strong correlation with tensile strength, in comparison to their previous combined analysis where they both showed only a medium correlation.

For nozzle diameter, the difference between the combined and infill orientation categorized results is even more stark. Originally, in the combined analysis neither of the two fiber-reinforced materials showed any correlation between nozzle diameter and tensile strength; however, after splitting them into orientations, only the carbon fiber reinforced samples that have been printed with an infill orientation of 45° remained the same, while their 0° oriented samples showed a low correlation. For glass fiber reinforced nylon, both of their infill orientation groups showed an almost identical strong correlation between nozzle diameter and tensile strength, which again showed no correlation at all before the differentiation of orientations.

When discussing the Pearson correlation between tensile strength and layer height, the two groups that change from the combined analysis are the 0° oriented glass- and 45° oriented carbon fiber reinforced nylon, which change from a low correlation to medium- and strong correlations, respectively.

One of the most unexpected changes that has occurred is regarding the relation between tensile strength and Young's modulus. Previously, all three material groups showed a very strong correlation between the two; however, after the categorization by infill orientation, the new groups showed vastly different correlations. For unreinforced nylon, only the 45° oriented group showed a strong correlation, while the 0° oriented one only showed a medium one. For carbon fiber-reinforced nylon, the 0° oriented group had a low Pearson coefficient, while the 45° one had a medium one. Again, in the glass fiber reinforced groups only the 0° one showed the original strong influence between the Young's modulus and tensile strength, while the 45° group only showed a medium one.

5.4.2 Pearson correlation between Young's modulus and material groups categorized by their infill orientation

In the case of temperature, the Pearson coefficient of differently oriented samples shows a very similar value for the fiber-reinforced nylon ones, albeit a step up for both materials in terms of correlation as they went from low to medium and medium to strong correlation when the combined values are compared. The unreinforced nylon samples went from a combined medium correlation to low and strong correlations as the 45° and 0° infill oriented respectively.

The nozzle diameter had a similarly stark change, coming from a combined effect to an infill orientation grouped one. The previously low effect of nozzle diameter on the Young's modulus values of unreinforced nylon changed to a medium one when the material group got separated into two orientations. Also, the carbon fiber-reinforced nylon that previously was on the threshold of low and medium correlation showed the strongest one in the case of the 45° infill oriented group at a Pearson coefficient of 0.87, while its 0° oriented counterpart showed only a low value of 0.18. The case was similar for the glass fiber one as well; the previously low coefficient value changed into a high one for the 0° oriented group, while the 45° one showed no significant correlation between this parameter and Young's modulus.

Layer height, which previously showed that in the unreinforced nylon case had a significantly higher impact on Young's modulus than the other two fiber-reinforced ones, with the grouping of samples showed it is not the case. The 45° oriented unreinforced group showed a very strong 0.8 coefficient value; however, surpassing that, the 0° oriented carbon fiber reinforced group showed a value of 0.85, while its 45° oriented group remained at a low value of 0.16.

To show why the categorization by infill orientation is important, the following case is presented:

When searching for the most influential parameter when using carbon fiber-reinforced nylon, the combined Pearson analysis shows that it is the orientation that influences it by far the most, then the temperature is a second one, and nozzle diameter and layer height have a very low or no influence at all. However, when the data is split into two groups based on infill orientation, the result is flipped on its head as the previously low to no influence becomes by far the most affecting parameters, reason being that they are the most influencing only for one of the orientations as the nozzle diameter becomes the strongest for the 45° oriented group (with a low one for the 0° group) and layer height becomes the strongest for the 0° oriented group (with a low one for the 45° group). The most influential parameter, highly dependent on the infill orientation, is likely the reason for the previously combined result that the infill orientation is the most impactful parameter in the case of Young's modulus when carbon fiber-reinforced nylon is used.

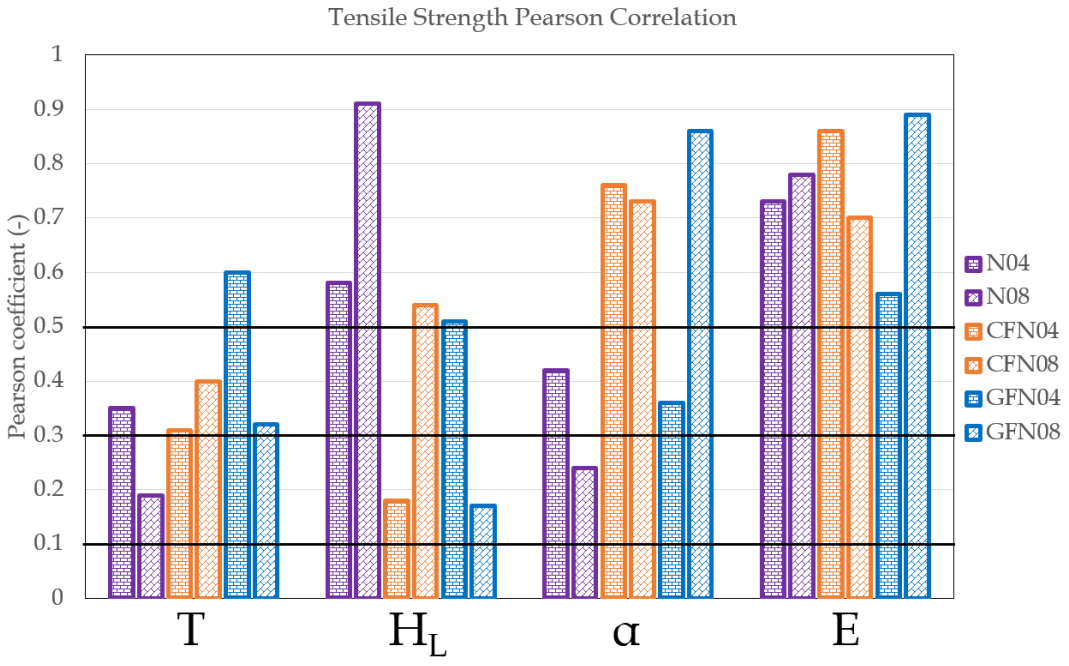


FIGURE 5.27: The tensile strength summarization of the Pearson coefficient values of all three materials grouped by their nozzle diameter

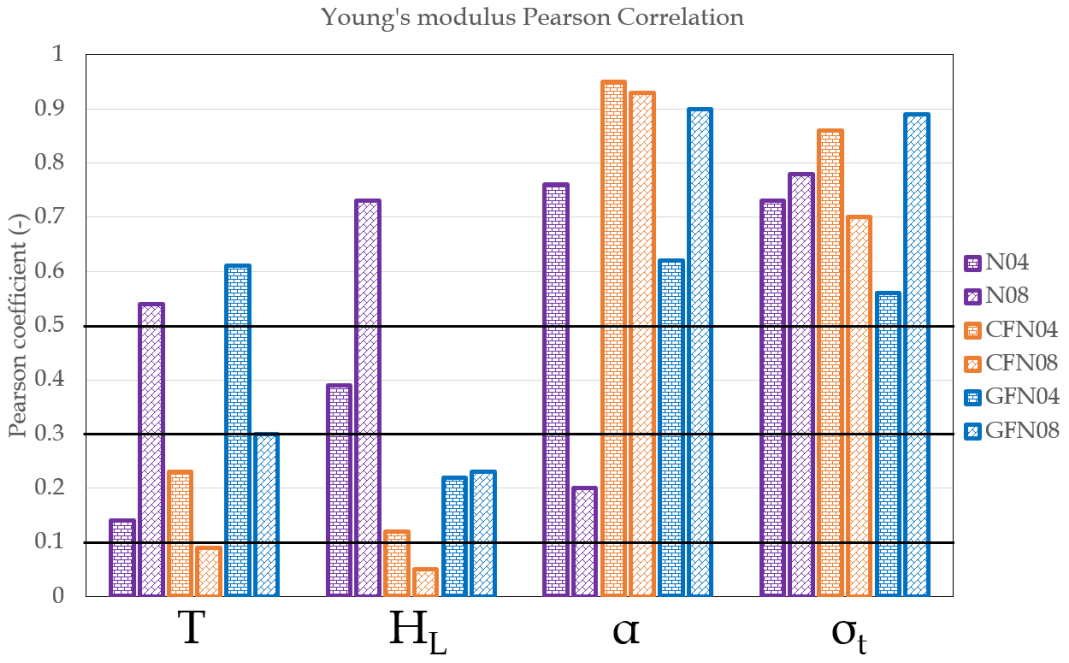


FIGURE 5.28: The Young's modulus summarization of the Pearson coefficient values of all three materials grouped by their nozzle diameter

5.4.3 Pearson correlation between tensile strength and material groups categorized by their nozzle diameter

When the data is categorized by nozzle diameter, the correlations are not significantly changed between temperature and tensile strength; the two exceptions occur in the unreinforced- and glass fiber reinforced groups that have been printed with a 0.4 mm nozzle.

When layer height is considered, the unreinforced nylon remains relatively the same, while for both fiber-reinforced nylons, the change from a combined low impact to a strong one when they were made by a 0.8 mm nozzle in the case of carbon fiber reinforcement and a 0.4 mm nozzle in the case of glass fiber reinforcement.

The infill orientation also remained relatively unchanged in the cases of unreinforced and carbon fiber reinforced nylon, while the glass fiber reinforced nylon only showed a very strong correlation when it was printed with a 0.8 mm nozzle; the ones that were printed with a 0.4 mm nozzle showed only a modest 0.36 value. Meaning that the glass fiber reinforced nylon tensile strength, when printed with a 0.4 mm nozzle, is mostly influenced by temperature and layer height, and when the same material is printed with a bigger 0.8 mm nozzle, the most influential parameter becomes the infill orientation, while temperature and layer height only play a medium and small part in it respectively.

The Pearson correlation between the two mechanical properties, the Tensile strength and Young's modulus, is again relatively unchanged from combined analysis to the nozzle diameter categorized one.

5.4.4 Pearson correlation between Young's modulus and material groups categorized by their nozzle diameter

In the case of temperature, the correlation between it and Young's modulus is not significantly changed when carbon fiber reinforced nylon was used. However, for both the unreinforced and glass fiber reinforced nylon, the combined medium correlation changed into a low and strong correlation. For unreinforced nylon, the 0.4 mm nozzle group showed a low correlation, while the 0.8 mm nozzle group showed a strong one; the opposite was true for glass-reinforced nylon.

When we observe the coefficient values at the layer height part, the two fiber-reinforced nylon samples did not change significantly, while the unreinforced one only shows a medium correlation when it was printed with a 0.4 mm nozzle.

Finally, when the previously (combined) most impactful parameter, the infill orientation, is examined, we still see very strong Pearson coefficients in the cases of fiber-reinforced nylons, while the previously low correlation value that the unreinforced one showed changed to a very high value when it was printed with a 0.4 mm nozzle.

To make another example for the importance of categorization of samples, change can be best seen with unreinforced nylon, as previously the layer height showed the strongest influence on Young's modulus and tensile strength. It remained true for the ones that were printed with a 0.8 mm nozzle, while the ones that were printed with a 0.4 mm nozzle showed a much greater correlation with infill orientation in the case of Young's modulus.

5.4.5 Conclusion

During the course of this chapter, measured data with Pearson coefficient analysis for creating a comprehensive investigation on the impact of parameters has been presented. The goal was to facilitate the understanding of complex effects between input printing parameters and output mechanical properties. It was expected that the fiber-reinforced nylons would behave similarly, but after the comparison was made with the test results presented in chapter 5, it was obvious that a different approach is needed. So the material groups were further categorized by their two structural parameters, which were the infill orientation and nozzle diameter, which finally reflected the aforementioned experimental results. A few of the most stark differences between the three material groups categorized by their infill orientation are the following:

- The influence each parameter has on the tensile strength of samples is mostly the same for both infill orientations, with the exception of layer height in the case of carbon fiber reinforced nylon, which shows a low influence in the 0° infill oriented group and a strong one in the 45° one.
- For unreinforced nylon, when grouped by their infill orientation, the nozzle diameter and layer height, both of which make up the extruded line size and shape, had a strong

correlation with tensile strength, while temperature only played a minor role. With correlation to the Young's modulus, the layer height, nozzle diameter, and temperature showed a strong, medium, and low impact when the specimens were printed with an orientation of 45°, respectively; however, these three parameters showed almost the same correlation when the samples were printed with an infill orientation of 0°.

- For the carbon fiber reinforced nylon 45° infill oriented group, the temperature and layer height had a strong correlation with tensile strength, while the nozzle diameter had no significant impact. However, the 0° group only had a high coefficient value with temperature, and the two-dimensional parameters only had a low one. Regarding Young's modulus, the layer height had by far the most impact when samples were printed with a 0° infill orientation and nozzle diameter when the samples were printed with a 45° one, while for both the temperature only played a medium role in the shaping of the Young's modulus values.

- The glass fiber reinforced nylon did not behave similarly to the other fiber reinforced nylon, as the nozzle diameter was the most impactful parameter for both of the differently oriented groups when correlation with tensile strength was analyzed. A very close second most impactful parameter for both groups was the temperature, while the layer height again had a very similar medium impact. These correlations between parameters and mechanical properties remain the same for Young's modulus as well, with the distinguishable difference that occurs in the case of nozzle diameter, where the 0° infill oriented group retains a high value, while its 45° counterpart shows an abysmal 0.04 value, which in practice means zero correlation.

After the more accurate categorization of materials by their infill orientation, the same categorizing had been carried out by their nozzle diameter, where the following observations were made:

- Both in the case of unreinforced and glass fiber reinforced nylon, the Pearson correlation values are very different for both mechanical properties based on the nozzle diameter that the samples were printed with; however, the carbon fiber reinforced nylon only showed this differentiation based on nozzle diameter when we observed the correlation between its layer height and tensile strength.

- When unreinforced nylon was printed with either of the nozzle sizes, the layer height always showed the strongest impact on its tensile strength, while the temperature and infill orientation had a very similar coefficient. The difference is mainly that the layer height shows a much higher value when the nozzle was the bigger 0.8 mm one, with a 0.91 Pearson coefficient, also having a lower temperature and infill orientation correlation that only shows a low correlation value, while the 0.4 mm nozzle group showed a medium one for both. For Young's modulus correlations, the layer height and temperature had a strong one, and the infill orientation had a low one when samples were printed with a 0.8 mm nozzle. However, when they were printed with a 0.4 mm nozzle, the infill orientation had by far the strongest effect on their Young's modulus value, while the layer height and temperature had a medium and low one, respectively.

- When samples were made with carbon fiber reinforced nylon, the tensile strength was mainly influenced by the infill orientation for both nozzle sizes, having correlation values over 0.7. For both sizes, the temperature also showed almost the same value, just over 0.3, value being a medium correlation, while the layer height showed a strong correlation when a 0.8 mm nozzle was used and a low one when a 0.4 mm nozzle was used. Impact of different parameters on the Young's modulus is especially stark when carbon fiber was used, as for both nozzle sizes the infill orientation showed Pearson correlations over 0.9. Contrasting these high values, the temperature and layer height values were so low that only in the case of the 0.4 mm nozzle were they able to be above the low correlation 0.1 value.

- Lastly, the glass fiber reinforced nylon samples showed a very strong correlation between the infill orientation and tensile strength (Pearson coefficient value of 0.86) when

they were printed with a 0.8 mm nozzle and only a medium and low one for temperature and layer height, respectively. The opposite was the case for the 0.4 mm nozzle samples, as the temperature and layer height displayed a strong correlation with tensile strength, while the infill orientation only showed a medium one. When we consider the effects of parameters on Young's modulus, the 0.8 mm nozzle ones remain relatively unchanged compared to tensile strength effects. However, the effect changes in the samples that were printed with a 0.4 mm nozzle, as the temperature now shows both a strong correlation with Young's modulus and the layer height shows only a low one. This is reflected in the tensile strength-Young's modulus correlations, as the Pearson coefficient is very high for the 0.8 mm nozzle and much lower for the 0.4 mm one; in the case of the 0.8 mm nozzle samples, the parameter effects were very close to one another for both mechanical properties.

One example to further improve the credibility of Pearson analysis by categorization is that we can read from Figure 5.28 that unreinforced nylon 0.8 mm nozzle samples Young's modulus values were mainly influenced by layer height and temperature, while the 0.4 mm nozzle samples were by the infill orientation, if we cross reference it with Figure 5.13 it shows that for 0.8 mm nozzle samples the 3 highest value samples were indeed of higher layer height, and the two highest were of high temperature, while the infill orientation were not significant as the 0° samples showed the highest and lowest values in that group while the 45° ones were in the middle. As for the 0.4 mm nozzle group, the 4 highest values can be attributed to all the 0° oriented samples, printed by low and high temperature alike, thus being the lowest Pearson correlation value for the 0.4 mm nozzle group in Figure 5.28.

Another case is the correlation between nozzle diameter and tensile strength, from Figure 5.25 we can read that it has a Pearson coefficient of 0.21 when the specimens were printed with an infill orientation of 0°, which is in the middle of the low correlation section, for reference the experimental results shown in Figure 4.12 are the same carbon fiber reinforced 0° infill oriented specimens that also show that the 0.4 mm nozzle samples had a little higher overall strength compared to their 0.8 mm counterparts.

To conclude the numerous observations presented above, the following conclusion can be drawn:

The effects of parameters on mechanical properties cannot be studied adequately unless the differently structured 3D printed samples are categorized by one of their structural parameters.

Even when the categories show the same effect between a parameter and a mechanical property combining the two categories when making a Pearson analysis can hide strong effects like in the case of glass fiber reinforced nylon, where their combined effect showed an almost 0 coefficient value for tensile strength (Figure 5.23), but after categorizing by their infill orientation both the 0° and 45° oriented category displayed a very similar 0.58-0.59 coefficient value (Figure 5.25), which translates to a strong correlation between this parameter and tensile strength.

Chapter 6

Modeling and simulating the complex structural 3D printed specimens based on different printing parameters

In the third chapter, my goal was to develop models using the experimental data that have been collected and shown in chapters 4 and 5 to predict the mechanical properties of nylon 3D printed parts based on their parameters.

6.1 The prediction of mechanical properties with model fitting

When choosing the model for the prediction of mechanical properties based on the parameters (parameter matrix in Table 5.1), Equation 6.1 was chosen. As seen in Figures 6.1 to 6.3, the performance of the model was excellent for every tensile strength and Young's modulus value, with one exception being the tensile strength of glass fiber reinforced nylon, albeit it still being very good at a 0.85 coefficient of determination. There is a need to distinguish the model performance in the case of carbon fiber reinforced nylon, which showed a 0.99 coefficient of determination, meaning a near-perfect prediction.

To approximate the measured data, we have chosen a polynomial function of the following form (Equation 6.1).

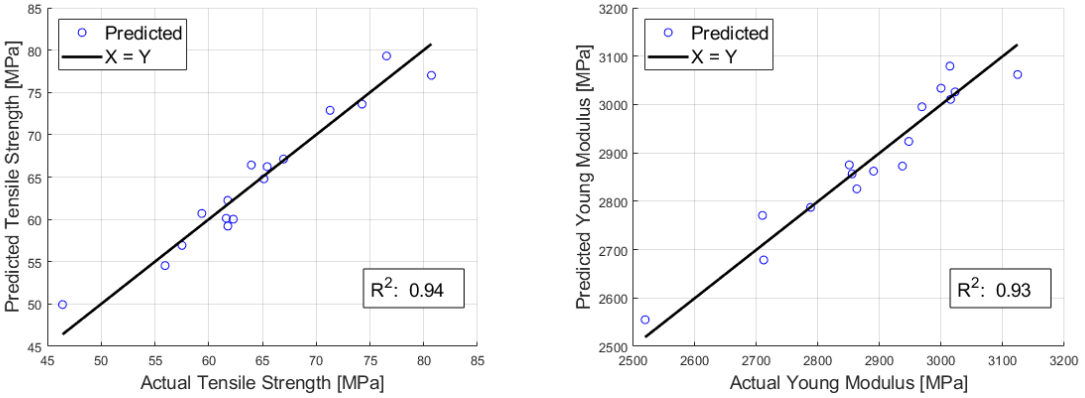
$$\Gamma = a + bD_N + cT + d\alpha + eH_L + fD_N T + gD_N \alpha + hD_N H_L + jT\alpha + kTH_L + lH_L \alpha \tag{6.1}$$

We only have the data for two points for each investigated characteristic, so the correlation contains only first-order, cross-effect, and bias terms. The function makes a connection between the nozzle diameter (D_N), the layer height (H_L), the printing temperature (T), and the infill orientation (α). For output, we have two examined properties, so the Γ symbol may be Young's modulus or tensile strength. For the determination of the parameters of Equation 6.1, we need to solve an extreme value search, which can be formalized in the following form (Equation 6.2).

$$\min_{\Omega} \sum_{i=1}^{n} \left(\Gamma_{\text{comp},i} - \Gamma_{\text{meas},i}\right)^2 \tag{6.2}$$
$$[a, b, \ldots, l] \in \Omega$$

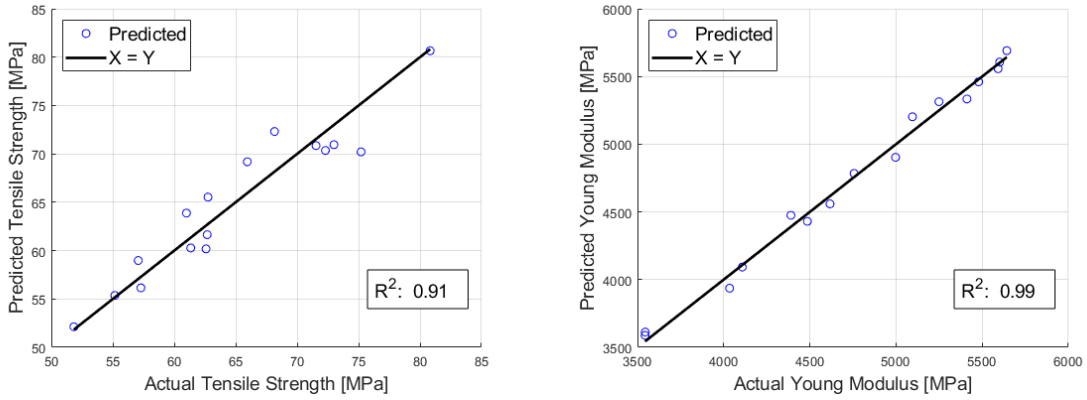
The solution to the minimization problem was obtained in the MATLAB environment, with the least squares algorithm. The performance of the model fitting can be characterized with the coefficient of determination (R^2), which can be formalized with the following equation (Equation 6.3), where $\overline{\Gamma}_{\text{meas}}$ symbolizes the mean of the measured data.

$$R^2 = \frac{\sum_i^n \left(\Gamma_{\text{meas},i} - \Gamma_{\text{comp},i}\right)^2}{\sum_i^n \left(\Gamma_{\text{meas},i} - \overline{\Gamma}_{\text{meas}}\right)^2} \tag{6.3}$$



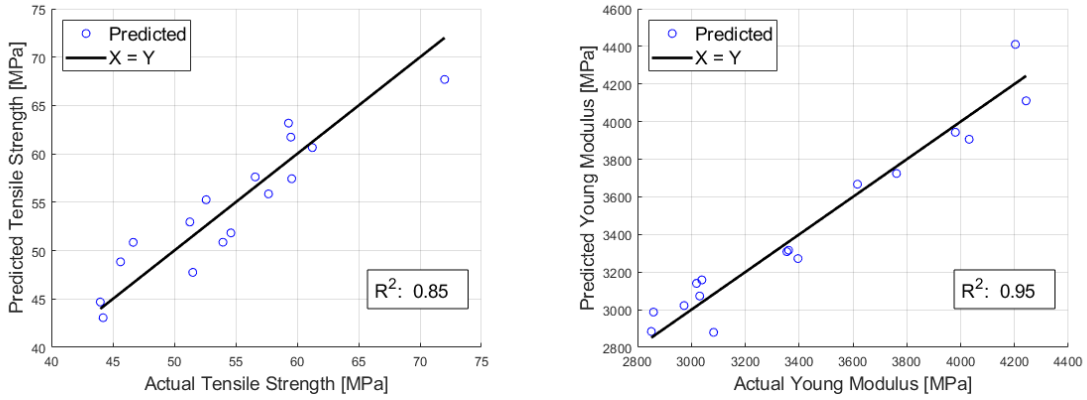
(a) (b)

FIGURE 6.1: The prediction model performance for unreinforced nylon samples' tensile strength (a) and Young's modulus (b) values.



(a) (b)

FIGURE 6.2: The prediction model performance for carbon fiber reinforced nylon samples' tensile strength (a) and Young's modulus (b) values.



(a) (b)

FIGURE 6.3: The prediction model performance for glass fiber-reinforced nylon samples' tensile strength (a) and Young's modulus (b) values.

The performance of the models has more than satisfactory accuracy, which can also be seen based on the R^2 values. The best fittings are in the cases of Young's modulus, while the cases of tensile strength fittings are just a little bit behind. Table 6.1. contains the values of the fitting parameters. The measured and computed values can be seen side by side in the appendix for all three material groups and two mechanical properties.

TABLE 6.1: The values of received parameters of each mechanical property

Parameter	**Unreinforced nylon mechanical property**		**Carbon fiber reinforced nylon mechanical property**		**Glass fiber reinforced nylon mechanical property**	
	σ_t	E	σ_t	E	σ_t	E
a	64.44	2888.41	64.92	4784.30	54.39	3425.33
b	1.74	55.51	2.78	113.79	2.79	191.17
c	4.44	-15.97	0.72	209.37	0.04	117.95
d	5.17	84.93	1.67	-61.96	1.88	-101.90
e	-2.18	-21.14	-5.68	-599.27	-4.71	-354.35
f	-0.35	41.72	0.68	-69.77	0.14	-30.64
g	-2.15	-28.72	1.24	45.16	0.37	-15.28
h	0.39	-34.11	-0.20	23.36	-0.22	-76.35
j	1.65	44.74	2.92	38.37	-0.34	-20.27
k	0.35	56.41	-0.54	167.90	-3.13	-126.04
l	-0.63	7.60	0.68	133.27	-0.35	12.57

When the Pearson coefficient analysis was carried out the observation has been made that for parameter influence the categorization by structural parameters have been much more informative, so to account for this phenomenon the same categorization by both infill orientation and nozzle diameter have been made and also a new simplified polynomial function (Equation 6.4) has been used for the same reason that the combined effect of parameters has been rendered nonsensical by the categorization of one parameter.

$$\Gamma = a + bD_N + cT + d\alpha + eH_L \tag{6.4}$$

Because of the rather large number of figures, due to the categorization by both structural parameters, instead of displaying them all, only their R^2 values are presented in Figure 6.4 and 6.5. The individual figures can be seen in the appendix.



FIGURE 6.4: The prediction model performance for both infill orientation- and nozzle diameter categorizations in the case of tensile strength.

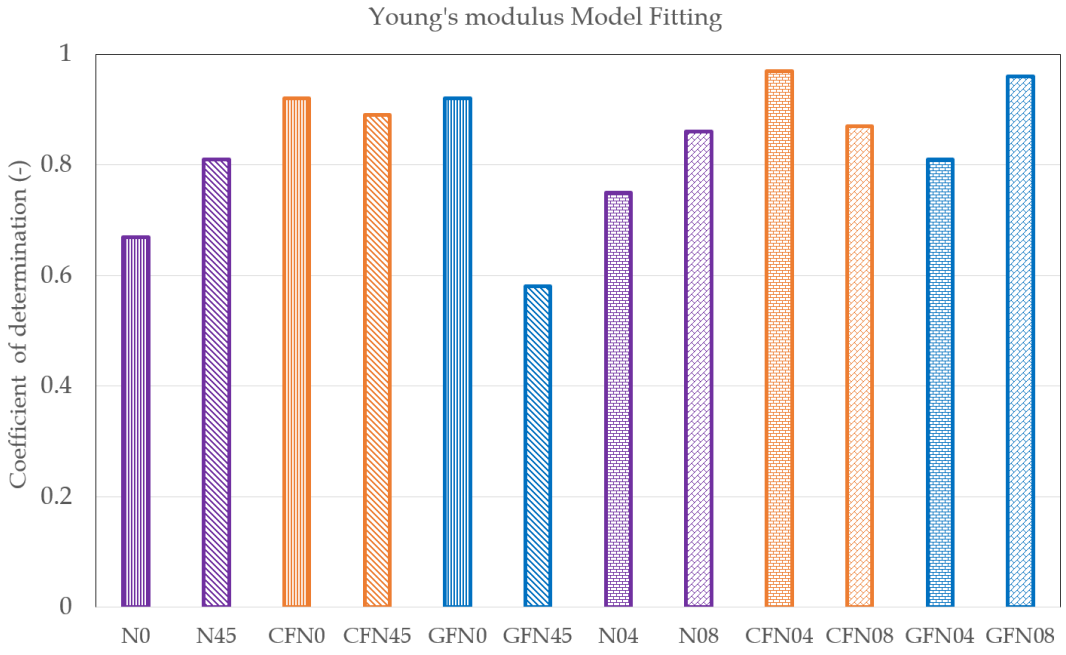


FIGURE 6.5: The prediction model performance for both infill orientation- and nozzle diameter categorizations in the case of Young's modulus.

After comparing the categorized, simplified, linear model performances (Figures 6.4 and 6.5) with the previously presented ones (Figures 6.1 to 6.3), they show a much worse performance, albeit still good performance overall, as they are all above a 0.6 value with one exception.

Meaning that when the data is categorized by parameters, the linear polynomial function isn't able to fully match the behaviour of the split-up groups, thus requiring the previously used Equation 6.1 and approach.

Utilizing this equation, further heat maps of tensile strength and Young's modulus values have been created for the 2 parameters that can assume values freely, them being the temperature and layer height. These heat maps (Figure 6.6 to 6.8) help visualize the predicted mechanical property values changing with the changing of the aforementioned 2 parameters.

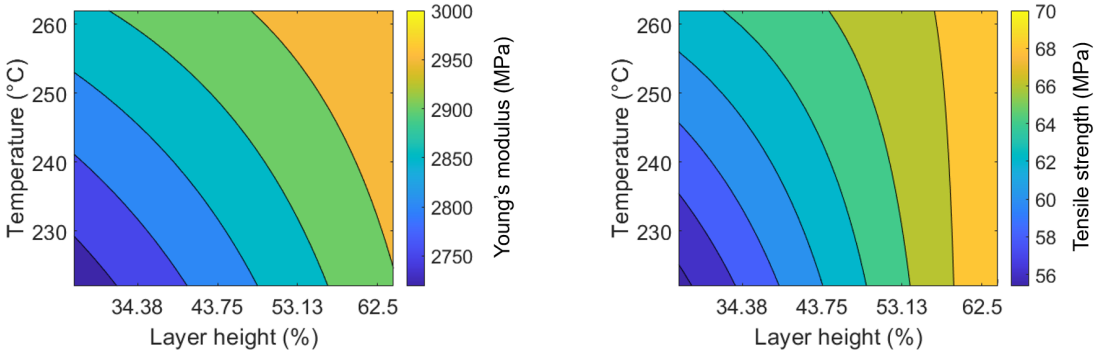


FIGURE 6.6: Young's modulus and tensile strength heat map for unreinforced nylon

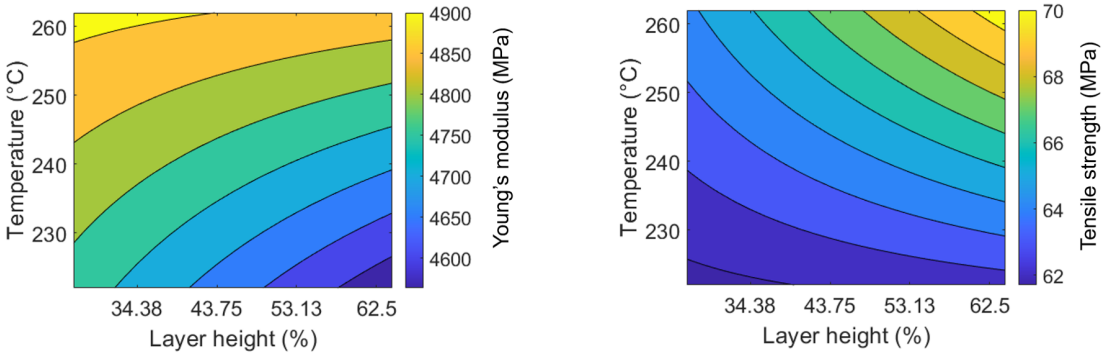


FIGURE 6.7: Young's modulus and tensile strength heat map for carbon fiber reinforced nylon

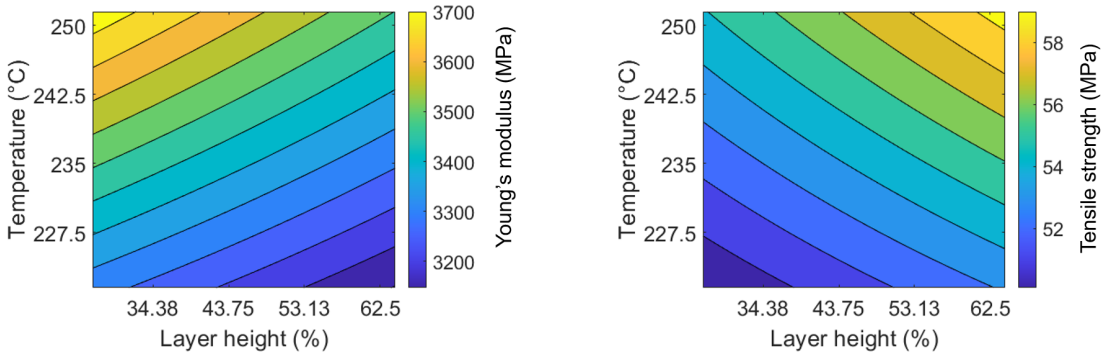


FIGURE 6.8: Young's modulus and tensile strength heat map for glass fiber reinforced nylon

There is a stark difference between the unreinforced nylon heat maps (Figure 6.6) and the fiber reinforced ones (Figure 6.7 and 6.8), as the fiber reinforced nylon maps show their highest and lowest values in the same corners, however both the tensile strength and Young's modulus heat maps of the unreinforced nylon show their highest values on their right side and their lowest values in the lower left corner. These characteristics mean an almost indifference to temperature change when a high layer height has been chosen but an increasing amount of influence with the decrease of layer height.

6.1.1 Conclusion

With the model fitting, the mechanical property values can be predicted for this set of parameters. As shown in the earlier section, the model used achieved very good results (model performance) with sometimes near-perfect matching of predicted and actual measured values. After the same model fitting has been done with a linear polynomial function for samples categorized by their two structural parameters, the conclusion has been made that the original, non-categorized approach was the superior one and the behaviours of 3D printed materials cannot be fitted with a linear model. The R^2 values achieved for the original approach are the following:

- For unreinforced nylon, tensile strength is 0.94 and Young's modulus is 0.93.
- For carbon fiber reinforced nylon, tensile strength is 0.91, and Young's modulus is 0.99.
- For glass fiber reinforced nylon, tensile strength is 0.85, and Young's modulus is 0.95.

Chapter 7

Conclusion

After verifying the comparability of 3D printed samples when different geometries are used, I investigated the complex behaviours of differently structured samples with regard to the 4 main printing process parameters. In this investigation, the change in the two main mechanical properties of plastics was studied and further clarified by the addition of Pearson correlation analysis. After which, the experimental data was used to make a prediction model of mechanical properties, with model fitting showing excellent performance.

7.1 I. Thesis point

With the presented evidence and observation, I have demonstrated that the size and shape of a carbon fiber reinforced nylon specimen bear no effect on its strength regardless of the structure and extruded lines that it is made up of when recommended printing parameters are set, thus making the results of differently shaped specimens comparable even in samples with low layer or extruded line count in the range of 2-4.

Furthermore, I have shown that after the material deposition calibration by pressure advance is done, the porosity of specimens may vary slightly; however, it does not influence their strength.

The published papers and presentations relevant to these findings are the following:

András Kámán, Armand Meszlényi, Miklós Jakab, András Kovács, and Attila Egedy.

Effect of geometry and size on additively manufactured short-fiber carbon-nylon composite under tensile loading. *Polymers*, 17(3), 2025.

András Kámán, Miklós Jakab, Attila Egedy. Influence of specimen size and geometry on the tensile strength of extrusion 3D printed nylon filament. *Műszaki Kémiai Napok 2025 Konferencia : Engineering Chemistry Conference*, 40, 2025.

7.2 II. Thesis point

I have presented the effects analysis of key printing parameters. I have presented the detailed influences of these parameters on different mechanical properties for all three materials used by using Pearson correlation and cross-referencing it with the measured data obtained through tensile testing. It was evident that a new approach was needed for analysing the data, that being the categorisation of samples based on structural parameters, here being the infill orientation and nozzle diameter.

- a, I have shown that the extruded line cross section area or ELCSA, does not affect the mechanical properties of 3D printed samples; rather, the two parameters that it consists of do, them being the nozzle diameter and layer height. Furthermore, the layer height should be given in relative value to the nozzle diameter and not as a stand-alone parameter with its own size value, as it eliminates the dependence of the two parameters when a correlation analysis is carried out and emphasises the meaning behind the layer height influencing the shape of the extruded lines.
- b, The only consistent trend among all three materials used was that higher temperature and 0° infill orientation always produced higher strength and Young's modulus values. This trend is mainly due to the fact that with higher temperature within the recommended range the bonding between the individual extruded lines becomes stronger, also with the orientation of said extruded lines being parallel to the tensile testing direction those bonds play a smaller role in the tensile strength of the entire specimen than with a 45° orientation, especially when fibers oriented the same direction are inside the extruded lines. Similar conclusions cannot be drawn for the other parameters.

The published papers and presentations relevant to these findings are the following:

Andras Kaman, Laszlo Balogh, Miklos Jakab, Armand Meszlenyi, Bálint Levente Tarcsay, and Attila Egedy. The effect of 3d printing process parameters on nylon-based composite filaments: Experimental and modelling study. *Chemical Engineering Transactions*, 100:481–486, Jun. 2023.

András Kámán, László Balogh, Bálint Levente Tarcsay, Miklós Jakab, Armand Meszlényi, Tamás Turcsán, and Attila Egedy. Glass fibre-reinforced extrusion 3d-printed composites:

Experimental and numerical study of mechanical properties. *Polymers*, 16(2), 2024.

András Kámán, Miklós Jakab, Attila Egedy. Experimental and simulation study of nylon-based extrusion 3D printed bodies. *Műszaki Kémiai Napok 2023 Konferencia : Engineering Chemistry Conference*, 47, 2023.

András Kámán, Miklós Jakab, Attila Egedy. Kompozit anyagrendszerek vizsgálata 3D nyomtatási technológiákban. *Pannon Egyetem, Mérnöki Kari Tudományos Konferencia*, 22, 2021.

7.3 III. Thesis point

I have proven that with polynomial Black-Box model fitting the prediction of mechanical properties could be carried out, unlike the Pearson correlation analysis, the model fitting showed much better results when the material groups were not categorized by their structural parameters, mainly due to the fact that by categorization the model that can be fitted is limited to be a linear one which proved insufficient to predict the behaviours of 3D printed samples.

So, the differentiation by structural parameters is not only not needed in the case of model fitting, but also produces much worse results, meaning that the effects of parameters cannot be predicted by a linear model.

The published papers and presentations relevant to these findings are the following:

Andras Kaman, Laszlo Balogh, Miklos Jakab, Armand Meszlenyi, Bálint Levente Tarcsay, and Attila Egedy. The effect of 3d printing process parameters on nylon-based composite filaments: Experimental and modelling study. *Chemical Engineering Transactions*, 100:481–486, Jun. 2023.

András Kámán, László Balogh, Bálint Levente Tarcsay, Miklós Jakab, Armand Meszlényi, Tamás Turcsán, and Attila Egedy. Glass fibre-reinforced extrusion 3d-printed composites:

Experimental and numerical study of mechanical properties. *Polymers*, 16(2), 2024.

András Kámán, Miklós Jakab, Attila Egedy. Nylon bázisú extrúziós 3D nyomtatott testek szimulációs vizsgálata. *Műszaki Kémiai Napok 2024 Konferencia : Engineering Chemistry Conference*, 49, 2024.

References

[1] Small resin prints. link. Accessed: 09.06.2026.

[2] Concrete house printing. link. Accessed: 09.06.2026.

[3] Powder bed mass 3d printing. link. Accessed: 09.06.2026.

[4] Powder bed safety. link. Accessed: 09.06.2026.

[5] Resin bath. link. Accessed: 09.06.2026.

[6] Fdm printer. link. Accessed: 09.06.2026.

[7] An extrusion 3d printer with visible layers. link. Accessed: 09.02.2026.

[8] A resin 3d printer with visible resin bath. link. Accessed: 09.02.2026.

[9] A powder bed 3d printer post production cleaning. link. Accessed: 09.02.2026.

[10] The rat rig v-core 3 3d printer. link. Accessed: 09.02.2026.

[11] Tengbo Ma, Yali Zhang, Kunpeng Ruan, Hua Guo, Mukun He, Xuetao Shi, Yongqiang Guo, Jie Kong, and Junwei Gu. Advances in 3d printing for polymer composites: A review. *InfoMat*, 6(6):e12568, 2024.

[12] Lu-Yu Zhou, Jianzhong Fu, and Yong He. A review of 3d printing technologies for soft polymer materials. *Advanced Functional Materials*, 30(28):2000187, 2020.

[13] Ilbey Karakurt and Liwei Lin. 3d printing technologies: techniques, materials, and post-processing. *Current Opinion in Chemical Engineering*, 28:134–143, 2020. Materials Engineering Separations Engineering.

[14] Utkarsh Chadha, Aarye Abrol, Naman Paras Vora, Agastya Tiwari, S. Kirubaa Shanker, and Senthil Kumaran Selvaraj. Performance evaluation of 3d printing technologies: a review, recent advances, current challenges, and future directions. *Progress in Additive Manufacturing*, 7(5):853–886, 2022.

[15] Utkarsh Chadha, Aarye Abrol, Naman Paras Vora, Agastya Tiwari, S. Kirubaa Shanker, and Senthil Kumaran Selvaraj.

[16] S. Garzon-Hernandez, D. Garcia-Gonzalez, A. Jérusalem, and A. Arias. Design of fdm 3d printed polymers: An experimental-modelling methodology for the prediction of mechanical properties. *Materials & Design*, 188:108414, 2020.

[17] K. Dave Harshit and Davim J. Paulo. Fused deposition modeling based 3d printing. *Springer Cham*, 1:2195–0911, 2021.

[18] András Kámán, László Balogh, Bálint Levente Tarcsay, Miklós Jakab, Armand Meszlényi, Tamás Turcsán, and Attila Egedy. Glass fibre-reinforced extrusion 3d-printed composites: Experimental and numerical study of mechanical properties. *Polymers*, 16(2), 2024.

[19] Mohammad Raquibul Hasan, Ian J. Davies, Alokesh Pramanik, Michele John, and Wahidul K. Biswas. Potential of recycled pla in 3d printing: A review. *Sustainable Manufacturing and Service Economics*, 3:100020, 2024.

[20] Eda Hazal Tümer and Husnu Yildirim Erbil. Extrusion-based 3d printing applications of pla composites: A review. *Coatings*, 11(4), 2021.

[21] Horvath Joan and Cameron Rich. Mastering 3d printing. *Apress Berkeley, CA*, 2:347, 2020.

[22] Patrick Guenoun, Laura Schittecatte, Valerie Geertsen, Thuy Nguyen, and Daniel Bonamy. From resin formulation and process parameters to the final mechanical properties of 3d printed acrylate materials. *MRS Communications*, 13, 03 2023.

[23] Yang Guo, Huseini Patanwala, Brice Bognet, and Anson Ma. Inkjet and inkjet-based 3d printing: Connecting fluid properties and printing performance. *Rapid Prototyping Journal*, 23, 04 2017.

[24] Md Nazmul Dipu. A review on 3d printing technology: Literature, components, generic process, printing categories, associated materials, advantages, disadvantages, and research gaps. 04 2024.

[25] Aniket Jadhav and Vijay S. Jadhav. A review on 3d printing: An additive manufacturing technology. *Materials Today: Proceedings*, 62:2094–2099, 2022. International Conference on Design, Manufacturing and Materials Engineering.

[26] Lucie Zarybnicka, Karel Dvorak, Zdeňka Dostálová, and Hana Vojáčková. Study of different printing design type polymer samples prepared by additive manufacturing. *Periodica Polytechnica Chemical Engineering*, 64:255–264, 10 2019.

[27] J.M. Chacón, M.A. Caminero, E. García-Plaza, and P.J. Núñez. Additive manufacturing of pla structures using fused deposition modelling: Effect of process parameters on mechanical properties and their optimal selection. *Materials & Design*, 124:143–157, 2017.

[28] Md Mahbub Morshed Haque, Suchinto Roy Dhrubo, Al-Fida Zubayer Pranto, Akash Ahmed, Md Miraj Arefin, Md Arifuzzaman, and Md Shariful Islam. Impact of process parameters and material selection on the mechanical performance of fdm 3d-printed components. *Hybrid Advances*, 10:100502, 2025.

[29] Hussein Hadi Jawad, Naser Kordani, Abbasali Bagheri, and Hamed Aghajani Derazkola. Optimization of 3d printing parameters for enhanced mechanical strength: Effects of glass fiber reinforcement and fill ratio using rsm and anova. *Journal of Composites Science*, 9(2), 2025.

[30] Muhammad Abas, Tufail Habib, Sahar Noor, Bashir Salah, and Dominik Zimon. Parametric investigation and optimization to study the effect of process parameters on the dimensional deviation of fused deposition modeling of 3d printed parts. *Polymers*, 14(17), 2022.

[31] Jerzy Bochnia, Malgorzata Blasiak, and Tomasz Kozior. A comparative study of the mechanical properties of fdm 3d prints made of pla and carbon fiber-reinforced pla for thin-walled applications. *Materials*, 14(22), 2021.

[32] S M Fijul Kabir, Kavita Mathur, and Abdel-Fattah M. Seyam. A critical review on 3d printed continuous fiber-reinforced composites: History, mechanism, materials and properties. *Composite Structures*, 232:111476, 2020.

[33] Thomas Hanemann, Alexander Klein, Siegfried Baumgärtner, Judith Jung, David Wilhelm, and Steffen Antusch. Material extrusion 3d printing of peek-based composites. *Polymers*, 15(16), 2023.

[34] Jaroslav Majko, Milan Vaško, Marián Handrik, and Milan Sága. Tensile properties of additively manufactured thermoplastic composites reinforced with chopped carbon fibre. *Materials*, 15(12), 2022.

[35] Ved S. Vakharia, Mrityunjay Singh, Anton Salem, Michael C. Halbig, and Jonathan A. Salem. Effect of reinforcements and 3-d printing parameters on the microstructure and mechanical properties of acrylonitrile butadiene styrene (abs) polymer composites. *Polymers*, 14(10), 2022.

[36] ES Zainudin, SM Sapuan, S Sulaiman, and MMHM Ahmad. Fiber orientation of short fiber reinforced injection molded thermoplastic composites: A review. *Journal of Injection Molding Technology*, 6(1):1–10, 2002.

[37] D. Teixeira, M. Giovanela, L.B. Gonella, and J.S. Crespo. Influence of injection molding on the flexural strength and surface quality of long glass fiber-reinforced polyamide 6.6 composites. *Materials & Design*, 85:695–706, 2015.

[38] Thanh Binh Nguyen Thi, Mizuki Morioka, Atsushi Yokoyama, Senji Hamanaka, Katsuhisa Yamashita, and Chisato Nonomura. Measurement of fiber orientation distribution in injection-molded short-glass-fiber composites using x-ray computed tomography. *Journal of Materials Processing Technology*, 219:1–9, 2015.

[39] Rafael Thiago Luiz Ferreira, Igor Cardoso Amatte, Thiago Assis Dutra, and Daniel Bürger. Experimental characterization and micrography of 3d printed pla and pla reinforced with short carbon fibers. *Composites Part B: Engineering*, 124:88–100, 2017.

[40] Pei Huang, Zhidong Xia, and Song Cui. 3d printing of carbon fiber-filled conductive silicon rubber. *Materials & Design*, 142:11–21, 2018.

[41] Tianyun Yao, Kai Zhang, Zichen Deng, and Juan Ye. A novel generalized stress invariant-based strength model for inter-layer failure of fff 3d printing pla material. *Materials & Design*, 193:108799, 2020.

[42] András Kámán, Armand Meszlényi, Miklós Jakab, András Kovács, and Attila Egedy. Effect of geometry and size on additively manufactured short-fiber carbon-nylon composite under tensile loading. *Polymers*, 17(3), 2025.

[43] Salman Pervaiz, Taimur Ali Qureshi, Ghanim Kashwani, and Sathish Kannan. 3d printing of fiber-reinforced plastic composites using fused deposition modeling: A status review. *Materials*, 14(16), 2021.

[44] Tom Fisher, José Humberto S. Almeida Jr, Brian G. Falzon, and Zafer Kazancı. Tension and compression properties of 3d-printed composites: Print orientation and strain rate effects. *Polymers*, 15(7), 2023.

[45] Jingjing Liu, Muhammad Awais Naeem, Mouaz Al Kouzbary, Hamza Al Kouzbary, Hanie Nadia Shasmin, Nooranida Arifin, Nasrul Anuar Abd Razak, and Noor Azuan Abu Osman. Effect of infill parameters on the compressive strength of 3d-printed nylon-based material. *Polymers*, 15(2), 2023.

[46] R. Venkatesh, J. Jerold John Britto, K. Amudhan, V. Anbumalar, R. Prabhakaran, and R. Thiyanesh Sakthi. Experimental investigation of mechanical properties on cf reinforced pla, abs and nylon composite part. *Materials Today: Proceedings*, 76:647–653, 2023. International Conference on Additive Manufacturing and Allied Technologies (ICAMAT 2022).

[47] Aditya Pulipaka, Kunal Manoj Gide, Ali Beheshti, and Z. Shaghayegh Bagheri. Effect of 3d printing process parameters on surface and mechanical properties of fff-printed peek. *Journal of Manufacturing Processes*, 85:368–386, 2023.

[48] Noshin Tasnim Tuli, Sinthea Khatun, and Adib Bin Rashid. Unlocking the future of precision manufacturing: A comprehensive exploration of 3d printing with fiber-reinforced composites in aerospace, automotive, medical, and consumer industries. *Heliyon*, 10(5), 2024.

[49] Muhammad Azfar Jamal, Owaisur Rahman Shah, Usman Ghafoor, Yumna Qureshi, and M. Raheel Bhutta. Additive manufacturing of continuous fiber-reinforced polymer composites via fused deposition modelling: A comprehensive review. *Polymers*, 16(12), 2024.

[50] Fatheali A. Shilar, Sharanabasava V. Ganachari, Veerabhadragouda B. Patil, I. Neelakanta Reddy, and Jaesool Shim. Preparation and validation of sustainable metakaolin based geopolymer concrete for structural application. *Construction and Building Materials*, 371:130688, 2023.

[51] Zhaorong Zhu, Yiyan Lu, and Man Zhou. Surface modification of recycled tire rubber powders with tannic acid and nano-tio2 for enhanced performance and photocatalytic

properties of rubberized cement-based materials. *Construction and Building Materials*, 399:132607, 2023.

[52] Zhijie Pi, Shibing Huang, Jianbo Xu, Ziwen Chen, Hao Li, Yongqi Shen, and Junshuo Tian. The reinforcement mechanism of basalt and polypropylene fibers on the strength, toughness and crack resistance of tailing mortar. *Construction and Building Materials*, 419:135531, 2024.

[53] Y. Asghari, S.E. Mohammadyan-Yasouj, M. Petrů, H. Ghandvar, and S.S. R. Koloor. 3d printing and implementation of engineered cementitious composites - a review. *Case Studies in Construction Materials*, 21:e03462, 2024.

[54] Alison J. Clarke, Andrew Dickson, and Denis P. Dowling. Fabrication and performance of continuous 316 stainless steel fibre-reinforced 3d-printed pla composites. *Polymers*, 16(1), 2024.

[55] Rafał Podgórski, Michał Wojasiński, Edyta Trepkowska-Mejer, and Tomasz Ciach. A simple and fast method for screening production of polymer-ceramic filaments for bone implant printing using commercial fused deposition modelling 3d printers. *Biomaterials Advances*, 146:213317, 2023.

[56] Csenge Toth and Norbert Krisztian Kovacs. Comparison of the accuracy of analytical models for basalt fiber–reinforced poly(lactic acid) composites prepared by injection molding and fused filament fabrication. *The International Journal of Advanced Manufacturing Technology*, 121:1–12, 07 2022.

[57] Sachini Wickramasinghe, Truong Do, and Phuong Tran. Fdm-based 3d printing of polymer and associated composite: A review on mechanical properties, defects and treatments. *Polymers*, 12(7), 2020.

[58] Henglun Sun, Dongsheng Li, You Qu, Quan Zhi, Xiaoyong Tian, Dichen Li, and Weijun Zhu. Near-perfect turning of robot-based 3d printing continuous carbon fiber reinforced nylon composites based on fiber-scale internal stress characterization. *Composites Part A: Applied Science and Manufacturing*, 175:107805, 2023.

[59] Gonghe Zhang, Xiaodong Zheng, Qinglin Wang, Yinxu Ni, Fenghua Liu, Kai Zhao, and Luoyu Roy Xu. Limitations of composite strength theory for predicting the ultimate strengths of layered 3d printing polymers. *Composites Part A: Applied Science and Manufacturing*, 185:108288, 2024.

[60] Shuai Wang, Jie Liu, Zhelong He, and Dongmin Yang. Concurrent optimisation of structural topology and fibre paths for 3d printing of continuous fibre composites based on chain primitive projection. *Composites Part A: Applied Science and Manufacturing*, 185:108333, 2024.

[61] Yu Long, Zhongsen Zhang, Cheng Yan, Zhen Huang, Kunkun Fu, and Yan Li. Multi-objective optimization for improving printing efficiency and mechanical properties of 3d-printed continuous plant fibre composites. *Composites Communications*, 35:101283, 2022.

[62] Shouling Ding, Bin Zou, Yuexi Zhuang, Xinfeng Wang, Zhiwei Feng, and Qingyang Liu. Effect of printing design and forming thermal environment on pseudo-ductile behavior of continuous carbon/glass fibers reinforced nylon composites. *Composite Structures*, 322:117362, 2023.

[63] Baosheng Liu, Boxiao Dong, Huimin Li, Ruishen Lou, and Yi Chen. 3d printing finite element analysis of continuous fiber reinforced composite materials considering printing pressure. *Composites Part B: Engineering*, 277:111397, 2024.

[64] Wenfei Peng, Zehui Ge, Yiyu Shao, Longfei Lin, He Li, and Moliar Oleksandr. Mechanical behavior of nacre-inspired cfrp composites by 3d printing. *Composite Structures*, 339:118167, 2024.

[65] Ivan Grgić, Mirko Karakašić, Hrvoje Glavaš, and Pejo Konjatić. Accuracy of fdm pla polymer 3d printing technology based on tolerance fields. *Processes*, 11(10), 2023.

[66] Klipper3d Team. Klipper documentation. link. Accessed: 09.02.2026.

[67] Rat Rig Team. Ratos documentation. link. Accessed: 09.02.2026.

[68] Klipper3d Team. Klipper documentation - extrusion. link. Accessed: 09.02.2026.

[69] Klipper3d Team. Klipper documentation - retraction. link. Accessed: 09.02.2026.

[70] Klipper3d Team. Klipper documentation - resonance compensation. link. Accessed: 09.02.2026.

[71] Klipper3d Team. Klipper documentation - pressure advance. link. Accessed: 09.02.2026.

[72] Klipper3d Team. Klipper documentation - skew correction. link. Accessed: 09.02.2026.

[73] Tim Osswald, J. Puentes, and Julian Kattinger. Fused filament fabrication melting model. *Additive Manufacturing*, 22, 04 2018.

[74] Ahmed Hadi, Abdulkader Kadauw, and Henning Zeidler. The effect of printing temperature and moisture on tensile properties of 3d printed glass fiber reinforced nylon 6. *Materials Today: Proceedings*, 91:48–55, 2023. 4th International Conference on Processing and Characterization of Materials Shortname: ICPCM 2022 (Rourkela).

[75] J. Majko, M. Vaško, M. Handrik, M. Gavlas, and F. Nový. Effect of printing parameters on the tensile properties of improperly stored chopped carbon fibres reinforced nylon. *Procedia Structural Integrity*, 51:160–165, 2023. 6th International Conference on Structural Integrity and Durability (ICSID 2022).

[76] eSUN Team. esun epa-cf filament data sheet. link. Accessed: 09.02.2026.

[77] eSUN Team. esun epa-gf filament data sheet. link. Accessed: 09.02.2026.

[78] eSUN Team. esun epa filament data sheet. link. Accessed: 09.02.2026.

[79] José Humberto S. Almeida, Arttu Miettinen, Fabien Léonard, Brian G. Falzon, and Philip J. Withers. Microstructure and damage evolution in short carbon fibre 3d-printed composites during tensile straining. *Composites Part B: Engineering*, 292:112073, 2025.

[80] Xia Gao, Shunxin Qi, Xiao Kuang, Yunlan Su, Jing Li, and Dujin Wang. Fused filament fabrication of polymer materials: A review of interlayer bond. *Additive Manufacturing*, 37:101658, 2021.

[81] Prusa Research Team. Arachne perimeter generator. link. Accessed: 09.02.2026.

[82] Flaviana Calignano, Massimo Lorusso, Ignanio Roppolo, and Paolo Minetola. Investigation of the mechanical properties of a carbon fibre-reinforced nylon filament for 3d printing. *Machines*, 8(3), 2020.

[83] L.G. Blok, M.L. Longana, H. Yu, and B.K.S. Woods. An investigation into 3d printing of fibre reinforced thermoplastic composites. *Additive Manufacturing*, 22:176–186, 2018.

[84] STLDenise3D. Speed benchy: Settings and rules. link. Accessed: 09.02.2026.

Appendix

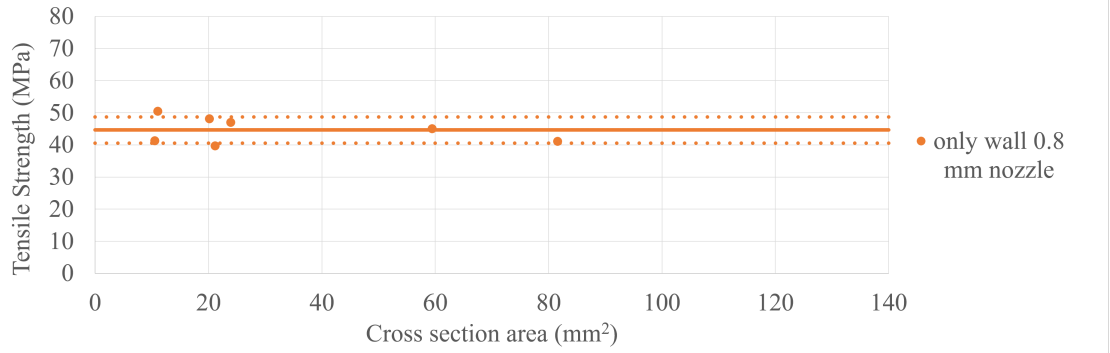


FIGURE 7.1: Individual specimen group with their mean value and deviations

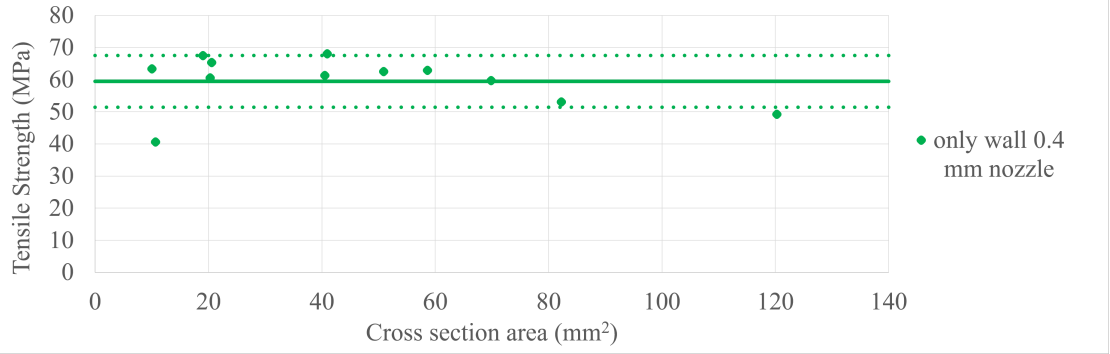


FIGURE 7.2: Individual specimen group with their mean value and deviations

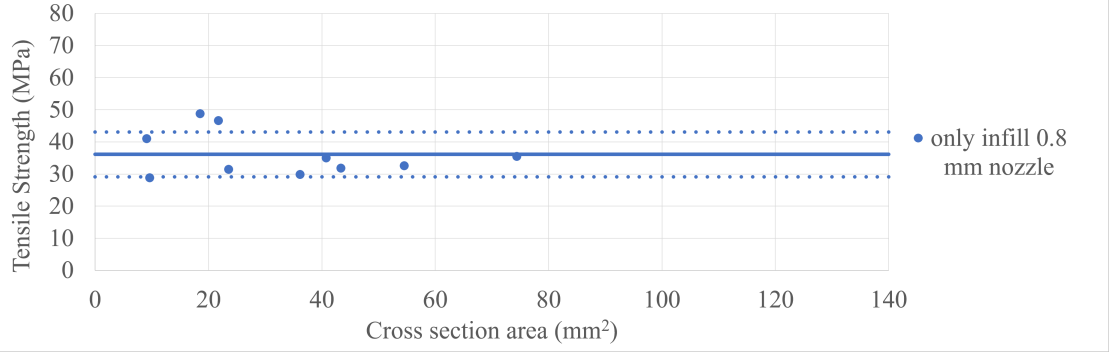


FIGURE 7.3: Individual specimen group with their mean value and deviations

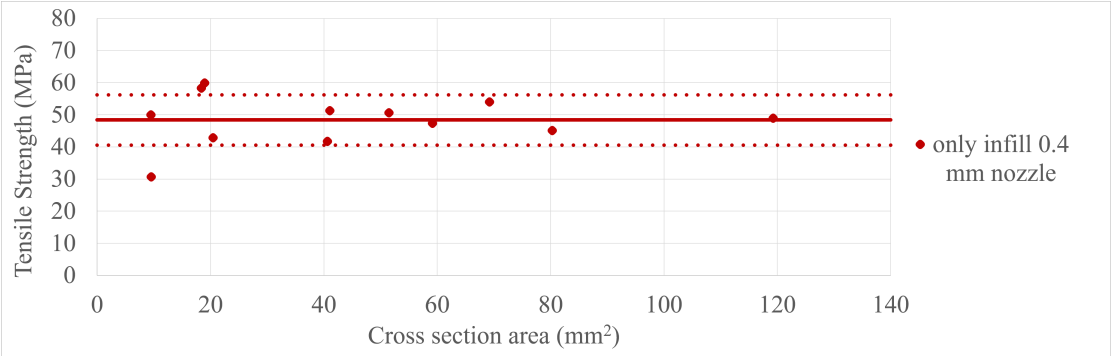


FIGURE 7.4: Individual specimen group with their mean value and deviations

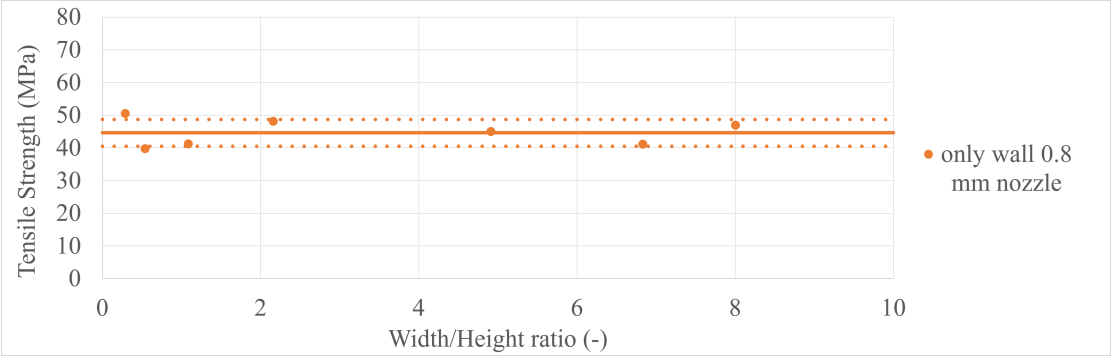


FIGURE 7.5: Individual specimen group with their mean value and deviations

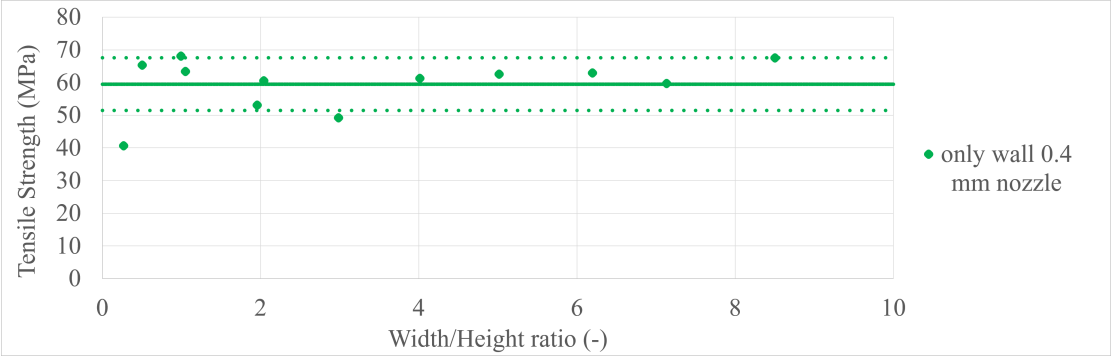


FIGURE 7.6: Individual specimen group with their mean value and deviations

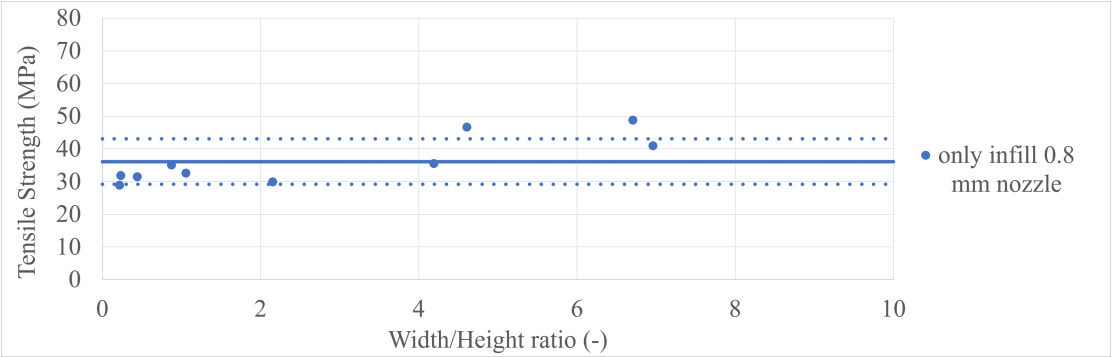


FIGURE 7.7: Individual specimen group with their mean value and deviations

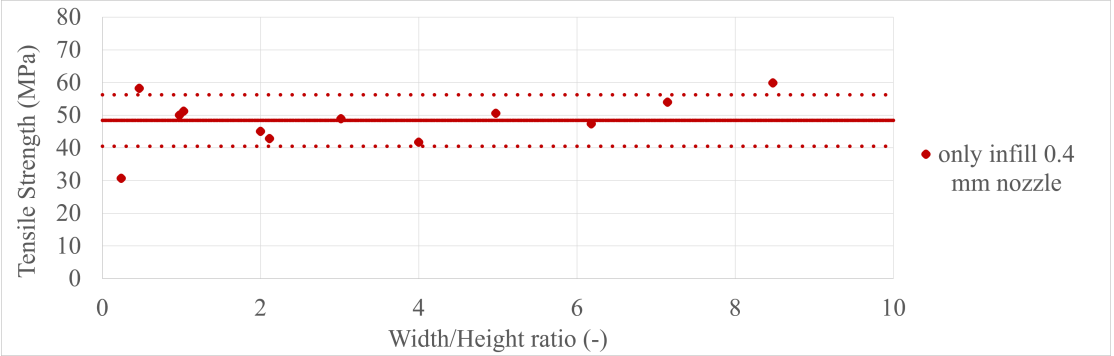


FIGURE 7.8: Individual specimen group with their mean value and deviations

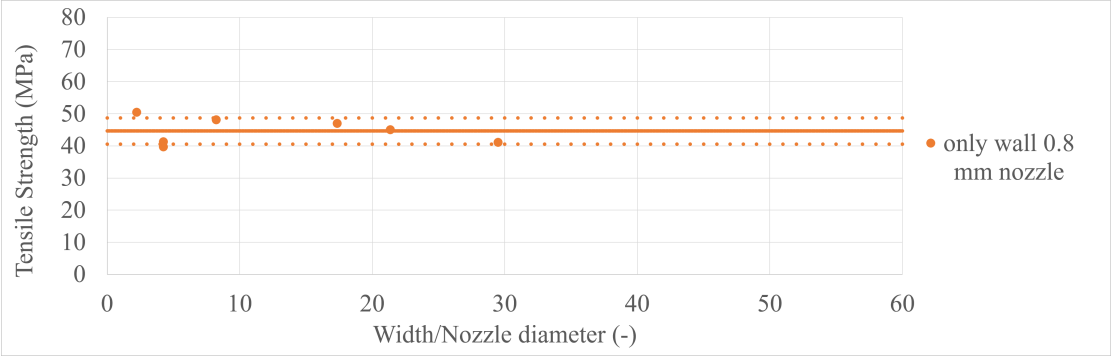


FIGURE 7.9: Individual specimen group with their mean value and deviations

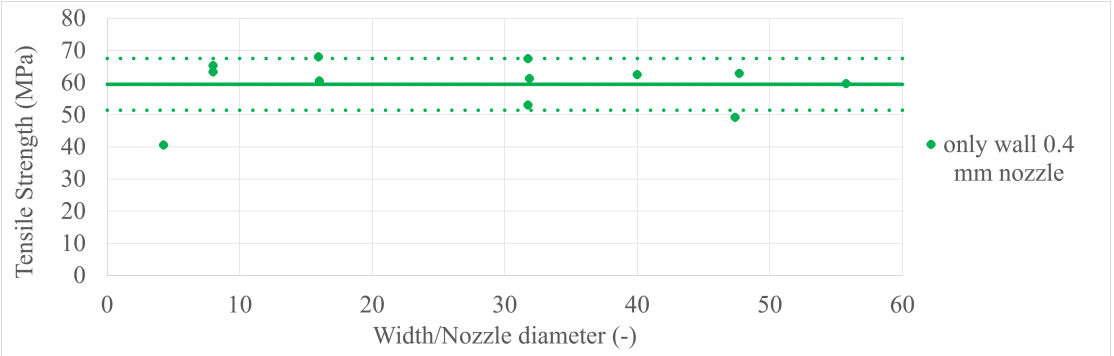


FIGURE 7.10: Individual specimen group with their mean value and deviations

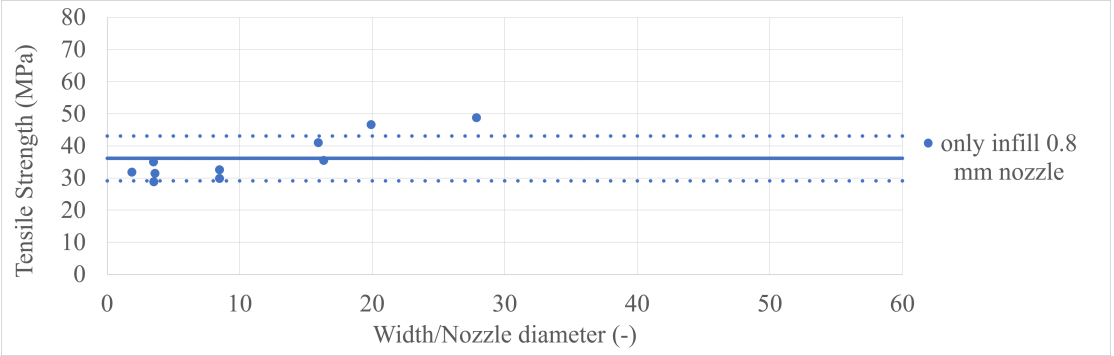


FIGURE 7.11: Individual specimen group with their mean value and deviations

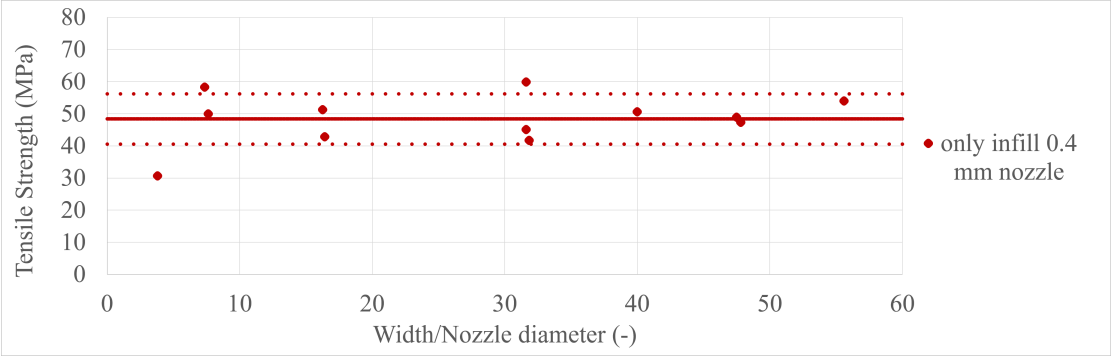


FIGURE 7.12: Individual specimen group with their mean value and deviations

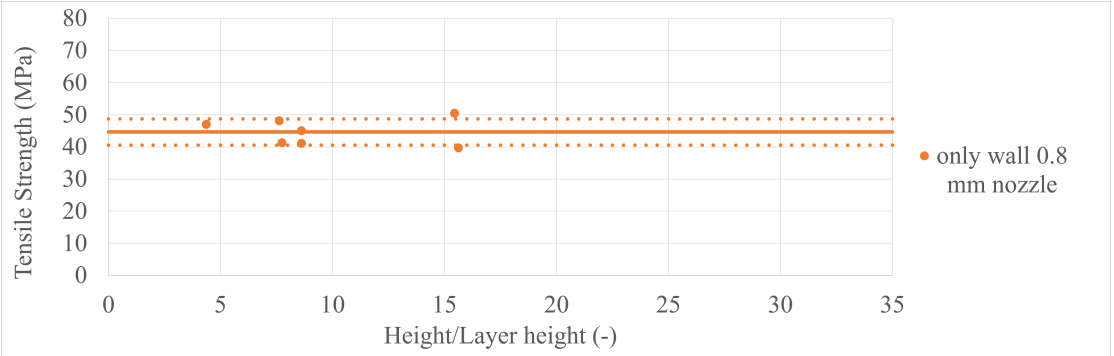


FIGURE 7.13: Individual specimen group with their mean value and deviations

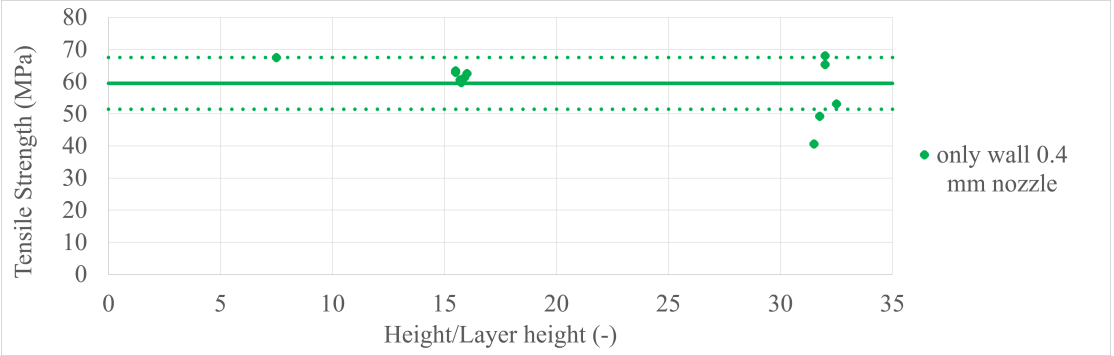


FIGURE 7.14: Individual specimen group with their mean value and deviations

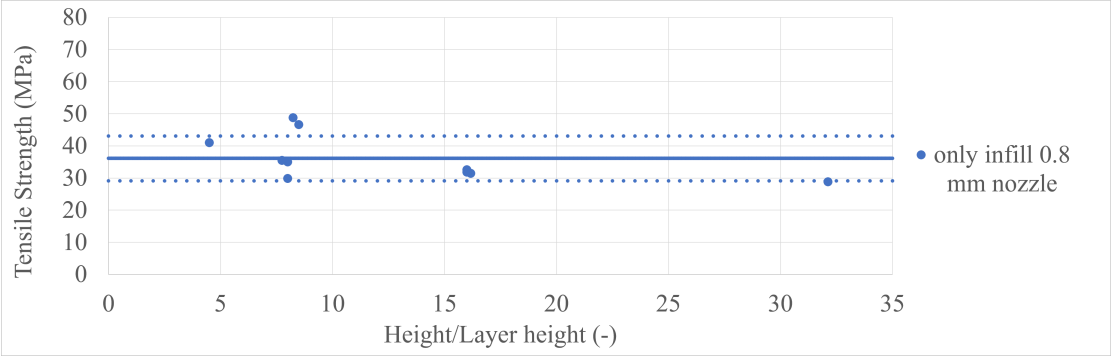


FIGURE 7.15: Individual specimen group with their mean value and deviations

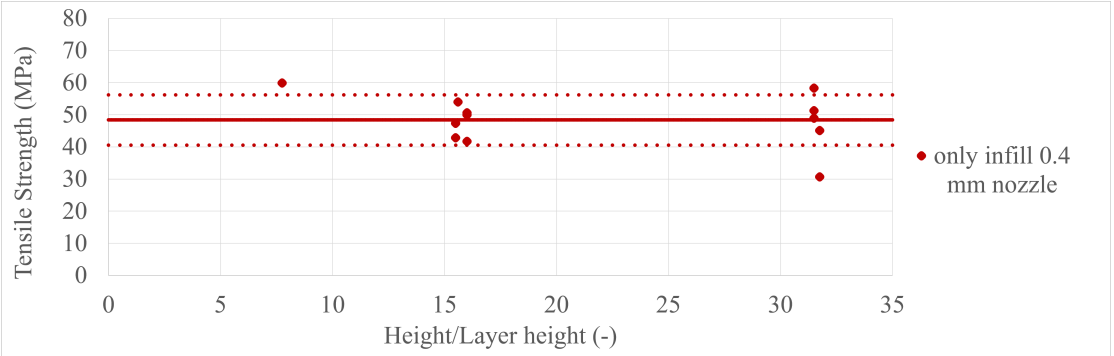
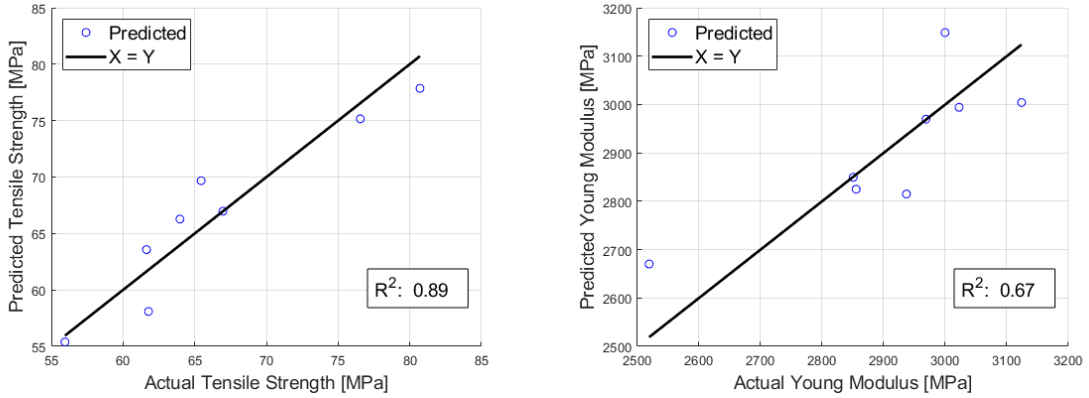
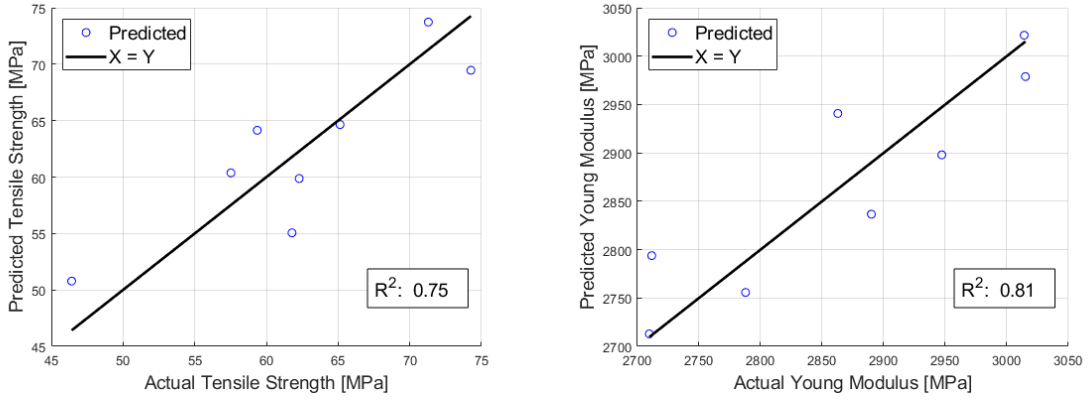


FIGURE 7.16: Individual specimen group with their mean value and deviations



(a) (b)

FIGURE 7.17: The prediction model performance for 0° infill oriented unreinforced nylon samples tensile strength (a) and Young's modulus (b) values.



(a) (b)

FIGURE 7.18: The prediction model performance for 45° infill oriented unreinforced nylon samples tensile strength (a) and Young's modulus (b) values.

TABLE 7.1: The measured mechanical properties and used parameters of every unreinforced nylon samples

Sample No. [−]	**Nozzle diameter** [mm]	**Layer height** [mm]	**Temperature** [$°C$]	**Infill Orientation** [°]	**Tensile strength** [MPa]		**Young's modulus** [MPa]	
					Average	Deviation	Average	Deviation
1	0.8	0.2	240	0	61.64	2.79	2519	160.29
2	0.8	0.5	240	0	76.55	6.19	2855	243.01
3	0.8	0.2	240	45	57.52	5.22	2712	111.59
4	0.8	0.5	240	45	74.26	7.96	3015	65.69
5	0.8	0.2	260	0	63.97	9.17	2851	22.76
6	0.8	0.5	260	0	80.72	5.83	3124	88.23
7	0.8	0.2	260	45	65.14	2.90	2890	24.38
8	0.8	0.5	260	45	71.29	3.26	3014	89.64
9	0.4	0.1	240	0	55.95	4.04	2937	63.94
10	0.4	0.25	240	0	66.97	1.12	2969	14.76
11	0.4	0.1	240	45	46.42	0.95	2710	11.27
12	0.4	0.25	240	45	62.29	1.60	2947	67.47
13	0.4	0.1	260	0	61.78	2.46	3022	34.94
14	0.4	0.25	260	0	65.45	6.22	3000	140.24
15	0.4	0.1	260	45	61.78	6.13	2788	107.92
16	0.4	0.25	260	45	59.36	0.41	2863	34.00

TABLE 7.2: The measured mechanical properties and used parameters of every carbon fiber reinforced nylon samples

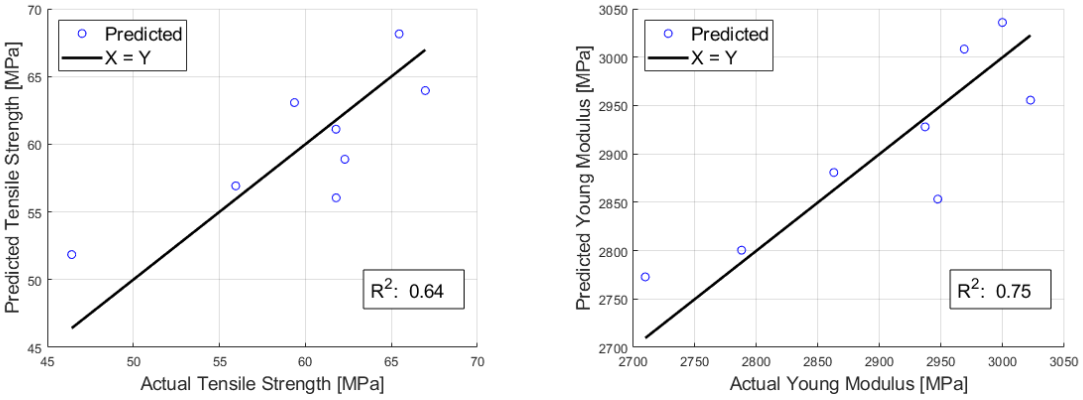
Sample No. [−]	**Nozzle diameter** [mm]	**Layer height** [mm]	**Temperature** [$°C$]	**Infill Orientation** [°]	**Tensile strength** [MPa]		**Young's modulus** [MPa]	
					Average	Deviation	Average	Deviation
1	0.4	0.1	240	0	75.20	3.43	5479	289.07
2	0.4	0.25	240	0	60.99	2.30	4997	96.12
3	0.4	0.1	240	45	63.88	0.74	3659	71.66
4	0.4	0.25	240	45	55.17	1.65	3544	246.22
5	0.4	0.1	260	0	68.16	2.46	5643	171.80
6	0.4	0.25	260	0	72.99	2.10	5249	330.67
7	0.4	0.1	260	45	61.35	5.34	4034	72.90
8	0.4	0.25	260	45	62.68	2.47	4108	156.82
9	0.8	0.2	240	0	62.74	6.01	5601	177.34
10	0.8	0.5	240	0	71.54	0.58	5095	54.48
11	0.8	0.2	240	45	57.96	9.50	4465	7.31
12	0.8	0.5	240	45	62.58	3.51	4617	43.42
13	0.8	0.2	260	0	72.30	2.67	5593	208.48
14	0.8	0.5	260	0	80.82	0.56	5412	115.26
15	0.8	0.2	260	45	57.28	6.27	4390	79.84
16	0.8	0.5	260	45	65.94	6.72	4757	195.87

TABLE 7.3: The measured mechanical properties and used parameters of every glass fiber reinforced nylon samples no. 1

Sample No. [−]	**Nozzle diameter** [mm]	**Layer height** [mm]	**Temperature** [$°C$]	**Infill Orientation** [°]	**Tensile strength** [MPa]		**Young's modulus** [MPa]	
					Average	Deviation	Average	Deviation
1	0.6	0.4	220	45	44.85	6.27	3322	906.03
2	0.6	0.4	250	45	39.17	1.86	2767	153.73
3	0.6	0.4	220	45	28.12	2.40	2417	97.83
4	0.6	0.15	220	45	30.29	1.15	2823	101.42
5	0.6	0.15	250	45	28.88	0.45	2497	94.67
6	0.6	0.15	220	45	31.01	2.55	3716	251.73
7	0.6	0.4	220	0	36.72	2.75	2943	189.45
8	0.6	0.15	220	0	34.77	2.87	3304	183.06
9	0.6	0.4	250	0	38.20	0.98	3018	33.38
10	0.6	0.15	250	0	43.33	1.55	3816	111.38
11	0.6	0.4	220	0	35.65	1.79	2789	215.70
12	0.6	0.15	220	0	37.25	12.39	3361	1018
13	0.6	0.4	220	45	35.05	5.08	2337	423.01
14	0.6	0.15	220	45	32.43	4.63	2308	293.98
15	0.6	0.4	250	90	36.86	2.69	2763	140.62
16	0.6	0.4	250	45	33.94	2.14	1854	124.32
17	0.6	0.15	250	0	32.71	2.12	2971	225.60
18	0.6	0.15	250	45	33.09	2.44	2265	209.53
19	0.3	0.2	220	45	36.09	0.84	2213	200.86
20	0.3	0.1	220	0	39.24	1.75	3951	460.87
21	0.3	0.2	220	0	35.00	3.91	2752	281.88
22	0.3	0.1	220	45	43.73	1.94	3400	167.57
23	0.3	0.1	220	0	28.94	3.01	2613	232.51
24	0.3	0.2	220	0	28.66	5.94	2270	421.09
25	0.3	0.1	220	45	27.08	1.14	1616	56.63

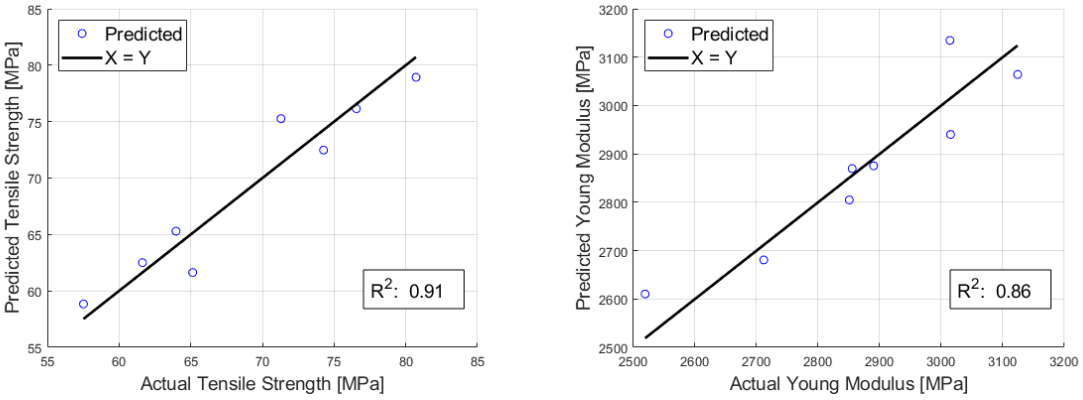
TABLE 7.4: The measured mechanical properties and used parameters of every glass fiber reinforced nylon samples no. 2

Sample No. [−]	**Nozzle diameter** [mm]	**Layer height** [mm]	**Temperature** [$°C$]	**Infill Orientation** [°]	**Tensile strength** [MPa]		**Young's modulus** [MPa]	
					Average	Deviation	Average	Deviation
26	0.3	0.2	220	45	24.88	1.69	1353	100.76
27	0.3	0.2	250	45	36.50	0.99	2065	195.60
28	0.3	0.1	250	0	47.47	3.83	5409	508.06
29	0.3	0.2	250	0	36.81	1.29	2701	219.35
30	0.3	0.1	250	45	43.54	3.43	3802	364.11
31	0.3	0.1	250	0	40.29	1.66	3598	340.19
32	0.3	0.2	250	0	30.75	1.58	2176	147.28
33	0.3	0.2	250	45	31.37	0.75	1981	73.07
34	0.3	0.1	250	45	29.68	2.27	1738	275.94
35	0.4	0.10	220	0	53.96	3.73	3361	400.54
36	0.4	0.25	220	0	52.60	2.43	3039	139.61
37	0.4	0.10	220	45	45.63	0.72	2859	125.08
38	0.4	0.25	220	45	54.61	4.89	3083	61.63
39	0.4	0.10	250	0	57.67	3.98	3981	208.52
40	0.4	0.25	250	0	59.49	2.27	3762	112.57
41	0.4	0.10	250	45	51.27	3.84	3355	121.64
42	0.4	0.25	250	45	59.56	2.92	3019	223.98
43	0.8	0.20	220	0	56.59	6.51	4032	180.94
44	0.8	0.50	220	0	61.24	1.93	3617	168.38
45	0.8	0.50	220	45	44.21	3.80	3031	116.94
46	0.8	0.50	220	45	43.98	5.56	2852	371.12
47	0.8	0.20	250	0	59.30	3.96	4203	154.19
48	0.8	0.50	250	0	72.00	7.10	4243	198.44
49	0.8	0.20	250	45	51.51	3.67	3396	176.39
50	0.8	0.50	250	45	46.66	4.45	2973	113.84



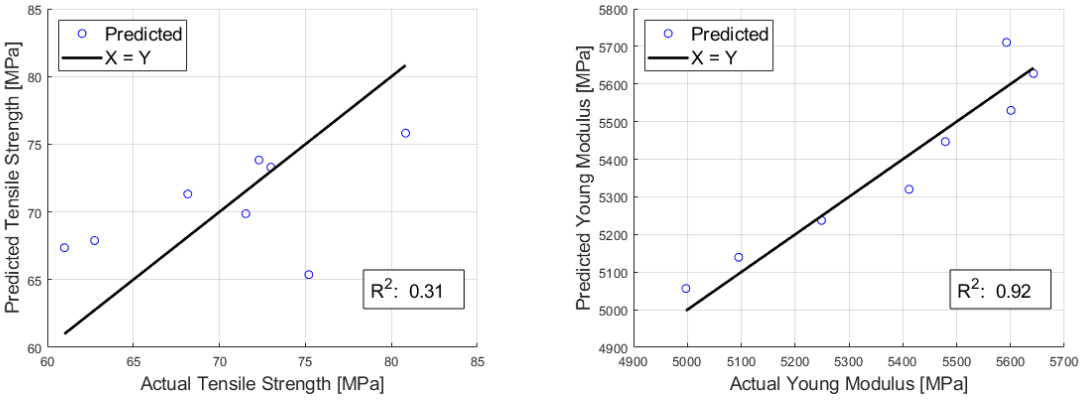
(a) (b)

FIGURE 7.19: The prediction model performance for 0.4 mm nozzle unreinforced nylon samples tensile strength (a) and Young's modulus (b) values.



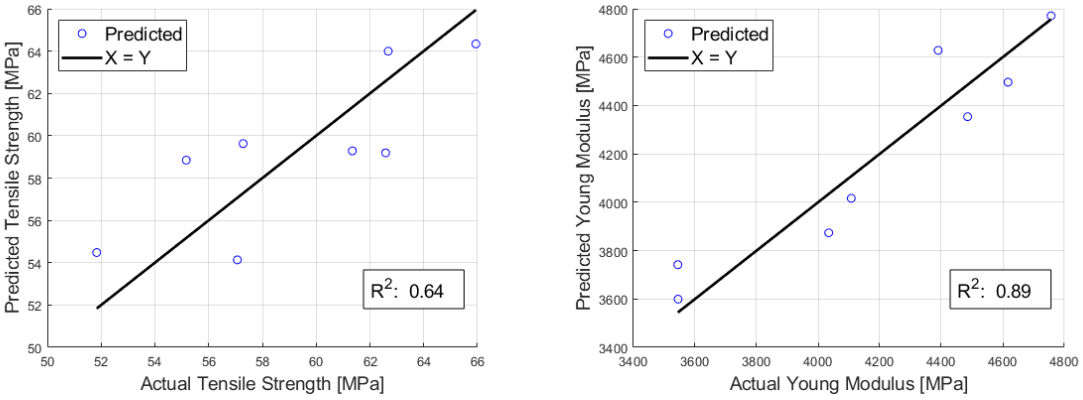
(a) (b)

FIGURE 7.20: The prediction model performance for 0.8 mm nozzle unreinforced nylon samples tensile strength (a) and Young's modulus (b) values.



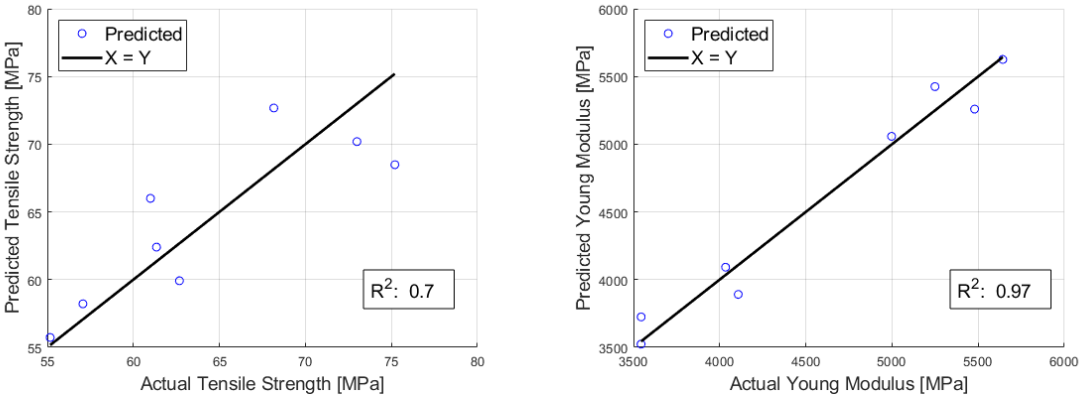
(a) (b)

FIGURE 7.21: The prediction model performance for 0° infill oriented carbon fiber reinforced nylon samples tensile strength (a) and Young's modulus (b) values.



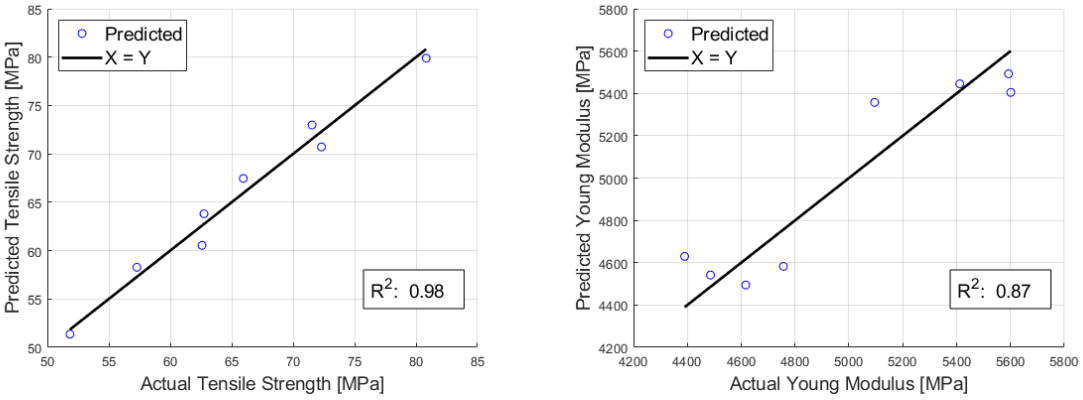
(a) (b)

FIGURE 7.22: The prediction model performance for 45° infill oriented carbon fiber reinforced nylon samples tensile strength (a) and Young's modulus (b) values.



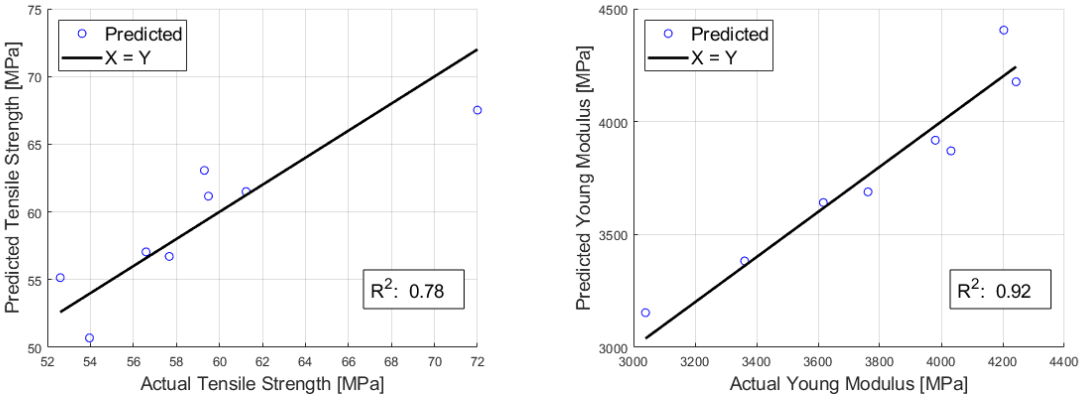
(a) (b)

FIGURE 7.23: The prediction model performance for 0.4 mm nozzle carbon fiber reinforced nylon samples tensile strength (a) and Young's modulus (b) values.



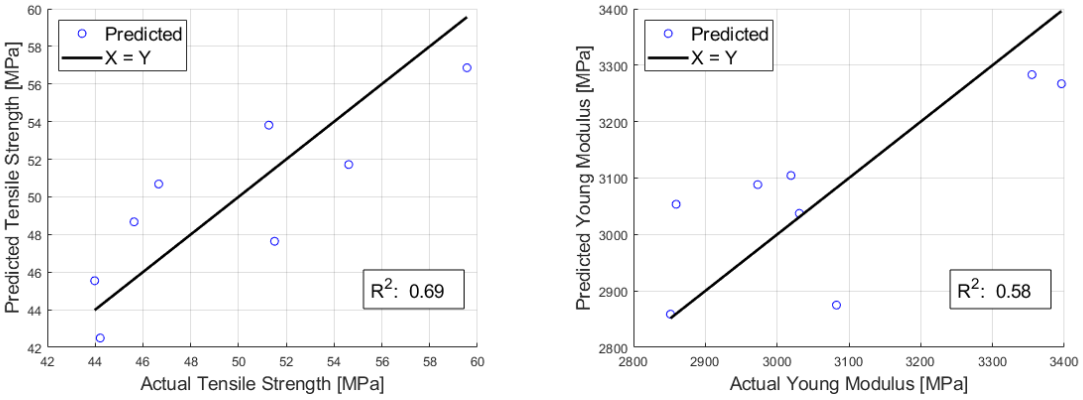
(a) (b)

FIGURE 7.24: The prediction model performance for 0.8 mm nozzle carbon fiber reinforced nylon samples tensile strength (a) and Young's modulus (b) values.



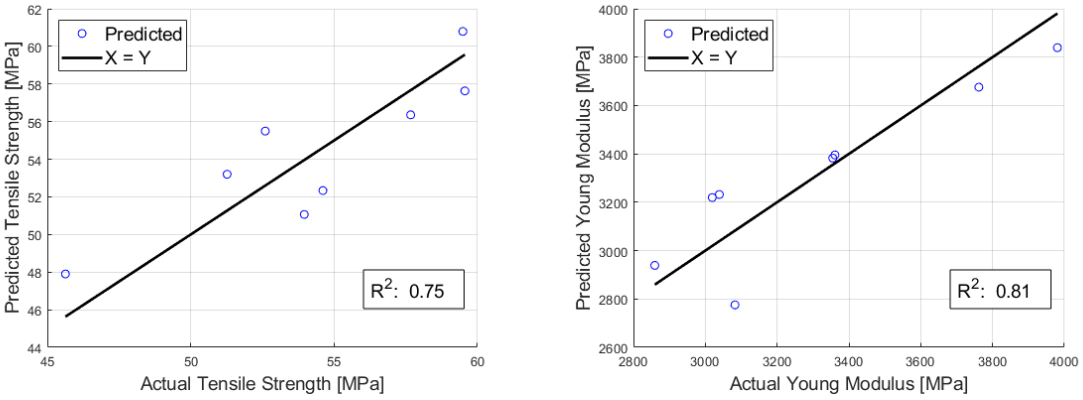
(a) (b)

FIGURE 7.25: The prediction model performance for 0° infill oriented glass fiber reinforced nylon samples tensile strength (a) and Young's modulus (b) values.



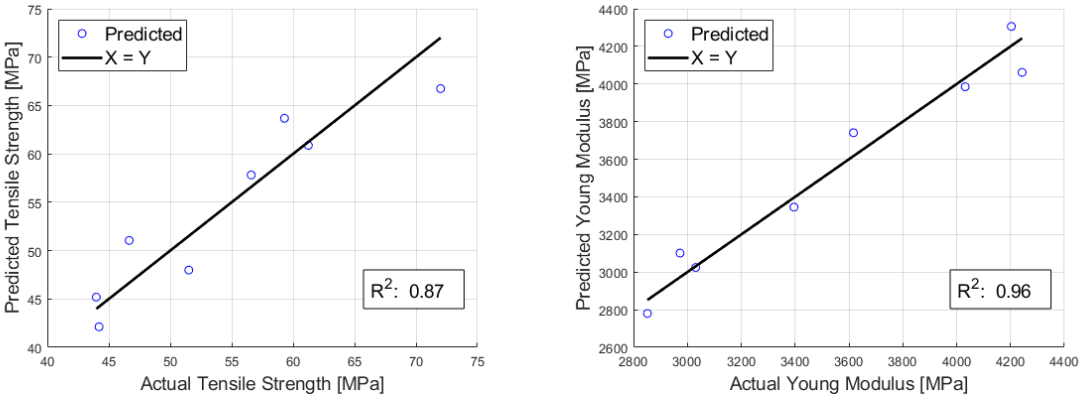
(a) (b)

FIGURE 7.26: The prediction model performance for 45° infill oriented glass fiber reinforced nylon samples tensile strength (a) and Young's modulus (b) values.



(a) (b)

FIGURE 7.27: The prediction model performance for 0.4 mm nozzle glass fiber reinforced nylon samples tensile strength (a) and Young's modulus (b) values.



(a) (b)

FIGURE 7.28: The prediction model performance for 0.8 mm nozzle glass fiber reinforced nylon samples tensile strength (a) and Young's modulus (b) values.